USE AND APPLICATIONS OF ELECTROCHEMICAL IMPEDANCE TECHNIQUES

TECHNICAL REPORT 24

TECHNICAL REPORT NUMBER 24

Use and Application of Electrochemical Impedance Techniques

TECHNICAL REPORT NUMBER 24

Claude Gabrielli

Ing Ecole Superieure d'Electricite

Docteur es Sciences

Centre National de la Recherche Scientifique

LP15 Physique des Liquides et Electrochimie

Universite P et M Curie, 4 Place Jussieu, T22

75252 Paris Cedex 05, France

Issue B: April 1997

Solartron Part No.: 12860013

To Bernadette, Genevieve and Julien.

Claude Gabrielli
September 1990

Contents

CHAPTER 3 : APPLICATIONS OF IMPEDANCE TECHNIQUES

Introduction

Numerous processes occurring when an electrical conductor (metal or semiconductor) is put in contact with an ionic conductor (liquid or solid electrolyte) are electrochemical by nature, or can be often considered as such. In some cases (e.g. atmospheric corrosion, corrosion in soil, metal lubrication, etc.), this nature is not obvious a priori, but a careful inspection will lead to this conclusion. The recognized testing techniques can be very time consuming (e.g. for corrosion: salt spray test, gravimetry, quantitative analysis of the dissolved metal...). Hence in many instances the electrochemical techniques are particularly attractive.

An "in situ" investigation of an electrochemical process which avoids the surface changes which are often the drawbacks of the "ex situ" analysis can often only be carried out by electrical techniques. In general an overall mechanism does not involve only one charge transfer reaction between the electrode and the electrolyte. It is the result of an ensemble of partial elementary phenomena, in series or in parallel, involving mass transport, chemical and electrochemical reactions. These various steps are characterized by their rates. If one of the steps is much slower than the others, it imposes its own rate on the overall mechanism and the plotting of the current-voltage curve in steady-state conditions gives information on the latter. However in the general case where several steps have rates of the same order this plotting is not sufficient to establish a fine description of the spatio-temporal imbrication of the elementary processes interacting at the electrode/electrolyte interface. However, whatever the point of view of the experimentalist, either fundamental for explaining the reaction mechanism and finding the characteristic parameters, or applied for optimizing the conditions of a reaction mechanism for economical purposes or devising a non-destructive material characterization, it is necessary to separate the various processes coupled together.

Even if a technique is used as a test for evaluating a complex process it is necessary to perform measurements on a system which can be considered of academic interest where the physico-chemical properties are well known in order to validate the technique. In this simpler case a model of the interface which takes into account the kinetics of chemical or electrochemical reactions and mass transport by means of some evolution equations which express mass and electrical charge balances can be proposed. However the derivation of the time response even to a small amplitude perturbing signal of a simple model is often inextricable. The expression of the frequency response is generally much simpler. From the experimental point of view by varying the frequency of analysis it is possible to separate the elementary phenomena which have different time constants. As the time constants are generally potential dependent, a potential change may lead to a better separation of the relaxation domains of the various processes and hence can lead to a better understanding of the overall process.

This second monograph about electrochemical impedance techniques is devoted to some practical aspects of the use and the applications of the frequency analysis of the electrochemical interfaces which have been developed since the issue of the first [1]. In the first part the performances of the frequency analysis are compared with the other established techniques. In the second part the two types of applications of the frequency analysis in electrochemistry are reviewed: derivation and comparison with experimental data of a model of simple systems of academic interest and evaluation and test of complex systems of practical interest.

It is of interest to note that some very useful books have been published in the field of electrochemistry since the publication of the first monograph and can be fruitfully consulted by the reader [2-4].

Chapter 1
Basic Electrochemical Techniques

1.1 Introduction

Electrochemical techniques can be used whenever a voltage controlled transfer of electrical charge occurs at the interface between an electrode and an electrolyte. The electrode and electrolyte form a "cell" in which physical/chemical reactions occur with varying degrees of complexity. In such cases the polarization of a cell with a dc potential induces a response in the form of an electric current. This is the basis of electrochemical techniques, where all the quantities which establish the state of the interface (temperature, pressure, area ...) are kept constant and the response of one of the electrical quantities (current or potential) is observed, while the other is perturbed. The electrical transfer provokes an oxidation, or a reduction, which obeys Faraday's law. Thus, the processes which lead to the charge transfer are called Faradaic processes.

The basic technique employed to study electrochemical phenomena is the plotting of the relationship between current and voltage (Fig. 1). This shows two different domains:

the cathodic current part due to the reduction of the solvent (generally water), or the reduction of a species in solution (e.g. metal deposition)

the anodic current part due either to the oxidation of the solvent or the oxidation of the electrode (e.g. metal dissolution), or the oxidation of a species in solution.

The anodic potentials are taken as positive. The anodic contribution of current is also generally taken as positive, but sometimes people who exclusively study cathodic processes may choose this contribution as positive. The potentials are measured and indicated versus a reference electrode e.g. saturated calomel electrode (SCE) or, when chloride ions have to be avoided, sulphate saturated electrode (SSE, where V/SCE = V/SSE + 0.44V). Given that the reference electrode has a constant composition, because no current flows through it, its potential is fixed and known. Hence any modification in the polarization of the cell is due to the voltage between the material being studied (working electrode) and the electrolyte. The working electrode is an anode if oxidation takes place and a cathode if reduction takes place. The current-voltage curve generally reveals a striking non-linear behaviour.

The interpretation of the rate of an electrochemical reaction which involves both electrons and chemical species is more difficult than for an homogeneous chemical reaction, because it is an heterogeneous process which only occurs at the interface between the electrode and the electrolyte. Information can be obtained by measuring the current versus the potential. When a steady-state is reached, after some transient phenomena, the magnitude of the current is often limited by the rate of one or several processes which are called kinetically determining steps. If several processes are determining steps the value of the steady-state current cannot give valuable experimental data as the data connected with these processes are inextricably entangled and it will be seen that only non steady-state techniques can be efficient.

In addition to these Faradaic processes, non-Faradaic processes have to be taken into account when electrochemical behaviour has to be interpreted. The double layer capacitance, due to a charge accumulation in the vicinity of the electrode only has to be taken into account-when non steady-state techniques are used. The electrolyte resistance, due to the finiteness of the electrolyte conductance, can obscure all the investigation techniques of the interface, especially for electrolytes of low conductivity, or for fast Faradaic processes.

As an example for a disc electrode of diameter d immersed in an electrolyte of conductivity γ the electrolyte resistance is equal to:

$$R_e = \frac{1}{2\gamma d}$$

The first step in testing electrochemical processes is based on the study of the steady- state regime. The second and major step is based on the study of the non steady-state behaviour.

1.2 Steady-state techniques

In order to study an electrochemical system by investigating the current-voltage relationship, it is necessary to control one of the variables (current or voltage). It is important to select the appropriate variable to be controlled, this being dependent on the current-voltage characteristics of the cell and the mechanism of the reaction, as well as the information required from the investigation.

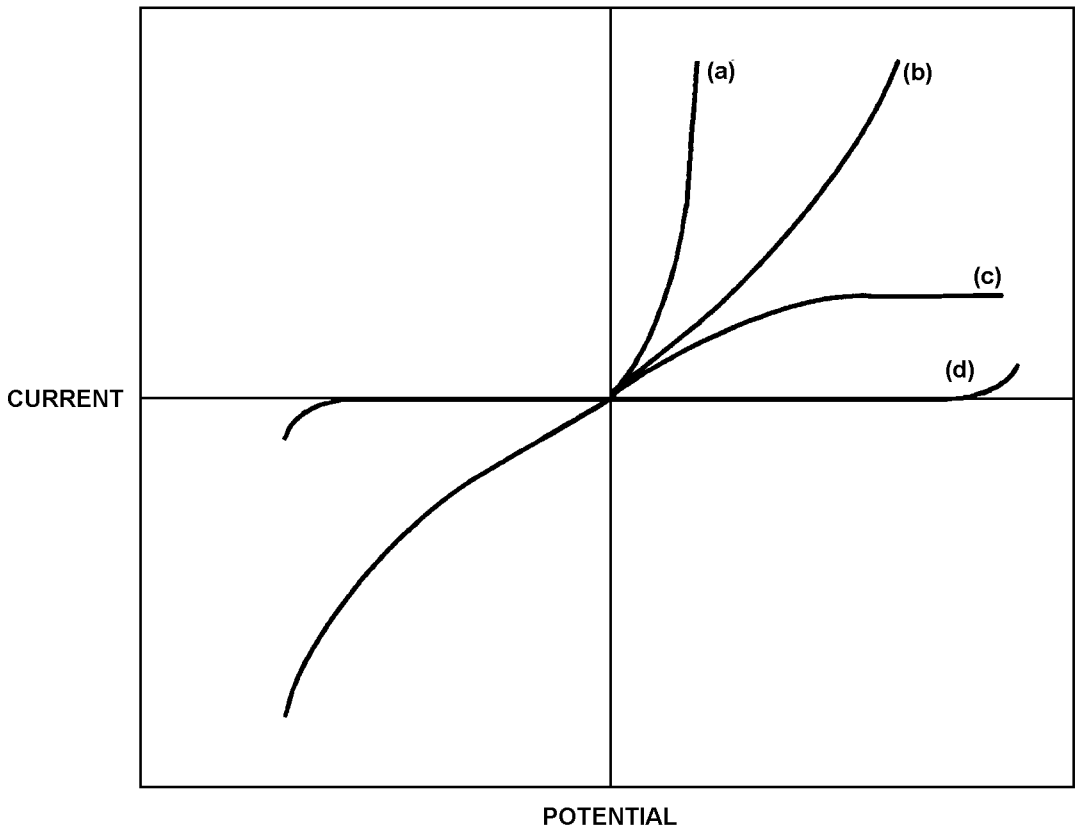

Fig.1 Current-voltage curves of different shapes.

For example, curve (a) in Fig. 1, which shows a steep increase in current for a relatively small increase in voltage, can be investigated with galvanostatic (current) control. Potentiostatic (voltage) control is better, however, in curves (b), (c) and (d). Curve (b) shows a slow increase in current for increasing voltage, while curve (c) shows a current plateau, caused by

a limitation in the mass transport of the reacting species. In curve (d), no transfer of charge occurs at the electrode, within the potential range investigated. Other reactions [1] give rise to S-shaped current-voltage relationships (which require galvanostatic control), or N-shaped curves (potentiostatic control).

In other cases the type of control is imposed by the system under study itself. For example, the study of corrosion potential needs galvanostatic control (I = 0). Control of the relevant parameter can be imposed by the use of a potentiostat/galvanostat, such as the Solartron 1286 Electrochemical Interface, as illustrated in Fig. 3. It can be seen that the control configurations are similar, although in the case of the galvanostatic mode the reference electrode connections (RE1 and RE2) are only necessary for measuring the cell potentials.

It has to be noted that the time needed by the electrochemical system to achieve a

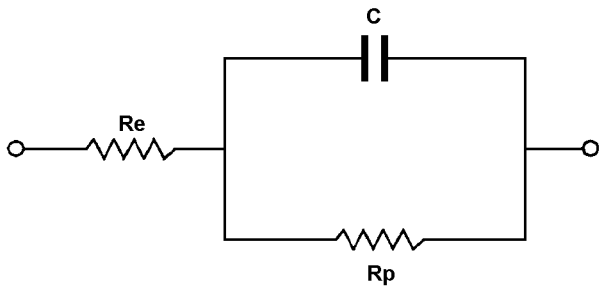

Fig. 2 Equivalent circuit of an electrochemical cell.
R_e: electrolyte resistance,
R_p. polarization resistance,
C : double layer capacitance.

steady-state is not the same in voltage and current control modes. If the interface is supposed equivalent to the circuit shown in Fig. 2, the current response, I(t), to a voltage step, ΔE, is [2]:

$$I(t) = \frac{\Delta E}{R_e(R_e + R_p)}\left[R_e + R_p\, exp\left(-t / \frac{CR_eR_p}{R_e + R_p}\right)\right]$$

If $R_e << R_p$ the time constant needed to achieve a steady-state in potentiostatic mode is: '

$\tau_p = CR_e$

The voltage response, E(t), to a current step, AI, is:

$$E(t) = \Delta I.R_e + \Delta I.R_p\left[1 - exp\left(-t / CR_p\right)\right]$$

and the time constant in galvanostatic mode is:

$\tau_g = CR_p$

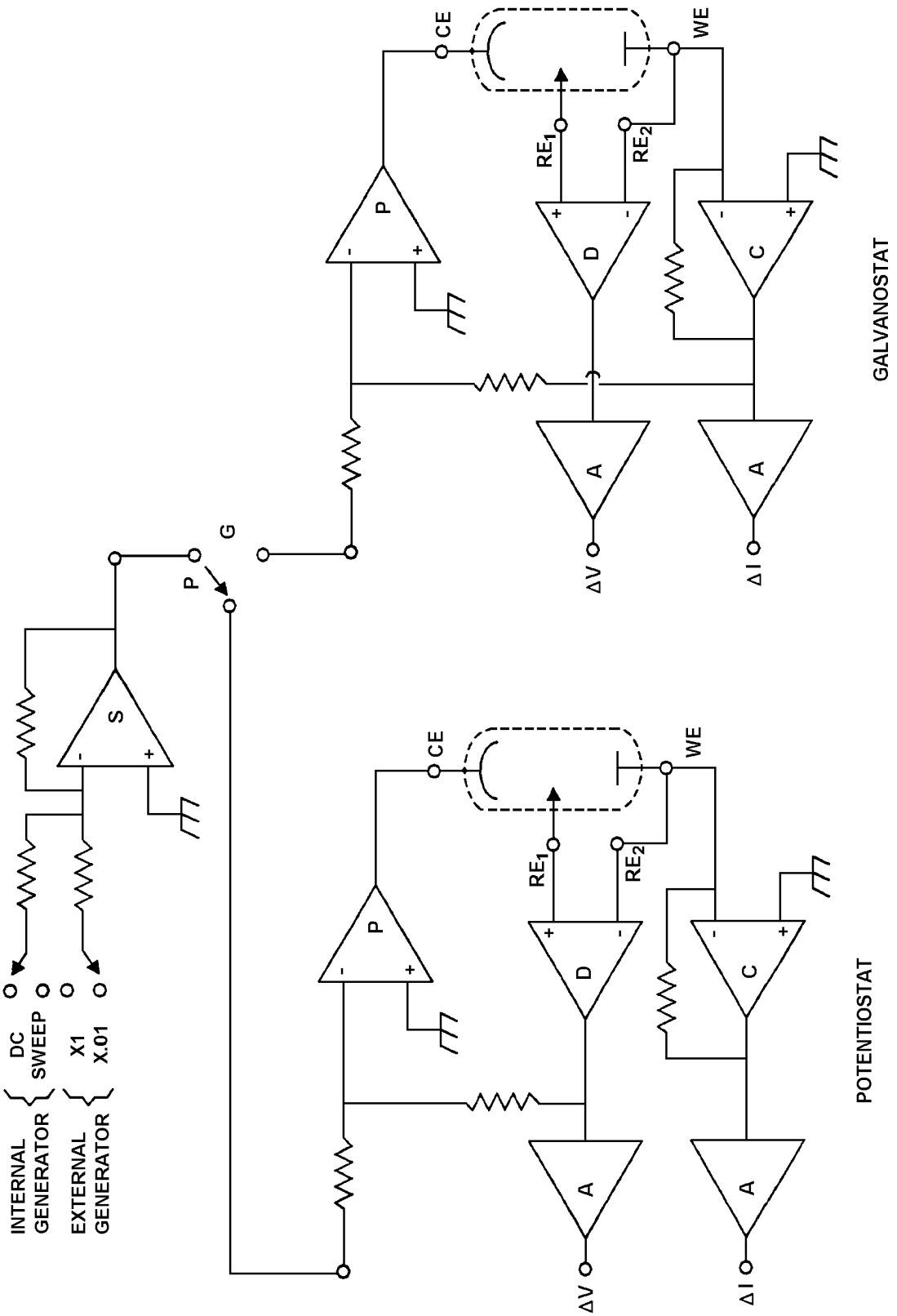
INTERNAL GENERATOR
DC SWEEP
EXTERNAL GENERATOR
X1
X.01
S
P
G
CE
WE
RE1
RE2
P
D
C
A
ΔV
ΔI
GALVANOSTAT
POTENTIOSTAT

Hence, for systems with high R_p value (e.g. metals with very low corrosion rates), hours may be required to achieve the steady-state. Therefore, in cases where R_p is very high the advantage of using potentiostatic instead of galvanostatic measurements becomes clear.

The I-V curves can be plotted either by imposing discrete and successive values of the controlled quantity (current or potential), or by imposing a voltage ramp sufficiently slow to obtain the steady-state curve (potentiodynamic plotting). In themselves, the form of these curves can bring some information to the electrochemist. The shape shows passivation of a metal in an aggressive medium if the current decreases when the potential increases. On the other hand, if the current becomes independent of potential then a limitation of the overall rate by mass transfer, or diffusion control, is indicated. Data analysis can also afford some attractive parameters. As an example, the plotting of log current vs potential can lead to the exchange current or the corrosion current (Tafel plot) by an extrapolation procedure (Fig. 4(a)).

The slope of the I-V curve (R_p^{-1} at zero current) leads to the corrosion current where b_a and b_c are Tafel coefficients:

$$I_{corr} = \frac{1}{R_p(b_a + b_c)}$$ (Stern-Geary method) (Fig. 4(b)).

However, in order to interpret current-voltage curves it is necessary to assume that the anodic and cathodic processes (e.g. dissolution of a metal and hydrogen evolution for a corrosion process) follow exponential laws, such as the Tafel law in corrosion:

$$I_a = I_{corr}\ exp\, b_a(E - E_{corr})$$

$$I_c = I_{corr}\ exp - b_c(E - E_{corr})$$

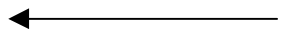

Fig. 3 Schematic of the cell polarization arrangement of the Solartron 1286 Electrochemical Interface in three terminal cell configuration.

S: summing amplifier;

P: control amplifier;

D: differential amplifier used for measuring the voltage across the interface;

C: current follower used for measuring the current flowing through the interface,

A : amplifier and filter of the current and voltage measurement channels.

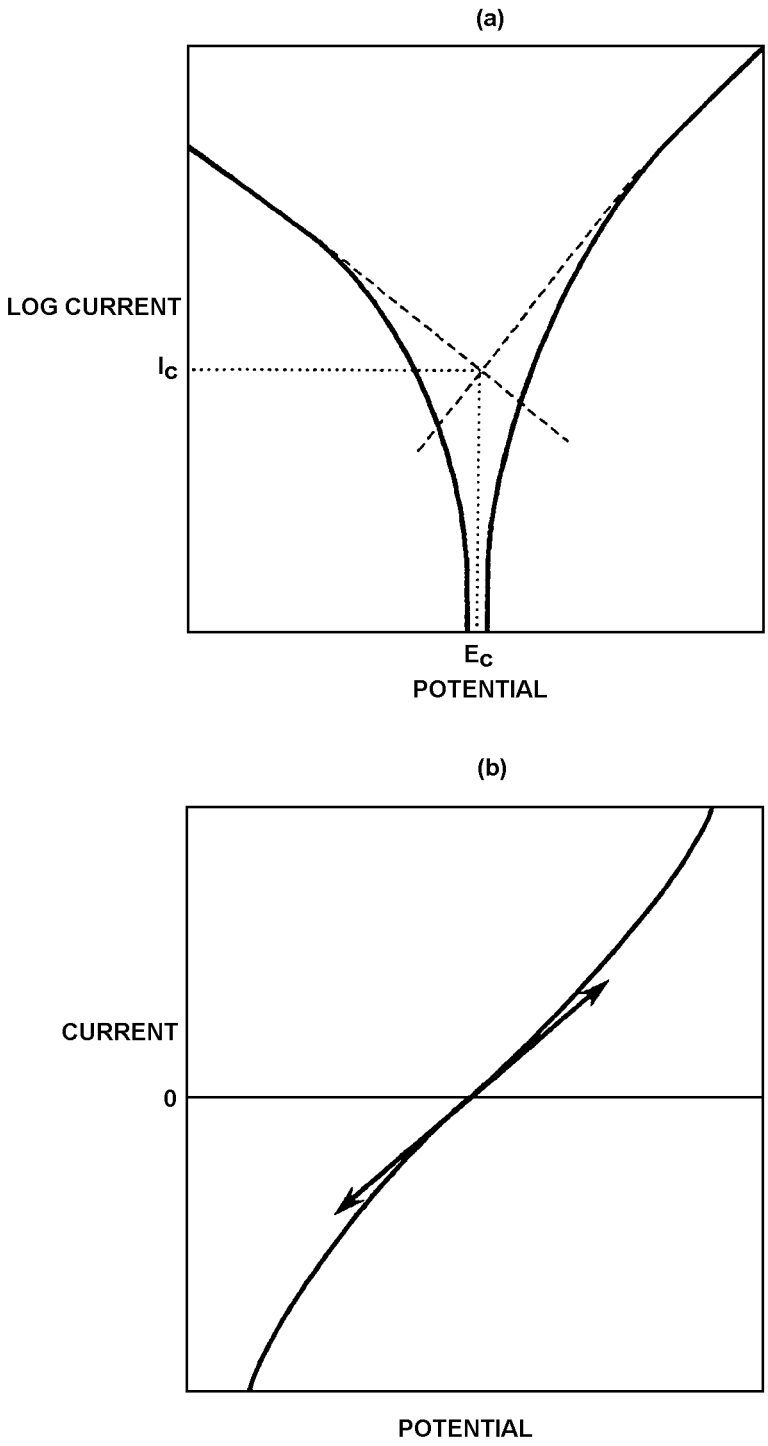

Fig 4 Examples of dc techniques:

(a) Measurement of corrosion current from the Tafel plot.

(b) Measurement of the polarisation resistance from the slope of the I-V curve.

In practice it is not easy to find a linear region in the log I-V plot and the determination of corrosion current needs the values of b_a and b_c, which necessitates the use of the Tafel plot. The limitations of steady-state techniques have been developed at length in the literature, especially in the case of corrosion [5]. The authors quoted the following occurrences which give rise to errors in the measurement of corrosion intensity by steady-state techniques:

- Tafel slopes are unknown, or vary with time
- lack of linearity of the polarization curve in the vicinity of the corrosion potential
- very high resistivity, due to the electrolyte itself, or the corrosion product layers
- variation of corrosion potential during the measurement
- pitting or localized corrosion
- the corrosion reaction is controlled by diffusion, or the metal is passivated
- equilibrium potentials of anodic and cathodic semi-reactions are very close to the corrosion potential
- the system being polarized requires a given time to achieve a steady-state
- perturbations in the working electrode - electrolyte interface during measurement.

These drawbacks of steady-state techniques can often be overcome by the use of non steady-state techniques.

1.3 Non steady-state techniques

Due to the strong limitations of steady-state techniques, numerous non steady-state methods have been proposed. They pertain either to large amplitude signal analysis, or to small amplitude signal analysis. The latter generally assumes a linear regime about a given polarization point and can be resolved either in the time or the frequency domains (Fig. 5).

These relaxation methods are based on the application of a transient (e.g. step) or continuous (e.g. sine wave) perturbation to an equilibrium or out-of-equilibrium steady-state and the subsequent analysis of the relaxation of the electrochemical system to a new steady-state. As the various elementary processes relax at different rates, the response has to be adequately analyzed in order to separate the various mechanisms involved in the overall response. However, as each process relaxes exponentially with time, the various elementary responses overlap between the origin of the perturbation and infinite time. This usually leads to a very complicated overall response, unless only one process is a determining step. In such a case this process imposes its own relaxation, with its own time-constant.

Among all these techniques, those which use small amplitude signals (a few mV peak-to-peak) superimposed on the dc potential of the interface have numerous advantages. The response is then a linear function of the applied perturbation and can be entirely described by the impedance of the electrochemical system. In these conditions, all the different types of perturbing signal (sine wave, white noise, step, etc.) give the same quantity (the impedance) and therefore lead to the same information.

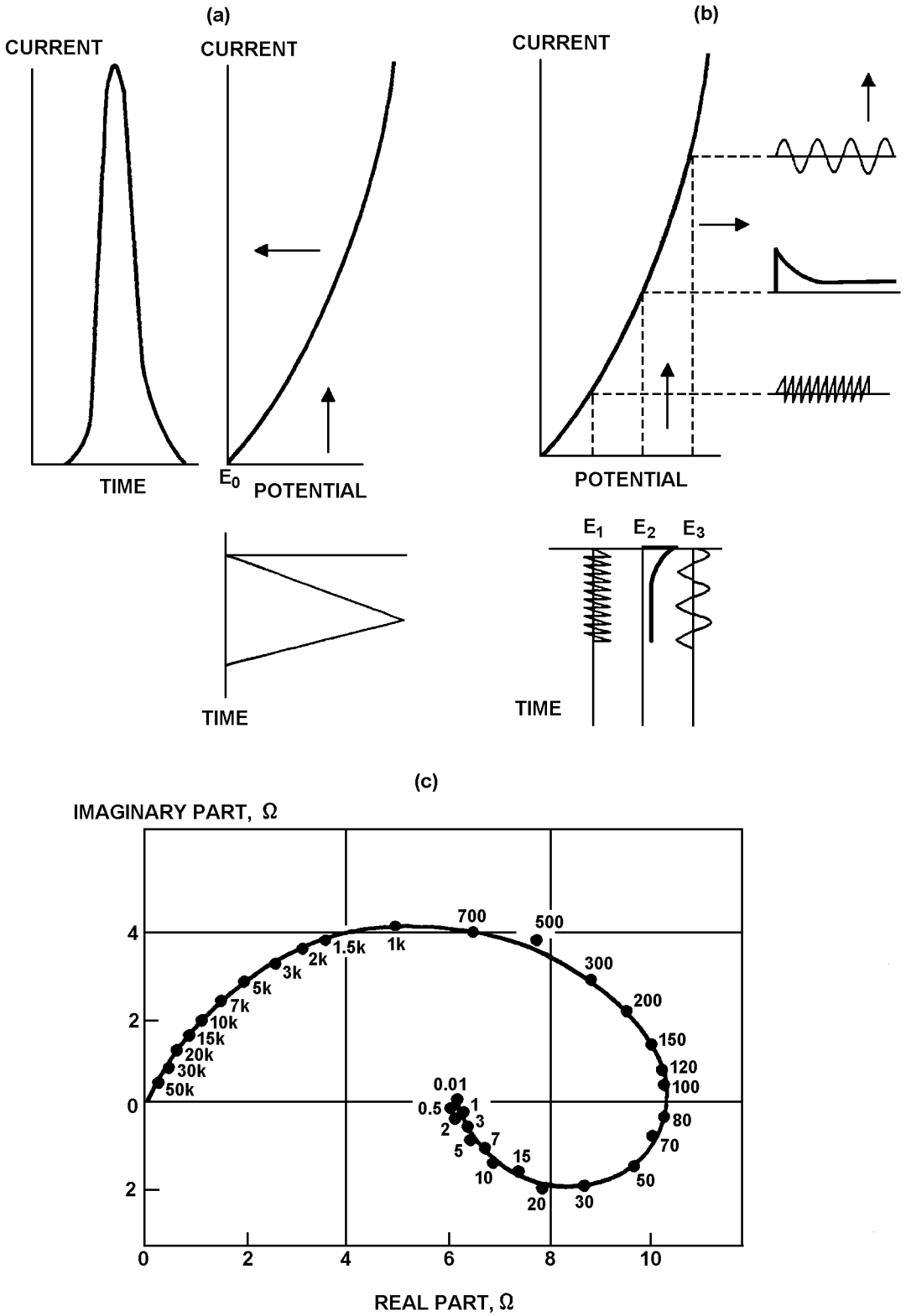

Fig 5 Principle of large signal analysis using (a) sweeping potential and (b) small signal analysis using a sine wave, step or white noise. The latter leads to an impedance (c).

As a linearized behaviour about the polarization point is assumed, a frequency analysis of the response usually yields an easy separation of the relaxation domain of the elementary steps of an overall mechanism whatever the applied perturbation. Since these small signal techniques can be used in a noisy environment and the electrochemical systems are generally not stationary over long times the choice of a particular technique (step, white noise, sine wave) is only based on consideration of signal processing and measurement efficiency. These constraints lead to a trade-off between the accuracy and the measurement time, as will be seen later. It is noticeable that this problem would not arise if electrochemical systems were truly linear systems, as any amplitude of the perturbing signals would be admissible and hence the error could be reduced at will.

Numerous experiments have shown that, for analysing the relaxation times of various electrochemical processes, the impedance has to be measured in a very large frequency range, which often spreads between 10^{-3}Hz to 10^{5}Hz (i.e. in the time domain, an analysis has to be carried out between 10μs and 1000s). The impedance can then be plotted as a parametric function of frequency in the complex plane (Fig. 5(c)). As the interface is a non-linear system the impedance is potential dependent.

In general impedances can be represented by an equivalent circuit, which can be schematized as in Fig. 2. The high frequency limit gives the electrolyte resistance. In general this term can be minimized by using a Haber-Luggin capillary as the reference but this technique has to be used with care for impedance measurements, as the capillary introduces parasitic terms. The low frequency limit gives the polarization resistance, which is equal to the inverse of the slope of the current-voltage curve.

Between these extreme values, in the higher frequency range, is found a capacitive loop which is generally due to the double layer capacity in parallel with the transfer resistance. Lower frequency loops are related to the Faradaic impedance, due to relaxation of the Faradaic processes.

Chapter 2
Performance of Non Steady-State techniques

2.1 Introduction

Comparison of the efficiencies of large signal analysis and small signal analysis for investigating the behaviour of an electrochemical system is not, in general, very easy. In fact, the theory of measurement based on large amplitude perturbing signals should take into account non-linear analysis, which is quite complicated. On the contrary, the theory of measurement based on small amplitude perturbing signals is founded on the well-known linear system theory. Hence this comparison has been carried out only on particular examples for large amplitude signals. For this reason a definition of comparative criteria has yet to be fully established.

Concerning a comparison between the various small signal techniques, the target is more easily attainable, although comparisons between the time domain techniques and frequency domain techniques is not straightforward. A comparison between frequency domain methods according to type of input perturbation and signal processing has, however, been extensively investigated in terms of a trade-off between measurement time and accuracy. This compromise has been estimated in the case of experiments carried out using step, sine wave and white noise for measurements characterized by the same level of perturbation (defined to maintain a linear response of the electrochemical system).

Non steady-state techniques are, therefore, reviewed in order to emphasize the benefit of the techniques, and their advantages and limitations compared with impedance methods.

2.2 Large Amplitude Signal Analysis

Many input signals have been proposed in the literature. In this paper, however, only the two most commonly used (ramp and sine wave) are discussed. These lead respectively to linear sweep voltammetry and higher harmonic analysis.

2.2.1 Linear Sweep Voltammetry

For linear sweep voltammetry, the simultaneous electrochemical adsorption of two electroactive species A_1 and A_2 [6] on two kinds of surface sites S_1 and S_2 of surface coverage θ_1 and θ_2 is considered, as an example:

$$\underset{(1-q_1)}{A_1 + S_1} + e^- \underset{K_1}{\overset{K_1}{\rightleftharpoons}} \underset{q_1}{S_1 A_1}$$

$$\underset{(1-q_2)}{A_2 + S_2} + e^- \underset{K_2}{\overset{K_2}{\rightleftharpoons}} \underset{q_2}{S_2 A_2}$$

where:

$$K_i = K_i^{\circ} \exp b_i E$$

$$\overline{K}_i = \overline{K}_i^{\circ} \exp \overline{b}_i E$$

The equations of the system are:

$$\frac{dq_1}{dt} = -K_1 q_1 + \overline{K}_1 (1 - q_1)$$

$$\frac{dq_2}{dt} = -K_2 q_2 + \overline{K}_2 (1 - q_2)$$

$$i_F = F\left(\frac{dq_1}{dt} + \frac{dq_2}{dt}\right)$$

$$i_F = Fv\left(\frac{dq_1}{dE} + \frac{dq_2}{dE}\right)$$

where v is the potential scan rate.

Linear potential scan voltammetry characteristics have been computed for this example in [6] depicted in Fig. 6(a) (where the reduced potential is given by $\psi = 39(E\text{-}E^\circ)$ in function of the potential E in volts). For the same process, after linearization of the equation set and then Fourier transforming, the impedance has been calculated in [7] for the same conditions as in [6]. The Faradaic impedance:

$$Z_F = \frac{1}{jwFA} \frac{1}{\frac{B_1}{jw + A_1} + \frac{B_2}{jw + A_2}}$$

where:

$$B_i = \frac{K_i \overline{K_i}}{K_i + \overline{K_i}} \left(b_i - \overline{b_i}\right) \quad \text{and} \quad A_i = K_i + \overline{K_i}$$

is plotted in Fig. 6(b) for various potentials. It has to be noticed that the formal values of the parameters chosen in [6] lead to unrealistic low frequency behaviour of the impedance. The variation of various parameters of interest versus the potential (Fig. 6(c)) also gives information about the processes. As examples, the graphical integration of the change of the low frequency capacity versus the potential gives 2F (where F is the Faraday) which indicates the total number of the electrons exchanged (n = 2). The peaks in the capacity change give the equilibrium potentials (E_i°) of the two elementary reactions. Hence the sweep voltammetry is useful for a rapid qualitative analysis but a further quantitative analysis of the processes is necessarily achieved by means of an impedance analysis.

→

Fig 6. Voltammogram (a) and impedance (b) calculated for an irreversible co-absorption of two electroactive cations:

(a) Dimensionless linear potential scan voltammetry

$$X = iRT / n^2 F^2 A \Gamma_{max} n; \; j = nF(E - E^\circ) / RT \; (\text{from [6]})$$

(b) Impedances calculated at various polarization points marked on the voltammogram:

(1) 0v (2) -0.15V (3) -0.2v

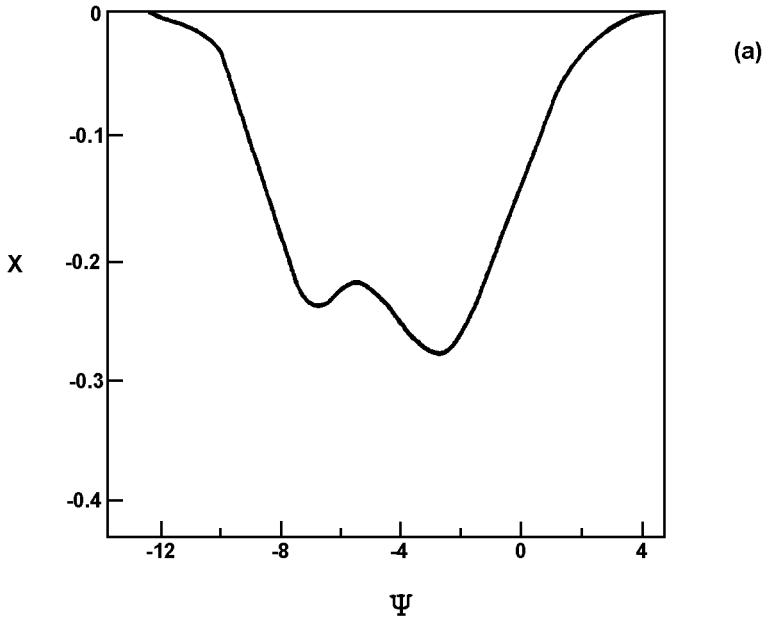
(a)
0
-0.1
-0.2
-0.3
-0.4
X
-12
-8
-4
0
4
Ψ

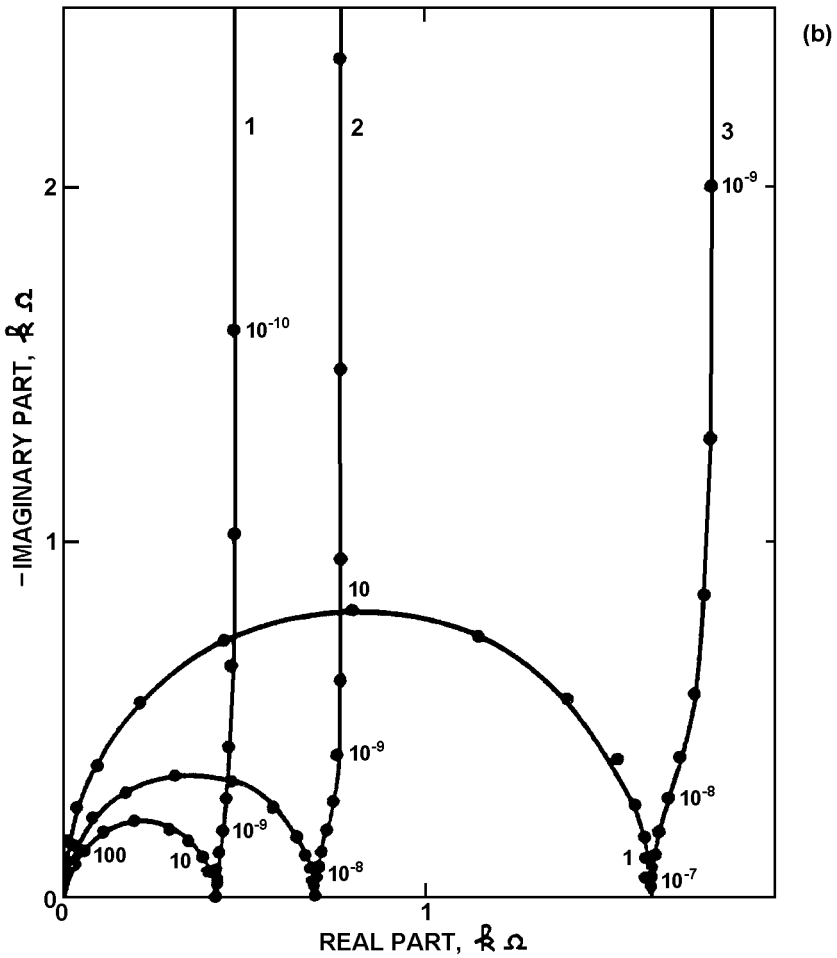
(b)
1
2
3
10^-9
10^-10
10
10^-9
10^-8
100
10
10^-9
10^-8
1
10^-7
2
1
0
0
1
– IMAGINARY PART, ℜ Ω
REAL PART, ℜ Ω

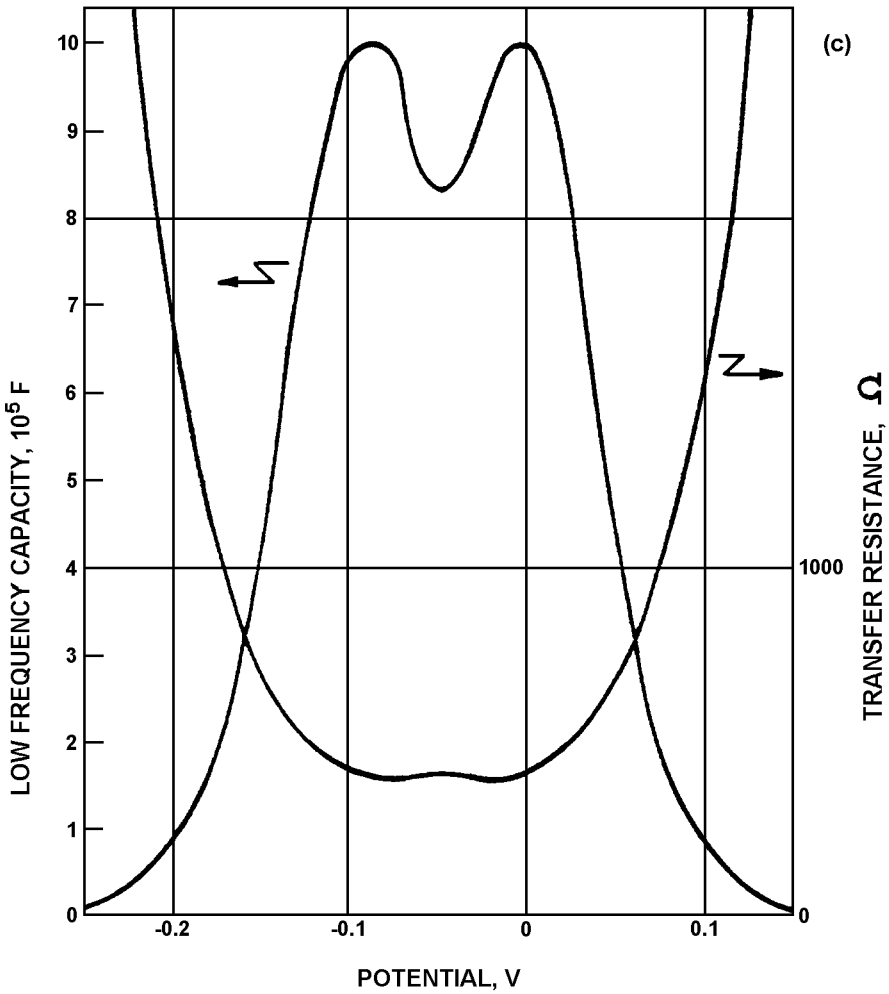

Fig 6c Variation of the low frequency capacity and of the transfer resistance versus the potential

2.2.2 Higher Harmonic Analysis

For a non-linear, large amplitude, sine wave response the calculation for the simple anodic and cathodic Tafel process is:

$$i = i_{corr}\left[exp\frac{\Delta E}{ba} - exp\frac{-\Delta E}{bc}\right]$$

If a large amplitude sine wave, $U_o \sin \omega t$, is imposed about the polarization potential E_o then $E_o + U_o \sin \omega t$ can be substituted for ΔE in this equation.

The current i can be expanded in a Fourier series approximated to the third order as:

$$i = i_{dc} + i_1 \sin wt + i_2 \cos 2wt + i_3 \sin 3wt$$

It can be shown that the measurement of the amplitude of the dc (Faradaic rectification), first, second and third harmonics, i_{dc}, i_1, i_2, i_3 respectively allows the corrosion current and the Tafel coefficients to be evaluated [8]:

$$i_{corr} = \frac{{i_1}^2}{\sqrt{48}\sqrt{2i_1 i_3 - {i_2}^2}}$$

$$\frac{1}{ba} = \frac{1}{2U_o}\left(\frac{i_1}{i_{corr}} + 4\frac{i_2}{i_1}\right)$$

$$\frac{1}{bc} = \frac{1}{2U_o}\left(\frac{i_1}{i_{corr}} - 4\frac{i_2}{i_1}\right)$$

It can be demonstrated that the measured second harmonic goes to zero at the point of inflection of the polarization curve as shown from the third term of the expression of the current. For this particular potential the Faradaic rectification current i_{dc}, is related to the corrosion current by (see Fig. 7):

$$i_{corr} = 0.6 i_{dc}$$

These two examples of large amplitude signals techniques take into account an irreversible charge transfer with Tafel laws for the anodic and cathodic reactions. However the mathematical derivation is already quite difficult. Other applications have been carried out in linear sweep voltammetry or ac polarography concerning various couplings of electrochemical reactions (E) homogeneous chemical reactions (C) and diffusion. Hence E, CE, EC, CEC, ECE, etc. mechanisms have been tested. However the reactive species are supposed to be transported in an infinite diffusion layer and the charge transfer is often supposed to be as infinitely fast. These hypotheses considerably simplify the derivation although a computer is nevertheless required. It can be concluded that it is necessary to assume very simplified approximations of the real world in order to use the non-linear techniques.

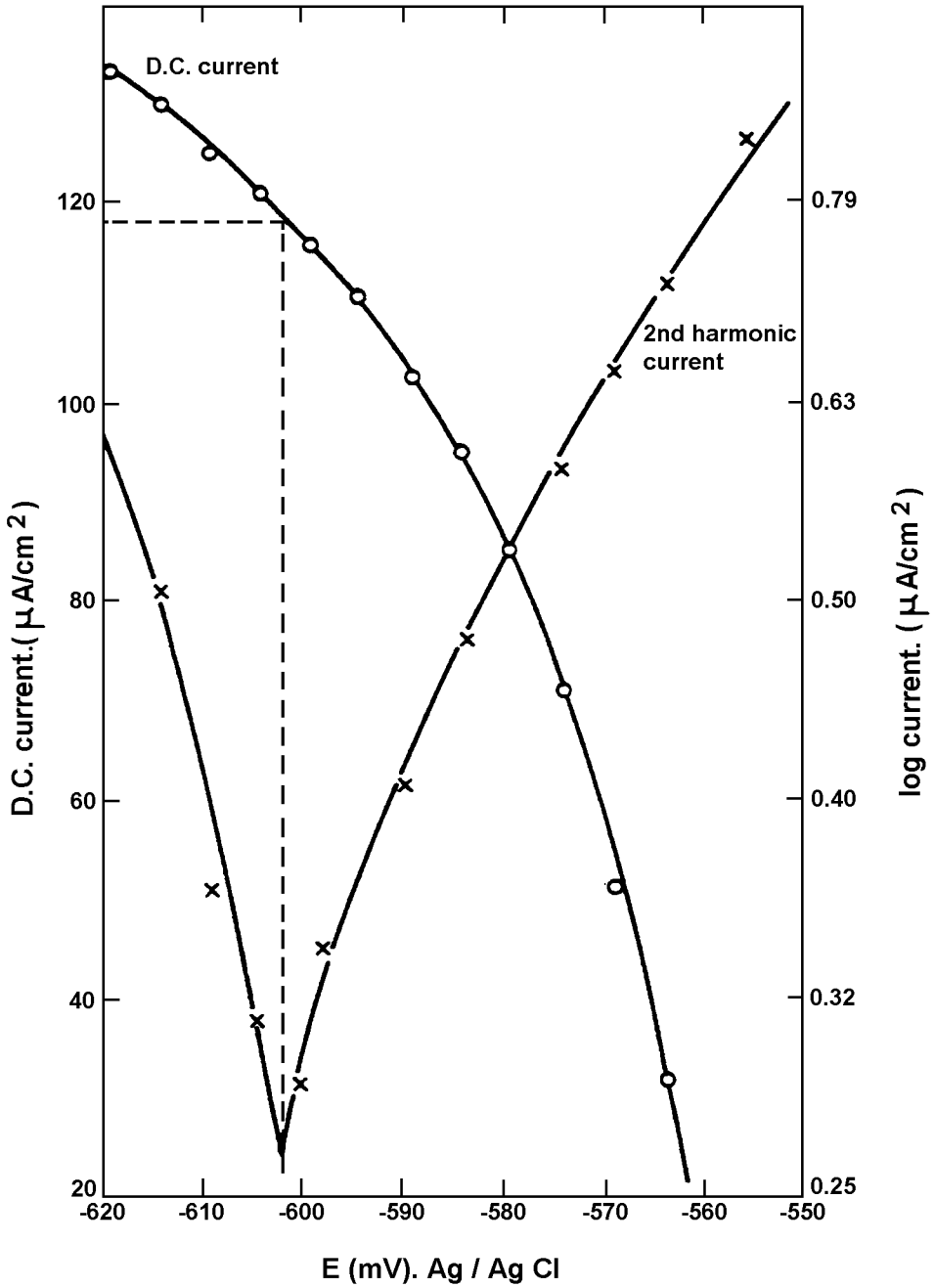

Fig 7 Variation of the second harmonic current and dc rectification current. The measurements have been performed by using a 10mV amplitude perturbation at 148mHz on 34cm^2 cold rolled 1.2mm mild steel test panels immersed 24 hours in 3% aerated Analar NaCl solution (from [8]).

2.3 Small Amplitude Signal Analysis

Linear relaxation techniques are based on the use of a perturbing signal having an amplitude sufficiently low that the processes can be linearized about a dc polarization point. From signal theory it is known that the information involved in the response of any input is the same, whatever the shape of the perturbing signal (step, ramp, sine wave, random noise, etc.). Although it has not yet been demonstrated in the general case, it seems that, except for a few cases, (non-linear systems involving delays, hysteresis, etc.) the information extracted by a linear analysis at a sufficient number of polarization points along the I-V curve is the same as the information extracted from a non-linear analysis.

The linear response of a system to a small amplitude perturbing signal can be utilised either in the time domain, or in the frequency domain.

2.3.1 Time Domain Resolution

The main perturbations used in this method are step and ramp signals. Various single, double, or more, current and potential steps techniques have been devised, essentially in order to study diffusion controlled electron transfer.

The measurement of polarization resistance, which is a typical application of step and ramp techniques will be examined. It is assumed that the equivalent circuit of the electrochemical interface is similar to that depicted in Fig. 2. As has been seen already, the current response to a voltage step ΔE, under potentiostatic control, reaches its steady-state with a time constant:

$$\tau = R_e C_d$$

if $R_e << R_p$

After a time $T = 5\tau$ the difference between the transient current and the final steady-state value, ΔI, is less than 1%. Hence, for a perfect, non-noisy step signal the polarization resistance can be estimated from:

$$R_p = \frac{\Delta E}{\Delta I}$$

Using a voltage ramp ($E = E_o + kt$) as the perturbing signal (potentiodynamic technique) the current response is [9]:

$$I(t) = \frac{kt}{R_e + R_p} + \frac{kCR_p^{\,2}}{(R_e + R_p)^2}\left[1 - exp\left(-t / \frac{CR_eR_p}{R_e + R_p}\right)\right]$$

where k is the voltage sweep rate.

Representing this expression in an I-V diagram, a deformed parallelogram is obtained (Fig. 8).

Hence for $t \to \infty$

$$\frac{dI}{dE} = \frac{dI/dt}{dE/dt} = \frac{1}{R_e + R_p}$$

For very low sweep rates, the quasi-horizontal sides of the parallelogram become straight lines of slope:

$$\frac{1}{R_e + R_p}$$

However, when the sweep rate is increased, an apparent R_p value between R_e and R_e+R_p may be obtained. An example is shown in Fig. 9, which shows that a maximum sweep rate is necessary in order not to under-evaluate R_p [5].

From this diagram a value of k = 10mV/min is the maximum for response A in order not to obtain an under-estimated value of R_p. This study also gives the maximum scan rate admissible for the potentiodynamic plotting of a current-voltage curve considered as being in steady-state condition. Hence the minimum measurement time necessary to measure the full parallelogram, with ΔE = 10mV and without under-estimation of R_p is:

$$2\frac{\Delta E}{k} = 120s$$

By the step technique, $R_e.C = 5 \times 9.8 \times 10^3 \times 1.2\ 10^{-3}$ = 60s is required.

The measurement time necessary to obtain R_p by time domain analysis will now be compared with frequency domain analysis.

From this example, and others in the literature, it can be concluded that a time domain analysis of the response to small amplitude signals can be useful to obtain the parameters of a known model in the case of a simple system. However, the extraction of the parameters is very complicated, not to say impossible, if a simple model (or equivalent circuit) is not assumed. In the case of a complicated model or for testing a model (non-parametric identification) it will be seen below that frequency domain analysis is superior.

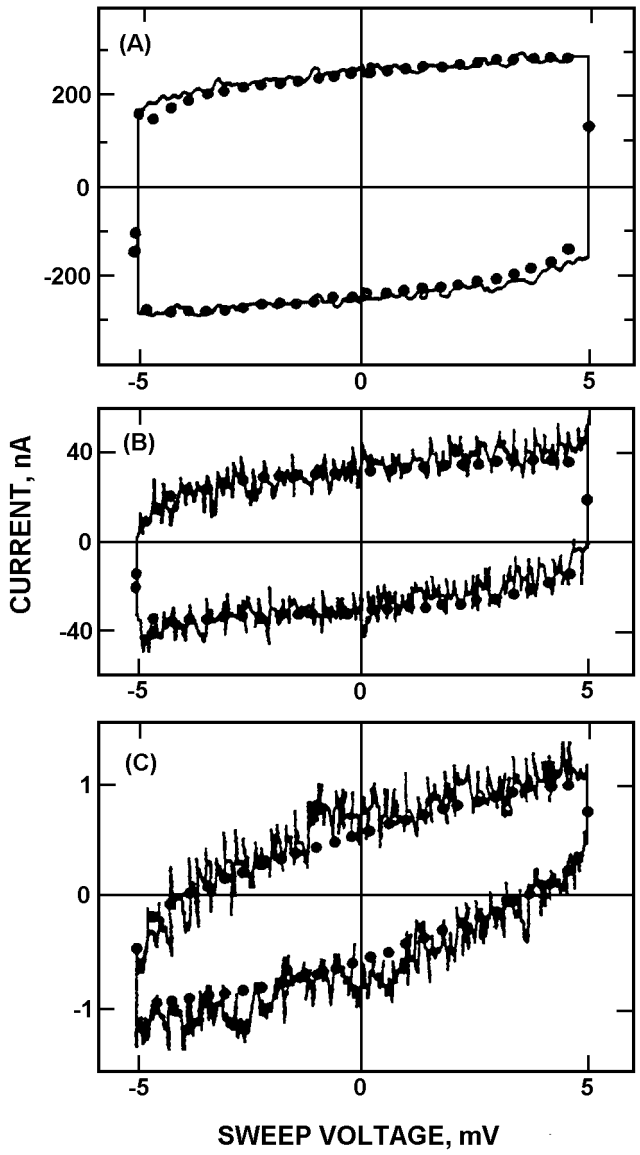

Fig. 8 Experimentally determined current-voltage cycle under a triangular voltage sweep. Steal Z2 CNDU 17-16. Electrode surface area: 4.2cm^2; air bubbled, 10vol% H_2S0_4 at room temperature.

Dots indicate calculated values from a theoretical derivation using the results of impedance measurements; period of triangular sweep: (a) 10s; (b) 100s; (c) 1000s (from [9]).

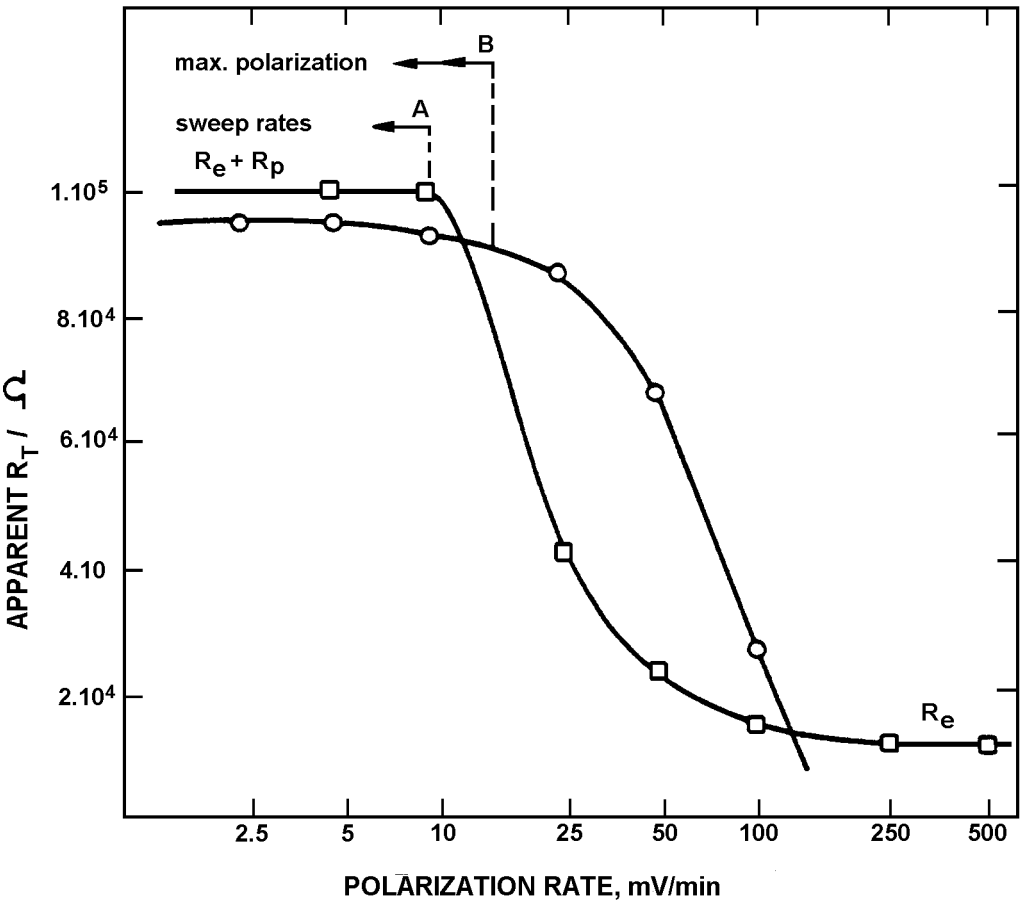

Fig. 9 The variation of the apparent R_p values of two electrical circuits A and B as a function of the polarization sweep rate:

A R_e =9.80kΩ; C = 1.2mF; R_p = 86kΩ

B R_e = 1kΩ; C ~ 1.3mF; R_p = 86kΩ (from [5]).

2.3.2 Frequency Domain Resolution

As we are mainly concerned with frequency response analysis of electrochemical systems, the instrumentation will be first summarized. In order to make a frequency analysis over a very large frequency range (eg. 10^{-3} to 10^{5}Hz) only two types of measurement arrangements can be used which depend on the type of perturbing signals under examination. Either a single sine wave is used and a frequency response analyzer (FRA) is employed, or a broadband perturbing signal (eg. step, white noise,...) is used and a computer which performs a frequency transform (often a Fast Fourier Transform algorithm) is employed (Fig. 10). On Fig. 11 a general arrangement which can involve a potentiostat / galvanostat 1286 and a FRA 1250 (or 1255, 1260) from Solartron is shown.

Other types of devices such as lock-in amplifiers and ac bridges cannot be so widely used as, in spite of their very good accuracy, they do not have a wide frequency range, in particular they are not able to perform measurements in the very low frequency range (lower than 1Hz), and they are not usually programmable.

The time varying systems which often characterize processes of practical interest (high current dissolution, battery discharges, ...) can restrict impedance measurements which have to be carried out in a steady-state regime. In this case it is tempting to decrease the time necessary for performing the measurement by using either frequency sweeping techniques for harmonic analysis or broadband signal stimulation for spectral analysis. However, the increase in speed can prejudice the accuracy of the results.

This problem will be illustrated with some examples where the advantages and pitfalls of the technique will be shown. First of all the measurement of the polarization resistance by optimizing impedance technique and an error arising from too high a sweep rate of the excitation will be quickly reviewed. Then a comparison between single sine approach and frequency transform of a broadband signal will be reported. This will be preceded by a short comparison between Laplace and Fourier transforms of a step signal which will illustrate the performances of the time to frequency transform techniques.

2.4 Impedance Techniques

Several techniques, in particular step and ramp electrochemical time responses, can lead to some attractive parameters useful for tests of practical applicability with good performances in terms of rapidity and/or accuracy. However as the choice of these parameters is not imposed by the complete knowledge of the processes involved, i.e. a model, their validity has to be proved by a preliminary investigation which compares the practical application to the parameter measurement. On the other hand, techniques involving impedance measurements, i.e. ac signal perturbation having a small amplitude, are the most powerful techniques especially when a fundamental investigation is carried out, e.g. the search for a model.

2.4.1 Measurement of the Polarization Resistance

Concerning the impedance technique, if the form of the equivalent RC circuit is known a priori (Fig. 2) it is not necessary to perform the measurement on the whole frequency range. Only a measurement at a high frequency (e.g. about 50kHz) to determine R_e and at a low frequency to determine R_p is necessary. In galvanostatic mode the impedance is directly measured and in order to obtain an accurate value for R_p it is necessary to go down to a frequency $(200\Pi.R_pC_d)^{-1}$ which is equivalent to 100 times the impedance time constant (R_pC_d).

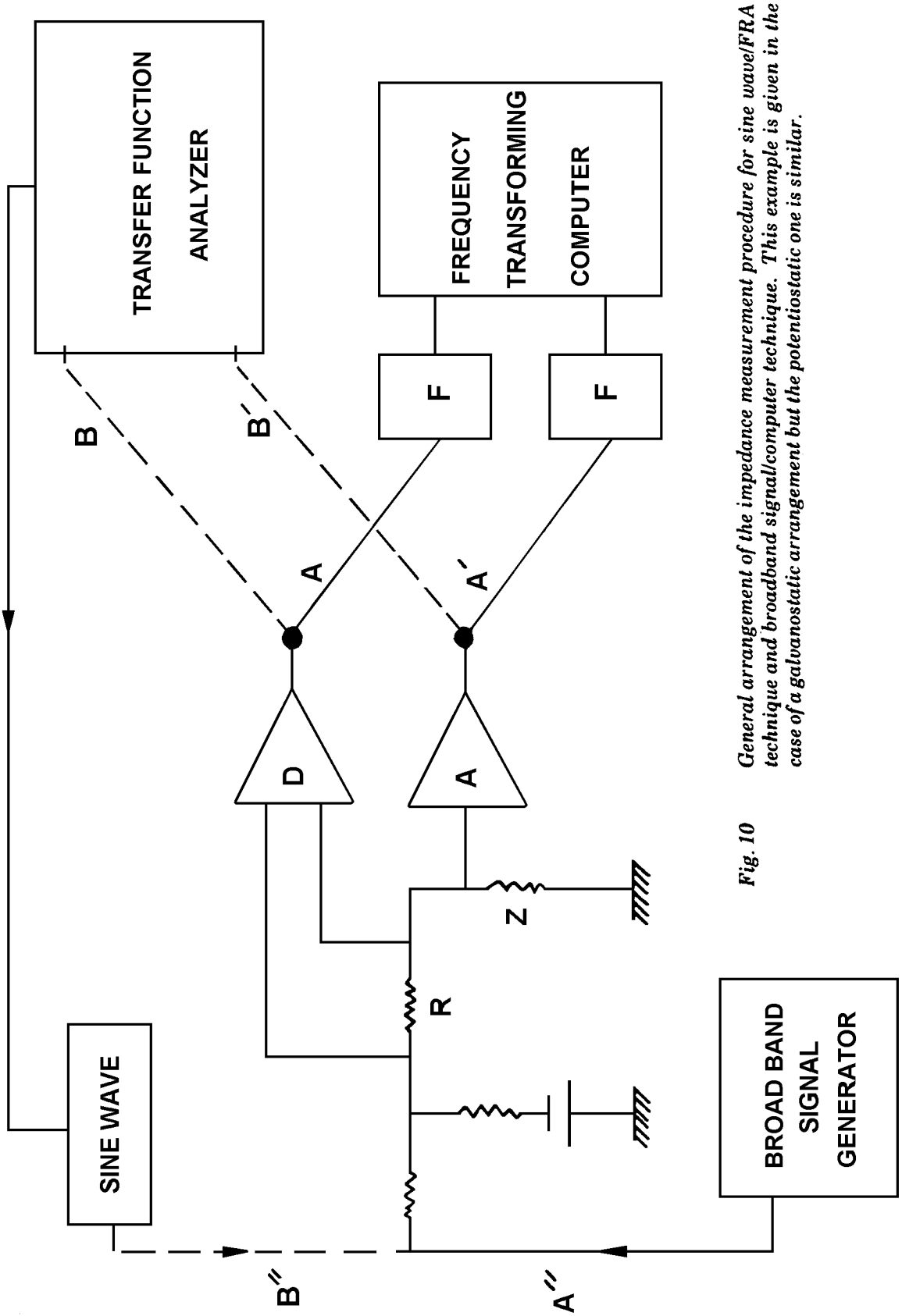

Fig. 10 *General arrangement of the impedance measurement procedure for sine wave/FRA technique and broadband signal/computer technique. This example is given in the case of a galvanostatic arrangement but the potentiostatic one is similar.*

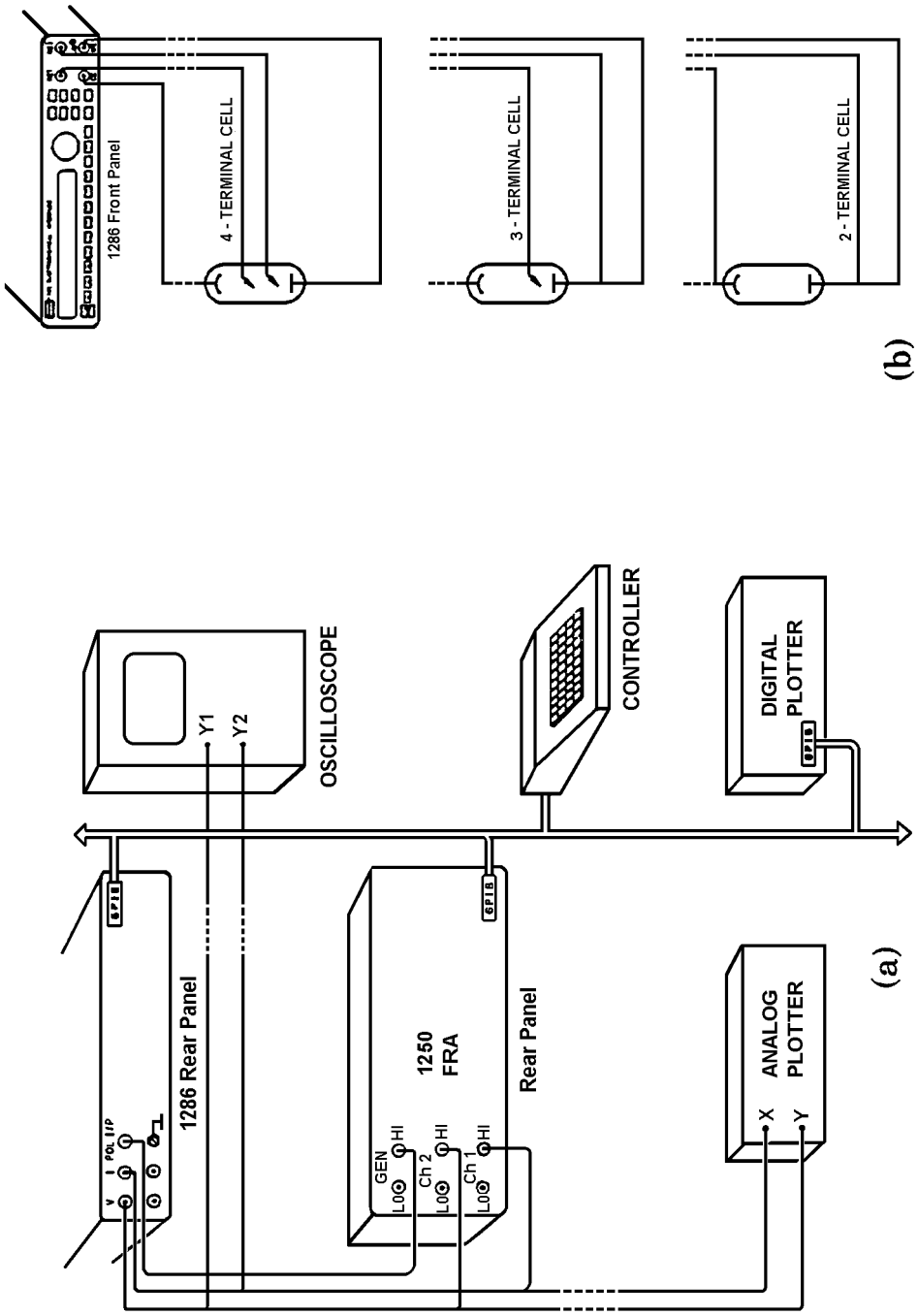

Fig 11 (a) General impedance measurement arrangement using a sine wave FRA technique with a Solartron 1250 FRA and 1286 ECI

(b) On the front panel the electrochemical cell is connected as shown

In potentiostatic mode the admittance is measured (time constant R_eC_d). For $R_p >> R_e$ and frequencies such as:

$$f < \frac{1}{2pR_pC_d} = f_c$$

the real part of the admittance is approximated by:

$$R_e[Y] \sim \frac{1}{R_p}\left(1 + \frac{w^2}{w_c{}^2}\frac{R_e}{R_p}\right)$$

where $\omega_c/2\pi$ is the characteristic frequency of the impedance:

Hence the relative error on R_p made at frequency f is equal to:

$$\frac{w^2}{w_c{}^2}\frac{R_e}{R_p}$$

where $w_c = \frac{1}{R_pC_d}$

e.g. for a circuit when $R_e/R_p = 10^{-3}$ and $R_pC_d = 100s$, a measurement performed at $\omega = 2/3\ \omega_c$ will give a 0.04 % error and needs a 15 minute measurement time.

The time necessary to obtain the value of R_p is longer by the frequency analysis than by the time technique but the accuracy is a lot better. The high level of parasitic noise, due to the pick up of electromagnetic radiation because of the high level of the impedance and to the fluctuations of the corrosion potential due to the hydrogen bubble evolution, etc., alters the measurement signals. The time techniques are particularly sensitive (e.g. see the parasitic noise in Fig. 8) to this alteration whereas the correlation technique used in frequency analysis assures a certain immunity to noise (see below). The only technique which can be used in the time domain is to repeat several times the measurement procedure and average the readings, but of course this increases the overall measurement time.

2.4.2 Systematic Errors arising from Fast Swept Sinusoidal Excitation for Single Sine Wave Measurements

In addition to estimation errors due to the presence of spurious noise which will be examined in the following, systematic errors may arise due to the signal processing itself. The use of a transfer function analyzer in connection with a single Sine wave perturbing signal may lead to a systematic error when the sinusoidal excitation is swept too quickly. For most electrochemical systems each frequency change leads to a transient regime. If the measurement is performed during this transient regime an error arises compared with the slow swept sinusoidal method where the frequency is changed sufficiently slowly for transients to be ignored. This transient regime can be calculated [10]. The error made by measuring the impedance at a frequency f2 following a change of frequency from f1 decreases when the integration time of the measurement increases, and when the frequency resolution increases. It depends upon the initial phase of the sinusoidal excitation at the time of the frequency change (the worst case is for a 90° initial phase) and on the time delay t_o between the time where the frequency has changed and the time where the measurement begins. For a RC circuit the maximum error is around its characteristic frequency f_c. It can be shown that $2/f_c$ delay is necessary to achieve a significant decrease of the error. However, from a practical point of view and in spite of the absence of a delay, this error can be

neglected when the measurement is carried out with a frequency sweep involving five steps per decade and 10 cycles of integration. This error is shown in Fig. 12.

The measurement error exhibited above is at first deterministic, but due to its dependence on the initial phase of the input signal, which is random, it appears to be random. Hence it can alter the measurement results in the same way as errors due to parasitic noise or system instabilities. These errors due to fast swept sinusoidal excitation ought to be decreased by keeping the initial phase of the input signal to zero or by delaying every measurement for several times the longest system time constant (a delay facility is provided with the 1170 and 1250 families of FRA).

The above calculation is valid for any frequency. However, in the higher frequency range the internal delays of the measurement device (0.2s for a Solartron 1170 instrument) lead to a very low error for frequencies greater than 10Hz ($t_o \geq 2\tau_o$). Hence only the lowest frequency range is now concerned with the present error but for a future quasi-perfect measurement device, i.e. with very low internal delays, this kind of error will alter the whole analyzed frequency range.

As this measurement error affects mostly the low frequency range, it may explain some scattering of the experimental measurement points in the complex plane often observed in electrochemical impedance measurements for frequencies below a few hundredths of a hertz.

2.4.3 Laplace and Fourier Analysis of Step Responses

Step signals resolved in the time domain were initially used as electrochemical perturbing signals. At the beginning of the sixties they were used in the frequency domain by means of Laplace transform. Then it was particularly developed by A.A. Pilla and coworkers [11]. The results are expressed in terms of an operational impedance. In the seventies the FFT algorithm was applied to the step responses [12].

For a steady-state, or at least quasi-steady-state linear system, the input x(t) / output y(t) relationship is given by:

$$y(t) = \int_0^\infty h(t - t')x(t')dt'$$

where h(t) is the impulse response of the device.

If the perturbing signal x(t) is sufficiently low in order not to drive the electrochernical system into non-linear regimes a transfer function can be defined at each polarization point by using the Laplace transform.

$$H(p) = \int_0^\infty h(t)e^{-pt}dt$$

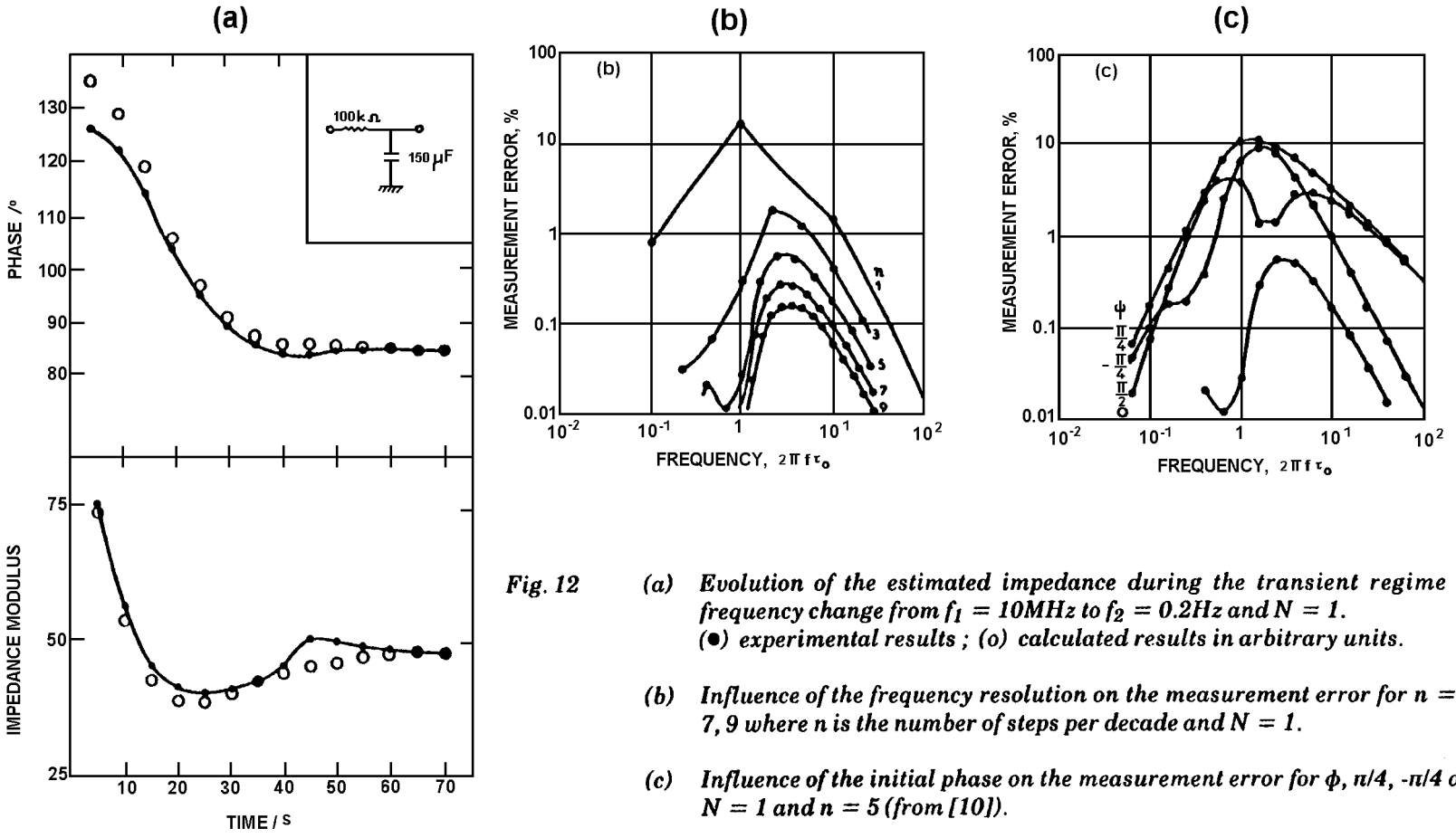

Fig. 12 (a) *Evolution of the estimated impedance during the transient regime for the frequency change from $f_1 = 10MHz$ to $f_2 = 0.2Hz$ and $N = 1$.*
(●) experimental results ; (o) calculated results in arbitrary units.

(b) *Influence of the frequency resolution on the measurement error for $n = 1, 3, 5, 7, 9$ where n is the number of steps per decade and $N = 1$.*

(c) *Influence of the initial phase on the measurement error for ϕ, $\pi/4$, $-\pi/4$ and $\pi/2$, $N = 1$ and $n = 5$ (from [10]).*

If x(t) is the voltage (respectively current) and y(t) the current (respectively voltage), H(p) is the admittance (respectively impedance) of the cell. Practically, H(p) is used either on the real axis ($\omega = 0$) or on the imaginary axis ($\sigma = 0$).

If ω is zero, H(p) becomes a real function of σ, called the operational transfer function such as:

$$H(s) = \int_0^\infty h(t) e^{-st} dt \ldots\ldots s > 0$$

If σ tends to zero and if h(t) is summable, H(p) tends to the usual complex transfer function:

$$H(f) = \int_0^\infty h(t) e^{-2pjft} dt$$

Hence $H(\sigma)$ and H(f) are theoretically equivalent. If the analytical expression of H(p) is known, $H(\sigma)$ and H(f) can be directly obtained by simply substituting σ or $2\pi jf$ for p in this analytical expression. However if $H(\sigma)$ is only experimentally known on the whole real axis, H(f) or h(t) cannot be simply reached. This problem arises because a usable inverse transform is not available for $H(\sigma)$.

Two types of errors decay the estimation of the spectra of a step signal and of its response. The systematic errors are inherent to the processing itself and the estimation errors are due to the presence of spurious noise especially in the measurement channels. The systematic errors arise from the signal processing in absence of noise. These errors are of two orders. Firstly a bias error due to the limited integration time of the step signal which has an infinite duration; secondly a random digital error due to the limitation of the dynamic range of the calculated spectrum.

If X and Y are respectively the input and output of the electrochemical system with transfer function $H(\omega)$ (impedance or admittance), after sampling (Xi, Yi) the two following quantities are computed:

$$f_{XX} = \sum_i X_i X_i^*$$

and:

$$f_{XY} = \sum_i X_i Y_i^*$$

where X_i^* is the complex conjugate of X_i (for Laplace transform $X_i^* = X_i$ as X_i is real) in order to obtain:

$$H(w) = \frac{f_{XY}}{f_{XX}}$$

The limited dynamic range of the calculated spectra due to the computer introduces random digital errors. These random errors can be eliminated by subtracting its limiting value (for $t \to \infty$) from the signal after acquisition. In order to avoid the bias error due to the fact that the step response does not tend to zero for $t \to \infty$ the response can be differentiated after digitizing. This processing leads to a drastic decrease of the spectrum in the low frequency range and an increase in the high frequency one. The differentiation while keeping the same total energy of the processed signal, performs a rearrangement of the distribution of the power density of the spectrum. Hence the processor has to cope with a quasi-white signal and the dynamic range problems are not so acute. After differentiation the signal is multiplied by a time window $W_o(t)$ such as [13]:

$W_o(t) = 1$ for $\quad o \le t \le K_o \Delta t$

$W_o(t) = 0$ elsewhere.

When parasitic independent Gaussian noises perturb the measurement signals x(t) and y(t) the estimation error can be calculated for the estimated modulus |H| and the estimated phase ϕ obtained from the measured perturbed quantities:

$$e^2\left(|\dot{H}|\right) = \frac{1}{2N_d} = \frac{Var\left(|\dot{H}|\right)}{\left[E\left(|\dot{H}|\right)\right]^2}$$

$$Var(f) = e^2\left(|\dot{H}|\right) \qquad \text{in radians}$$

Where Var (|H|) and E (|H|) respectively mean variance and average values of |H|.

For a Fourier transform, it can be shown that:

$$e^2\left(|\dot{\mathrm{H}}|\right) = \frac{1}{2N_d}\left(\frac{1}{h_i} + \frac{1}{h_o} + \frac{1}{h_i h_o}\right)$$

where η_i and η_o, are respectively the input and output signal-to-noise ratios and N_d is the number of averages.

In order to evaluate the efficiencies of the Fourier and Laplace transform techniques a comparison of the estimation errors has been plotted in Fig. 13 for the two cases in various conditions.

The quantity of information contained in the operational impedance and in the complex impedance are theoretically equivalent. Hence the test of a theoretical model is possible either in complex or in real frequency domain. However, the passage from one type of impedance to another is very difficult, or impossible, from the practical point of view.

As far as the measurement is concerned, the choice between the two techniques is difficult. A very narrow window ($K_o\Delta t$) gives a little advantage to the Fourier transform; however this type of window cannot always be chosen. However, the existence of a Fast Fourier Transform algorithm for Fourier transformation which is not the case for the Laplace transform, gives a strong advantage in terms of computing time. In addition in the Laplace domain the signal processing is not as well known as in the Fourier domain, particularly sampling theory and anti-alias filtering.

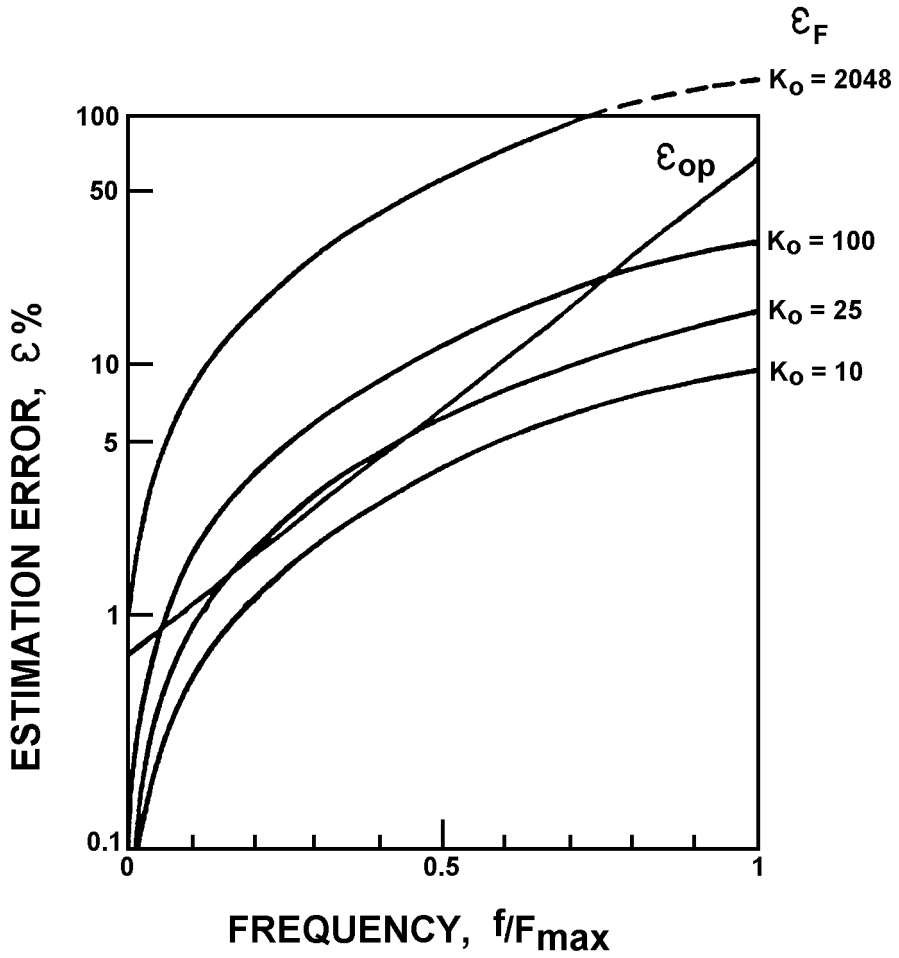

Fig. 13 Estimation errors due to parasitic noise for a step signal analysis by means of a Fourier (ε_F) or a Laplace (ε_{op}) technique for various time windows $K_o(t)$ for the same RC circuit (from [13]).

2.4.4 Comparison of the Performance of a Step, White Noise and Single Sine Wave Analysis

Impedance measurements performed by means of a step signal (SS) or a white noise (WN) through spectral analysis (SA) and a single sine wave through harmonic analysis (HA) have been compared. It has been shown that the estimation errors on the impedance measurements with galvanostatic control (Fig. 10) are given for the whole frequency range and with reasonable signal-to-noise ratios by [14]:

$$e_{SA}^{\,2}\left(\left|\hat{Z}\right|\right) = \frac{1}{2N_d}\left(\frac{1}{h_i} + \frac{1}{h_o}\right)$$

for spectral analysis and:

$$e_{HA}^{\,2}\left(\left|\hat{Z}\right|\right) = \frac{1}{2BtN_d}\left(\frac{1}{h_i} + \frac{1}{h_o}\right)$$

for harmonic analysis.

Where η_i and η_o are the signal-to-noise ratios at the input and/or the output of the system, N_d is the number of averages, B the bandwidth of the parasitic noise and t the measurement time for the analysis of one frequency.

In potentiostatic regime (Fig. 3) the estimation errors on the admittance measurement are given by:

$$e_i^{\,2}\left(\left|\hat{Y}\right|\right)_{pot} = \left[e_i^{\,2}\left(\left|\hat{Z}\right|\right)\right]_{gal}\left|\hat{Z}\right|^2 \frac{S_{nn}(I)}{S_{nn}(V)}$$

where i means either HA or SA and where $S_{nn}(I)$ is the power spectral density in A^2/Hz of the current sources in a potentiostatic arrangement and $S_{nn}(V)$ is the power spectral density in V^2/Hz of the voltage sources in a galvanostatic arrangement of parasitic noises which are supposed to be equal at the input and at the output.

In order to compare the three techniques it is necessary to choose the same measurement conditions:

1. Same amplitude of the perturbing signal.

   As all these techniques are characterized by an estimation error which tends towards zero when the signal-to-noise ratio tends to infinity, they are equivalent for a linear system as it is only necessary to increase the level of the perturbing signal to improve the accuracy. However, in the case of electrochemistry, where the processes are basically non-linear, the level of the perturbation has to be limited.

   In the case of a harmonic analysis or a step signal analysis the level of the perturbation is easily stated at a given value "a" which is not large enough to drive the system into non-linear behaviour (i.e. to stay in a linear regime). In the case of spectral analysis using white noise, if the anti-aliasing filters which are necessary because of the sampling are tuned at F_{max}, the mean power density of the current noise ϕ_{ii} is equal to $\sigma^2/2F_{max}$ where σ is the standard deviation of the random signal. As for a Gaussian process the signal has a 95.4% probability of lying between -2σ and 2σ, if a is the maximum

amplitude of the current allowed because of the non-linear distortion the analyzing white noise has to be chosen such that:

$$s^2 = \frac{a^2}{4}$$

2 Same parasitic noise power density S_{nn}.

3 Same resolution between the two lowest analyzed frequencies.

For spectral analysis the impedance measurement is made at K/2 frequencies equally separated by:

$\Delta f = 2F_{max} / K$

For a harmonic analysis carried out by using a logarithmic sweep of n frequencies per decade in the frequency bandwidth (f_{min}, f_{max}) where $f_{max} = 10^m f_{min}$, i.e. a measurement over m decades, the sequence of analyzing frequencies for the first decade is:

f_{min}, $10^{1/n} f_{min}$, $10^{2/n} f_{min}$, ……, $10^{(n-1)/n} f_{min}$, $10 f_{min}$

The frequency resolution Δf is a constant for a spectral analysis from where $\Delta f/f$ decreases when f increases. For a harmonic analysis the resolution $\Delta f = f_{min}$

$(10^{p/n} – 10^{(p-1)/n})$ at an analyzed frequency $f = f_{min} 10/^{(p-1)/n}$ increases when f increases,

$$\frac{\Delta f}{f} = 10^{\frac{1}{n}} - 1 \left(e.g. \frac{\Delta f}{f} \approx 0.78 . for . n = 4 \right)$$

and:

is constant over the whole frequency range.

Hence for the lowest part of the frequency range the resolution is equal to:

$\Delta f = f_{min}(10^{1/n} – 1)$ for harmonic analysis

$= 2F_{max}/K$ for spectral analysis

4. Same analysed minimum frequency

$f_{min} = 2F_{max}/K$

From the last two equations it is necessary to choose:

$10^{1/n} = 2$

i.e.

$n = 1 / \log 2$

Hence it is necessary practically to take at least n = 4 steps per decade to obtain the same resolution in the lowest frequency range for a harmonic and a spectral analysis.

5. Same measurement time.

For a spectral analysis the measurement time is equal to:

$T_{SA} = N_{SA}.T$

$= N_{SA}. 1 / f_{min}$

where SA, for spectral analysis, means WN or SS. For a harmonic analysis where the frequency is logarithmically swept over one decade of n frequencies per decade the time necessary to generate n frequencies is the sum of the periods of the analysing frequencies and is equal to:

$$t_1 = \frac{1}{f_{min}} . \frac{0.9}{10^{1/n} - 1}$$

For an analysis over m decades, the total time necessary to generate one period of each measuring frequencies, including the time necessary to generate f_{min} is:

$$t_m = \frac{1}{f_{min}} \left[\frac{0.9}{10^{1/n} - 1} \left(1 + \frac{1}{10} + ... + \frac{1}{10^{m-1}} \right) + 1 \right]$$

so:

$$t_m \approx \frac{1}{f_{min}} . \frac{1}{1.10^{-1/n}}$$

whatever the number of decades. Hence from a practical point of view and for $n \geq 3$:

$$t_m \approx \frac{2}{f_{min}}$$

i.e. the measurement time is roughly equal to twice the period of the minimum analysing frequency.

Example: for a logarithmic analysis carried out between 0.01 and 10Hz (m = 3) with five frequencies per decade (n = 5) the analysing frequencies are 0.01, 0.0158, 0.025, 0.0397, 0.063, 0.0996, 0.158, 0.25, 0.397, 0.63, 0.996, 1.58, 2.5, 3.97,6.3 and 0.96Hz. Hence:

$t_3 = 271s$

In practice, a transfer function analyzer (Solartron 1174) needs 276s including the calculation time for such a sequence. For a linear sweep, to obtain the same resolution in the lower frequency range (i.e. 0.0058Hz) 1566s are necessary (i.e. 1245 for the acquisition time and 321s for the total calculation time). Of course 1724 frequencies are analyzed in this case.

To obtain the actual measurement time the number of cycles of integration N_{HA} has to be taken into account:

$$T_{HA} = N_{HA}\left(\frac{1}{f_{min}\left(1-10^{-1/n}\right)} + nmt_o\right)$$

Where t_o is a delay between each low frequency measurement added in order to avoid transient regimes, this delay is equal to several times the longest time constant of the system investigated (see above).

For the critical value n = 1/log2

$$T_{HA} = N_{HA}\left(\frac{2}{f\,min} + nmt_o\right)$$

If the measurement is performed by using a sufficient number of measurement frequencies per decade (n≥4) and a sufficient number of cycles of integration (N≥10) the last term can be neglected and:

$$T_{HA} \approx N_{HA}\frac{2}{f_{min}}$$

So:

$$\frac{T_{HA}}{T_{SA}} = 2\frac{N_{HA}}{N_{SA}}$$

Hence to perform the measurements in the same measurement time it is required to average twice as long for spectral analysis as for harmonic analysis:

$$N_{HA}=N_{SA}/2$$

It should be noted that the older generation of transfer function analysers (1170 Series from Solartron) had two inputs with one correlator; thus channels were measured sequentially. The new generation (1250 Series) have two analyzers for simultaneous measurements. The newer instruments therefore take half the time to make a measurement.

By taking into account the relationship between the numbers of averages, the following quantities have been plotted in Fig.14 for the whole frequency range.

This figure shows that the step analysis is very poor in the high frequency range and that the sine wave analysis is better than the white noise analysis in the whole frequency range (the estimation error is the same for F_{max}).

In Fig. 15 the estimation errors have been compared in the lower frequency range.

This figure shows that for:

$$f < F_{max}\,\frac{2}{p}\sqrt{\frac{1}{K_o}}$$

the step signal analysis is better than the white noise analysis. It is also remarkable that in a very narrow bandwidth:

$$\left[\frac{F_{max}}{4}\cdot\frac{K_o}{K},\frac{4F_{max}}{K_o p^2}\right]$$

the step signal analysis is better than the harmonic analysis for:

$$K_o < \frac{4}{p}\sqrt{K}\,(i.e. K_o \le 80 for K = 4096)$$

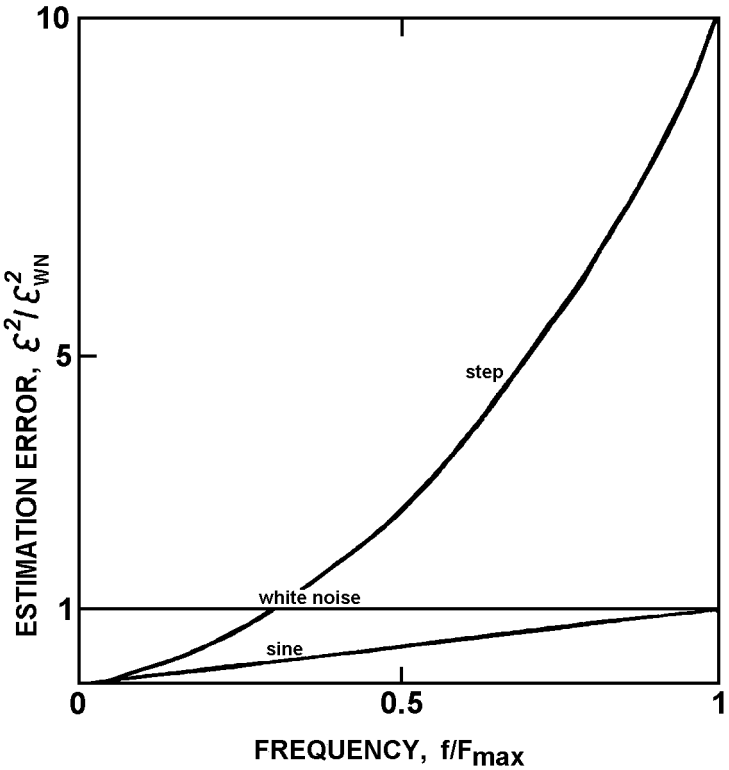

Fig 14 Comparison in the higher frequency range of the estimation errors of the electrochemical impedance measured by means of sine wave, white noise and step signal for the same frequency range, measurement time, resolution and perturbing signal of equivalent amplitude (from [14]).

However this advantage is so localized in frequency that very special purposes are necessary for preferring the step signal analysis in the very low frequency range. As a conclusion, if the case of use is also taken into account the sine wave analysis, used with a logarithmic sweep of four or five frequencies per decade, is generally the most efficient technique for measuring electrochemical impedances.

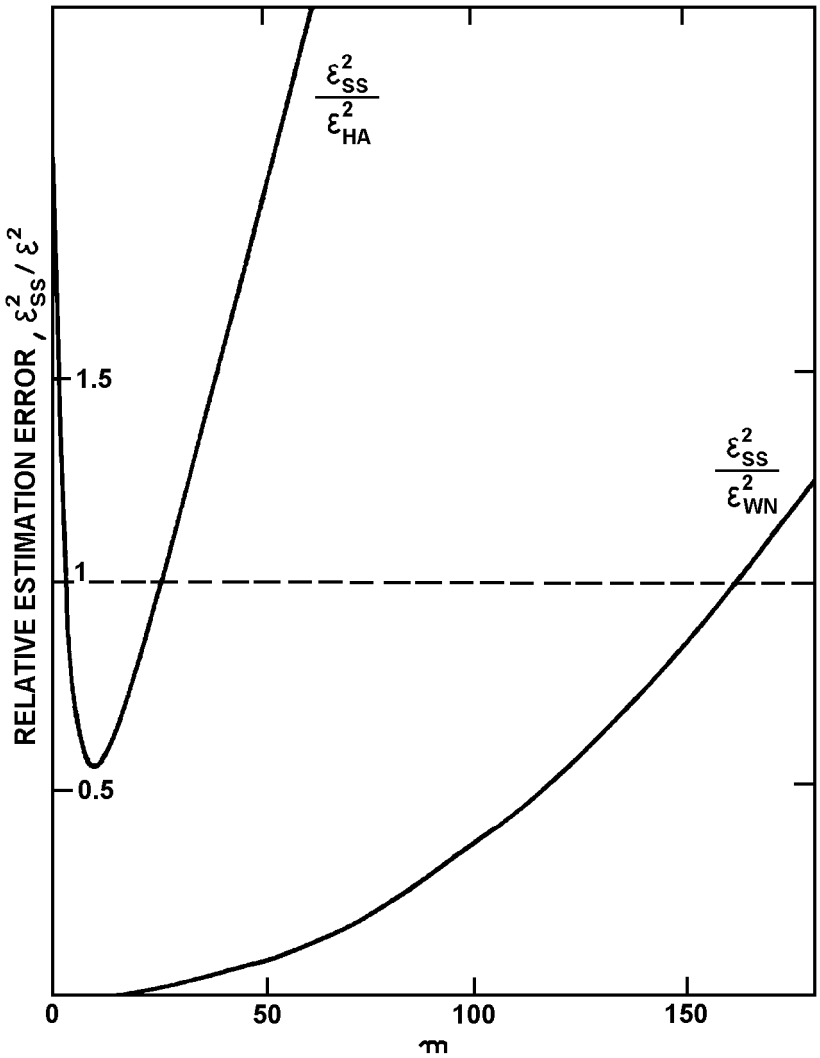

Fig. 15 Comparison in the lower frequency range (20% of the useful frequency range) of the estimation errors on the measurement of an electrochemical impedance measured from a step signal perturbation combined with spectral analysis and:

(i) a harmonic analysis (curve $\varepsilon_{ss}^2/\varepsilon_{HA}^2$) and;

(ii) a white noise combined with spectral analysis (curve $\varepsilon_{ss}^2/\varepsilon_{WN}^2$) for K = 2048 and a ($f_o/200$ - $5f_o$) analysed frequency range (from [13]).

TFA	1172	1174/1255	1250/1255
Input of one analyzer	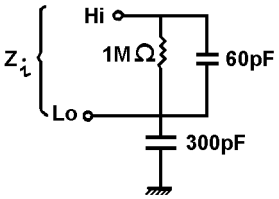	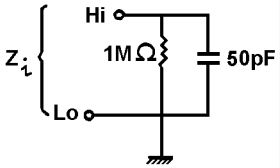	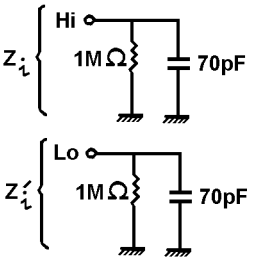
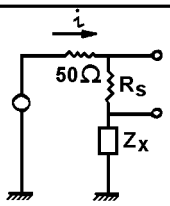	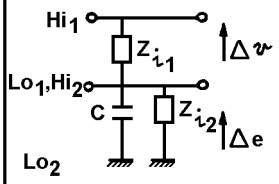	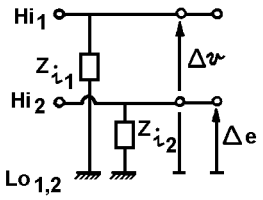	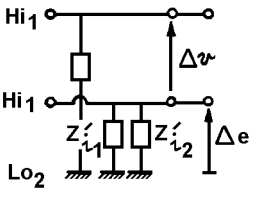
Δc Δv $\tilde{Z}_x = \frac{\Delta c}{i} = R_s \frac{\Delta c}{\Delta v}$	$\frac{i}{\frac{1}{Z_x} + j C\omega + \frac{1}{Z_{i_2}}}$ $\frac{i}{\frac{1}{R_s} + \frac{1}{Z_{i_1}}}$ $R_s \frac{\frac{1}{R_s} + \frac{1}{Z_{i_1}}}{\frac{1}{Z_x} + j C\omega + \frac{1}{Z_{i_2}}}$	$\frac{Z_{i_1} \cdot i}{1 + (Z_{i_1} + R_s)(\frac{1}{Z_x} + \frac{1}{Z_{i_2}})}$ $\frac{Z_{i_1} \cdot i \left(R_s + \frac{1}{\frac{1}{Z_x} + \frac{1}{Z_{i_2}}}\right)}{Z_{i_1} + R_s + \frac{1}{\frac{1}{Z_x} + \frac{1}{Z_{i_2}}}}$ $R_s \frac{1}{1 + R_s + \frac{1}{Z_x} + \frac{1}{Z_{i_2}}}$	$\frac{Z_{i_1} \cdot i}{1 + (Z_{i_1} + R_s)(\frac{1}{Z_x} + \frac{1}{Z_{i_2}})}$ $\frac{Z_{i_1} \cdot i}{Z_{i_1} + R_s + \frac{1}{\frac{1}{Z_x} + \frac{1}{Z_{i_2}}}}$ $\frac{Z_x}{1 + \frac{Z_x}{Z_{i_2}} + \frac{Z_x}{Z'_{i_1}}}$
at f = 0 and $R_s = Z_x$ Z_x = 100 kΩ Z_x = 1 MΩ	Z_x Z_x	0.47 Z_x 0.33 Z_x	0.83 Z_x 0.33 Z_x
input capacitance in parallel on Z_x	360 pF	50 pF very low for 1255	140 pF very low for 1255

Fig 16 Schematics and effects of the input impedance of various Solartron transfer function analyzers. The 1255 TFA can be used in either the 1174 or 1250 input configuration, however the input capacitance is a lot lower than the latter.

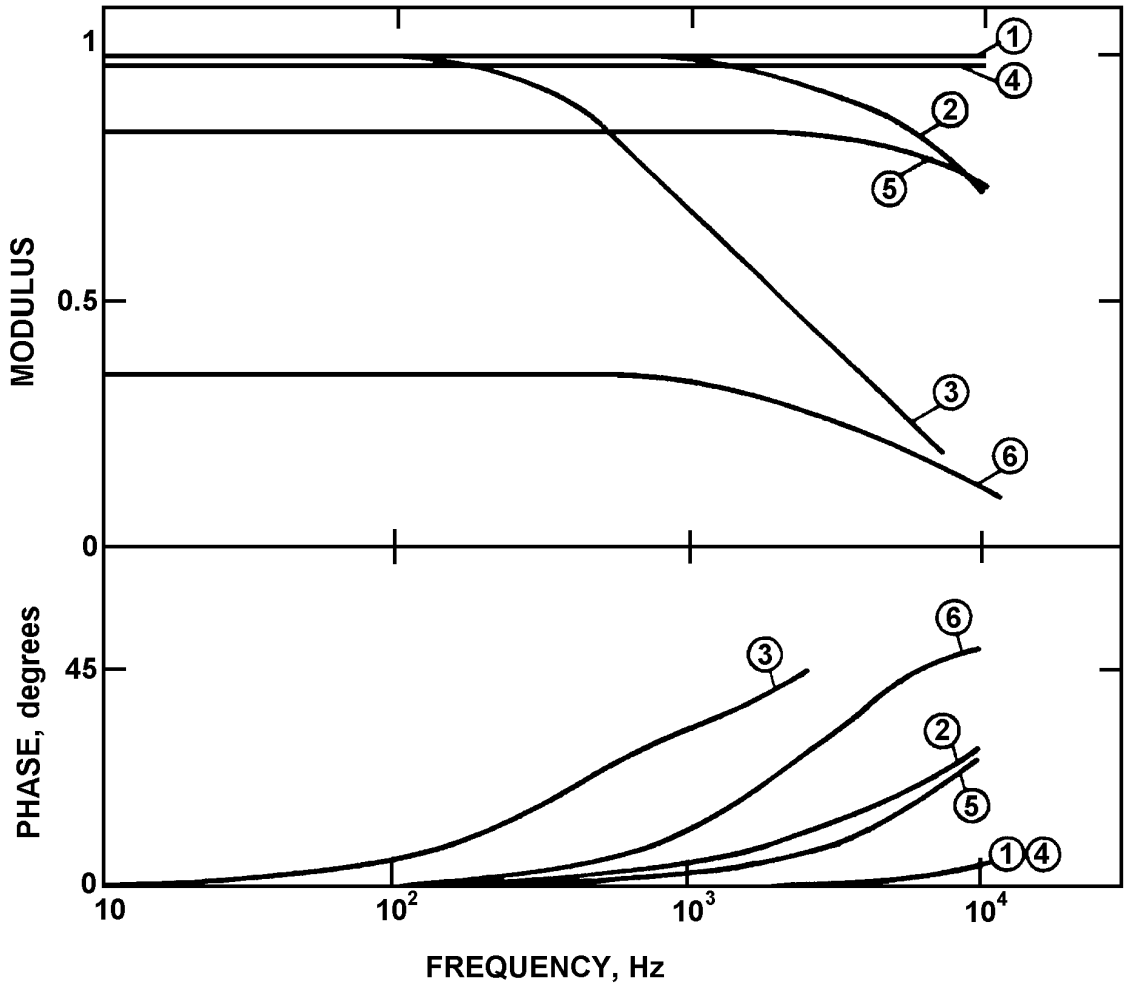

Fig. 17 Measurement of some resistances directly plugged to the transfer function analyser

(1) 1172 TFA - $R_L = Z_x = 10k\Omega$

(2) 1172 TFA - $R_L = Z_x = 100k\Omega$

(3) 1172 TFA - $R_L = Z_x = 1M\Omega$

(4) 1250 TFA - $R_L = Z_x = 10k\Omega$

(5) 1250 TFA - $R_L = Z_x = 100k\Omega$

(6) 1250 TFA - $R_L = Z_x = 1M\Omega$

2.5 Distortions in the Measurement of the Impedances of Extreme Values

For electrochemical impedances of mid-range value ($1 < |Z| < 10^4\Omega$) no special problems arise concerning the measurement in the ($0\text{-}10^4$HZ) frequency range. However for impedances of very low modulus (IZI < 1Ω) or of very large modulus ($IZI > 10^4\Omega$) some distortions may occur which increase when the frequency increases. These distortions are due to the parasitic components of the cell, the polarization device and/or the measuring instrument.

2.5.1 Distortions in the Measurement of the Impedances of Large Values (IZI > 10kW)

Instruments used to measure electrochemical impedances (amplifiers, transfer function analysers) have finite input impedances which limit the range of validity of the measurement. As examples, in Fig. 16, the input impedance of various Solartron instruments is shown which have been used to measure impedance, but the same problem arises when amplifiers or differential amplifiers are employed. The errors due to the finiteness of the input impedances are given for direct measurement (without any buffering amplifiers) of an impedance Zx by means of a standard resistor R_S used for measuring the current. It is noticeable that in some arrangements the measured value is biased even at low frequency. In Fig. 17 the variation of the errors versus the frequency are given. It is concluded that the measurement of impedances larger than $10^3\Omega$ is really questionable when direct measurement with no buffering amplifier is carried out. In addition in these conditions the reference electrode is connected to the ground through the input impedance of the measuring transfer function analyzer, ie. 1MΩ, which is generally inadequate as no current has to flow through the reference electrode.

As a general rule it is required to use measuring instruments (usually buffer amplifiers) which have input impedances at least 100 times larger than the impedance to measure. If this is not the case a calibration procedure is necessary. In the case of measurement of the impedance of a cell the use of an electrochemical interface (potentiostat or galvanostat plus the prerequisite buffer amplifiers) ensures good quality measurements in the widest experimental conditions (see Fig. 18).

It is shown that the measurement of an impedance by means of a 1286 electrochemical interface (potentiostat mode, bandwidth type C) allows a 100MΩ resistance to be directly measured, i.e. without calibration, up to 10Hz. For greater values errors arise (10% for 200MΩ, 20% for 300MΩ,etc.) due to the finite input impedance of the measuring amplifier (10GΩ) and hence a pre-calibration is necessary. It is to be noticed that thanks to the driven shielded inputs the parasitic capacitance that limits the frequency range of the measurement is only 5pF and the parasitic capacitance of the shielded leads (50pF/m) do not interfere with the measurement.

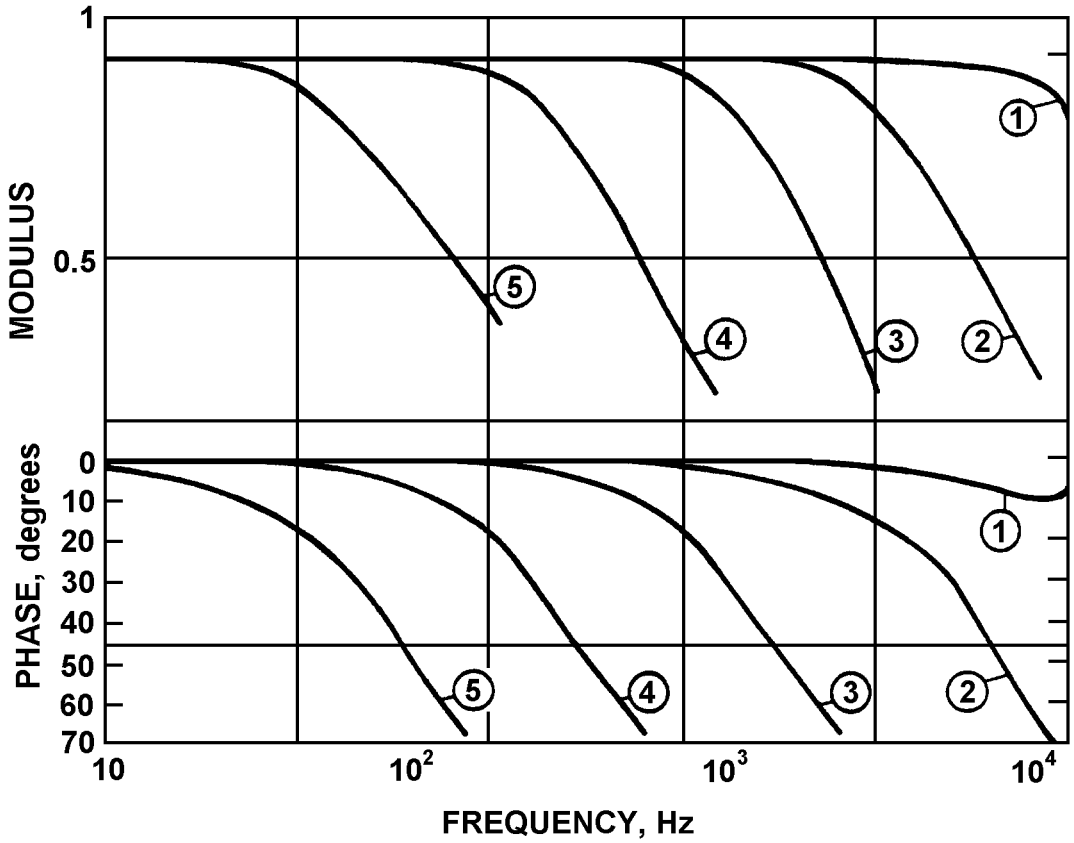

Fig. 18 Measurement of some resistance R by using a 1286/1174 equipment and a current measuring resistance R_S:

(1) R = 10kΩ, R_S = 10kΩ

(2) R = 100kΩ, R_S = 100kΩ

(3) R = 1MΩ, R_S = 100kΩ

(4) R = 10MΩ, R_S = 100kΩ

(5) R = 100MΩ, R_S = 100kΩ

2.5.2 Distortions in the Measurement of the impedance of Very Low Amplitude (IZI - 1W)

The measurement of the electrode impedance at frequencies above 10 or 100kHz, and sometimes less for very small amplitude impedances (see Fig. 19(b)) can be distorted by spurious effects which, to a first approximation, often correspond to that of an inductance connected in series with the electrode impedance.

The general equivalent circuit taking into account all the parasitic components is given in Fig. 19 (a). The impedance under investigation which is equivalent to R_e (electrolyte resistance) in series with $C_d||Z_f$ (double layer capacity in parallel with the Faradaic impedance) is tentatively measured. If a sine wave perturbation is imposed an apparent value Z_a is obtained through the measured potential U_m which deviates from the actual potential U because of the lead inductance L and of the impedance of the reference electrode (Rp,C). The measurement of the current is made through a standard resistor R_m with parasitic components L_m and C_m. which gives a voltage proportional to the measuring current $U(I_m)$. The other parasitic components are due to the cell geometry: the electrolyte resistance R between the counter electrode (CE) and the reference electrode (RE), and a stray capacity C' between the counter electrode and the reference electrode [15].

Depending on the experimental conditions various cases can arise. The inductive behaviour of the leads can often be minimized by shortening them. The effect of the capacity of the reference electrode C, which is often added to the capacity of the potentiostat, can be important in the very high frequency range, but special arrangement of the geometry of the reference electrode and care in the design of the electronic circuit of the potentiostat can decrease the R_p and C values. On the general point of view it seems that the capacity C' leads to a parasitic inductive behaviour such as:

$$L' = R_P R C'$$

By shielding the reference electrode, the value of this inductance can be decreased.

Even for very good quality standard resistors parasitic components appear for low and high values of R_m. For high values ($R_m > 10k\Omega$) a parasitic capacitive behaviour (C_m) hinders the measurement; for low values ($R_m < 1\Omega$) a parasitic inductive behaviour (L_m) predominates. In the latter case an additional problem arises due to the non-zero resistance of the leads which link the standard resistor to the potentiostatic circuit (eg. 0.12Ω has been found in [16]). In this case a calibration procedure is necessary.

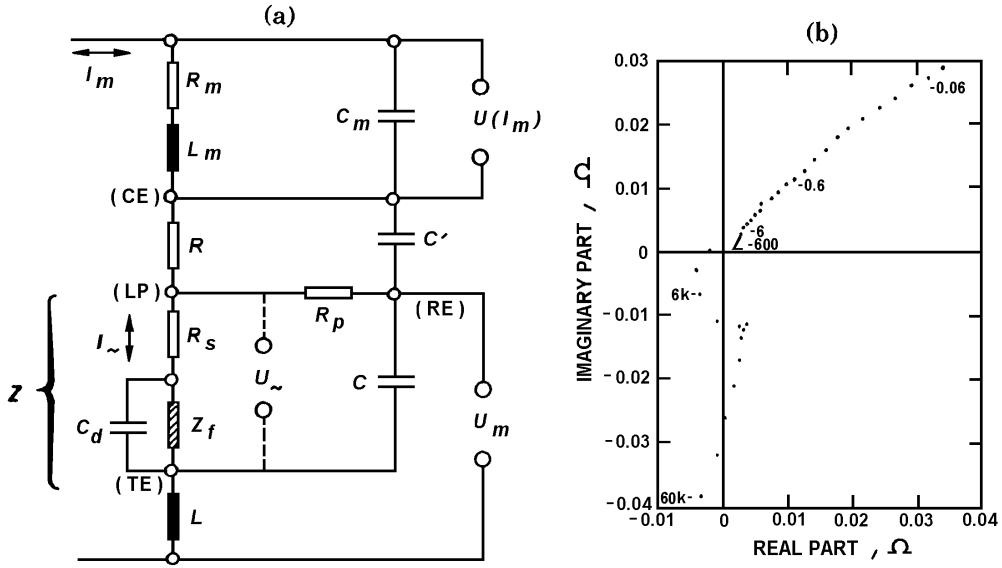

Fig. 19 *Problems arising in the measurement of small impedances:*

(a) Model circuit describing the measurement of the alternating signals I_m and U_m of the current and potential used to derive the measuring value Z_a of the apparent impedance (from [15]).

(b) Impedance of a 25Ah sealed lead-acid cell using a sense resistor of 10Ω (from [16]).

2.6 Data Analysis

Once the experimental raw data have been obtained the problem is to extract the parameters of interest. Two types of plotting can be considered depending whether a model is known a priori or not. If no model is known it is necessary to show the data without any pre-interpretative postulate: this is the case for Nyquist or Bode plane plotting. If a model is known, or believed to be known, various plottings, more or less based on a transfer and diffusion mechanism, are proposed in the literature.

2.6.1 Non-interpretative Plottings: Nyquist and Bode

The Nyquist plane or complex plane: negative of the imaginary part of the impedance (or admittance) versus the real part of the impedance (or admittance), has been used for a long time. The choice of the special, and surprising, sign convention is due to the fact that at the beginning the impedance measurements were made in the high frequency range and then the interface seemed to exhibit only a capacitive behaviour. Hence, in order to have the diagram conveniently plotted in the first quadrant of the complex plane this sign convention has been adopted. The use of the Bode plane is more recent in electrochemistry. Here the modulus and the phase are plotted versus the logarithm of the frequency. Before its introduction in our domain, it was widely used elsewhere and especially in electronics as the asymptotic trends (for $f \rightarrow \infty$) are easily determined to give the order of the system (1st order is 3dB/octave decrease of the modulus versus the frequency, 2nd order is 6dB/octave etc.). In the complex plane only one diagram is necessary to summarize all the experimental data. In the Bode representation two graphs are displayed, one for the modulus and one for the phase. However, except for the non-minimal phase shift systems, only one diagram should be necessary as from the Bode relationships there is a strict relation between the modulus and the phase of a transfer function. But of course as the nature of the system is not known a priori, it is usual to plot the two graphs.

For electrochemical work, the choice between the two types of display is not obvious, although most workers favour complex plane plotting. In fact, in the complex plane the impedance diagrams of some processes have very characteristic shapes: $\pi/4$ slope for a diffusion process, negative resistance for a passivation process, depressed semi-circle for a Cole-Cole distribution. These shapes are, without any doubt, more easily revealed in this representation than in a Bode representation. Only for special conditions is the latter chosen. When a very large modulus variation (e.g. from 10Ω to $10^6\Omega$) of the impedance occurs when the frequency varies, it is not easy to plot all the data in the same complex plane and a Bode representation (logarithm of the modulus versus the frequency) can be a more adequate alternative. Also if for a RC circuit only the C value changes when some parameter varies it is difficult to plot the change of impedance diagram in the same complex plane for various parameter values as they only show a shift in the frequency distribution. In this case too a Bode plot is more convenient. Other illustrations will be reported in the following and some examples are given in Fig. 20.

Usually it is the impedance which is plotted either in complex or Bode representation. However, especially for the complex plane, an admittance display can be more advisable when an infinite branch is shown in the graph. In some cases it is easier to determine a time constant from a finite loop than from an infinite one.

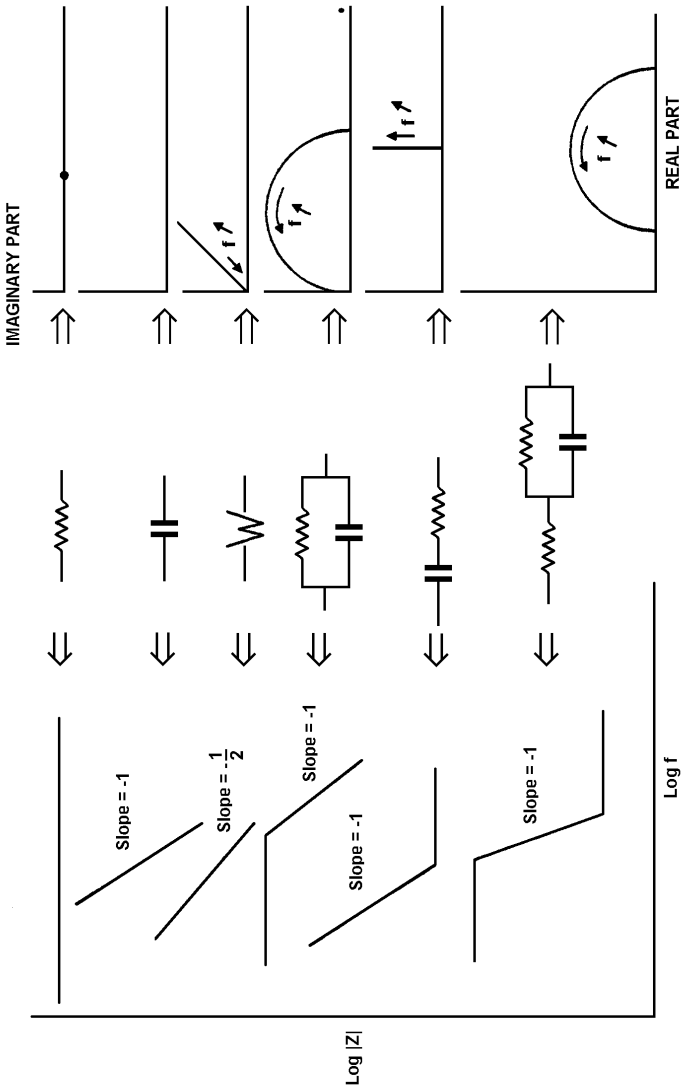

Fig. 20 Examples of Nyquist and Bode plane plottings.

2.6.2 Interpretative Plottings

If a quasi-reversible reaction limited by a diffusion process is considered the Randles circuit is often used (Fig. 21). The impedance of such a circuit has been calculated in [1]:

$$Z_F(w) = R_{ct}\left(1 + \frac{l}{\sqrt{jw}}\right)$$

When:

$$l = \frac{K_f}{\sqrt{D_o}} + \frac{K_b}{\sqrt{D_R}}$$

Where R_{ct} is the charge transfer resistance, K_f and K_b the forward and backward reaction rates of the oxydo-reduction process, D_o and D_R are the diffusion coefficients of the oxidized and reduced species.

To obtain the whole impedance of the circuit depicted in Fig.21 it is necessary to take into account the double layer capacity C_d and the electrolyte resistance R_e. In this case the real part and imaginary part are in the intermediate frequency range:

$$Re(Z) = R_e + R_{ct}\left(1 + \frac{l}{\sqrt{2w}}\right) - {R_{ct}}^2 l^2 C_d$$

$$Im(Z) = \frac{R_{ct}\, l}{\sqrt{2w}}$$

Hence the plotting of Re(Z) versus $\omega^{-1/2}$ (Randles plot) gives a straight line. One can obtain simultaneously $R_{ct}\lambda$ which is the slope of the straight line and $R_e+R_{ct}-{R_{ct}}^2\lambda^2 C_d$ which is the ordinate of the intersection of the straight line with the y-axis (Fig. 22(a)).

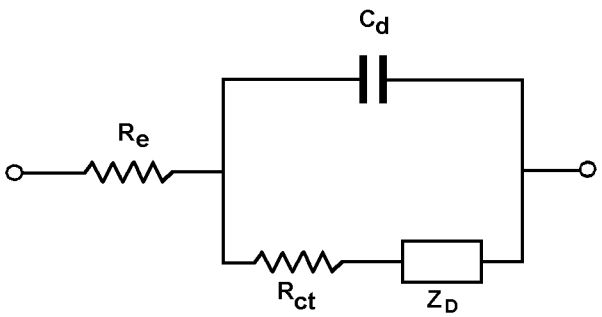

Fig. 21 Randles equivalent circuit. R_e: electrolyte resistance; C_d: double layer capacity; R_{ct}: charge transfer resistance; Z_D: diffusion impedance.

The vectorial subtraction of C_d from the interfacial impedance where R_e has been eliminated yields the Faradaic impedance for the system. Z_f can be plotted in a plane $R_e[Z_f]$, $-\omega I_m[Z_f]$. A straight line is fitted to the low frequency data, and extrapolation to zero frequency gives the polarization resistance $R_p = R_e [Z_f(\omega = 0)]$. The slope can be used for determination of the diffusion coefficient of the reacting species (Fig. 22(b)).

For the high frequency part of the impedance (R_e in series with $C_d||R_t$) a plot of Re(Z) versus - Im(Z)/ω gives a straight line whose intersection with the y-axis obtained for $\omega \rightarrow \infty$ leads to R_e, the slope is equal to $1/R_{ct}C$ and the end point (Fig. 22(c)) yields R_{ct} and $R_{ct}^2C_d$. From these the double layer capacity value can be obtained.

For the impedance of a blocking electrode (strongly adsorbed electroactive species) the impedance is often equivalent to a double layer capacity C_d in parallel with a capacity C and a resistor in series. The plotting of Y/ω where $Y = Z^{-1}$ in the complex plane gives a circle centred on the imaginary axis. The intersection of the latter with the y-axis directly gives the two involved capacitances (Fig. 22(d)).

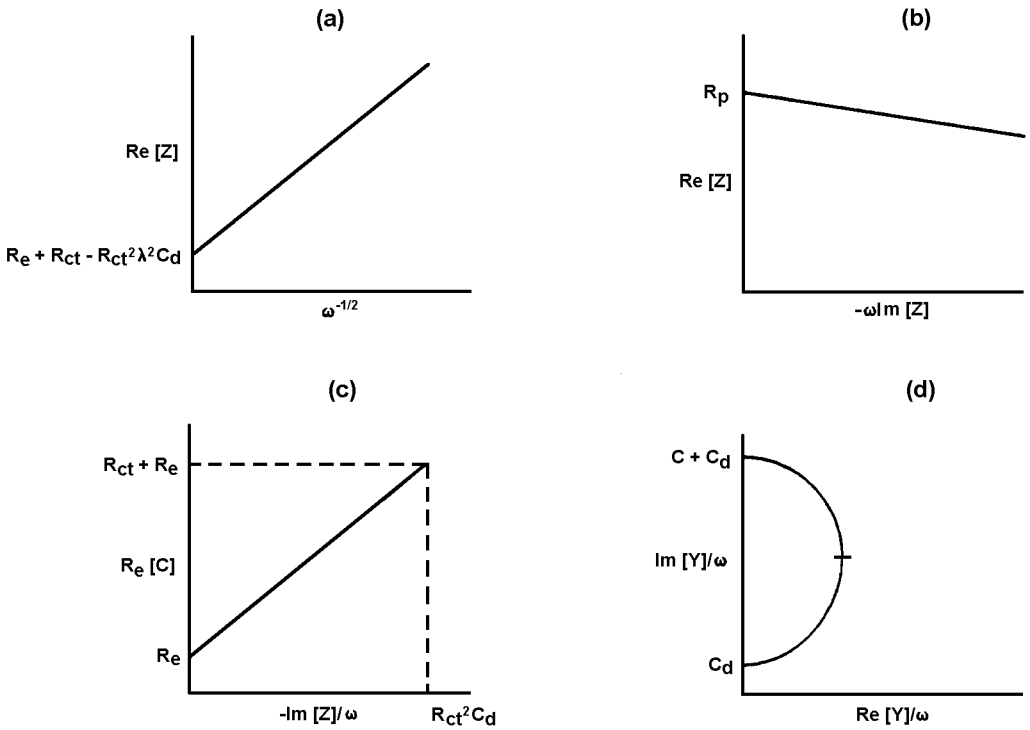

Fig. 22 Examples of specialized plots:

(a) Re[Z] vs $\omega^{-1/2}$. Randles plot.

(b) Re[Z] vs ωIm[Z] plot after elimination of C_d and R_e.

(c) Re[Z] vs Im[Z]/ω plot for the high frequency part of the impedance.

(d) Im[Y]/ ω vs Re[Y]/ ω plot for a blocking electrode.

2.6.3 Application of Kramers-Kronig Transforms in the Analysis of Electrochemical Systems

The Kramers-Kronig transforms have been used in electrochemistry for two purposes. First of all for obtaining the polarization resistance (e.g. for estimation of the corrosion rate) from the frequency-dependent imaginary component. Second, they were used as a general diagnostic for validating the experimental data. This can be very useful because of the need to employ low amplitude excitation and working with noisy systems.

The derivation of the K-K relationships is based upon four quite general conditions of the system being fulfilled: causality, linearity, stability and the impedance must be finite valued at $\omega \rightarrow 0$ and $\omega \rightarrow \infty$ and must also be a continuous and finite valued function at all intermediate frequencies. Two of the more important transforms may be stated as follows:

$$Z'(w) - Z'(\infty) = \frac{2}{p} \int_0^\infty \frac{xZ''(x) - wZ''(w)}{x^2 - w^2} dx$$

and:

$$Z'(w) - Z'(0) = \frac{2w}{p} \int_0^\infty \frac{\frac{w}{x} Z''(x) - Z''(w)}{x^2 - w^2} dx$$

where Z'(ω) and Z''(ω) are the real and imaginary components of the impedance, respectively.

Another couple of transforms exist which relate the modulus and the phase of an impedance.

The first relation can be firstly used, by taking $\omega = 0$, in order to obtain the polarization resistance R_p:

$$R_p = \frac{2}{p} \int_0^\infty \frac{Z''(x)}{x} dx$$

as $R_p = Z'(\phi) - Z'(\infty)$

This integral is evaluated in a piece-wise fashion by fitting a fifth order polynomial to experimental Z'' versus frequency (x) data using a least square technique. The integration is then performed over the whole frequency range.

As examples of illustration of the K-K transformation method for validating polarization resistance measurements in particular and for verifying impedance data in general, two systems, TiO_2 - coated steel in a HCl/KCl solution of pH = 2, (curve a, b) and Al - 0.1P - 0.1 In - 0.2 Ga - 0.01 TI alloy in 4M KOH, (curve c, d) are depicted in Fig. 23. For the two systems the polarization resistance is calculated from the high and low frequency limits of the impedance diagrams (curve a and c). The experimental Z" versus $\log_{10}\omega$ are plotted in curve b and d together with data calculated from the least squares piece-wise fit of a fifth order polynomial to the experimental data. The value of R_p is calculated from the integral. The calculated R_p agrees with the experimental value to within 0.7% in the first case. In the second case a larger discrepancy is due to the lower quality of the data, as expected for a rapidly corroding system, but also a less extensive data set, particularly in the critically low frequency region [17].

By using another type of K-K transform, R_p has been evaluated from the imaginary component at high frequencies, thus avoiding the need to obtain the impedance data at time-consuming low frequencies. However this procedure is limited to systems that exhibit single semi-circles in the complex plane that are either depressed or centred on the real axis, i.e. when the plot of Z" versus $\log\omega$ is symmetrical [18].

The K-K transforms can be used as diagnostic criteria for determining the validity of complex electrochemical impedance data. They provide a powerful means of assessing the validity of impedance data with respect to spurious errors that are present in either or both the real and imaginary components and with respect to system stability. The transforms coupled with statistical analysis, appear to be capable of detecting errors of a few percent in the experimental data [19].

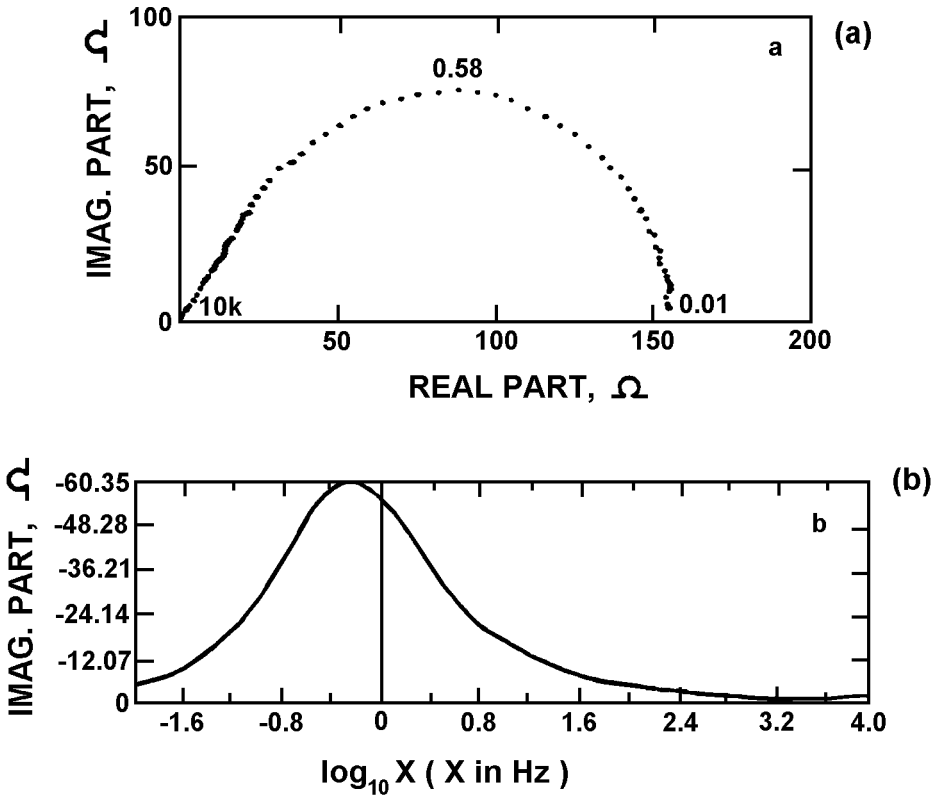

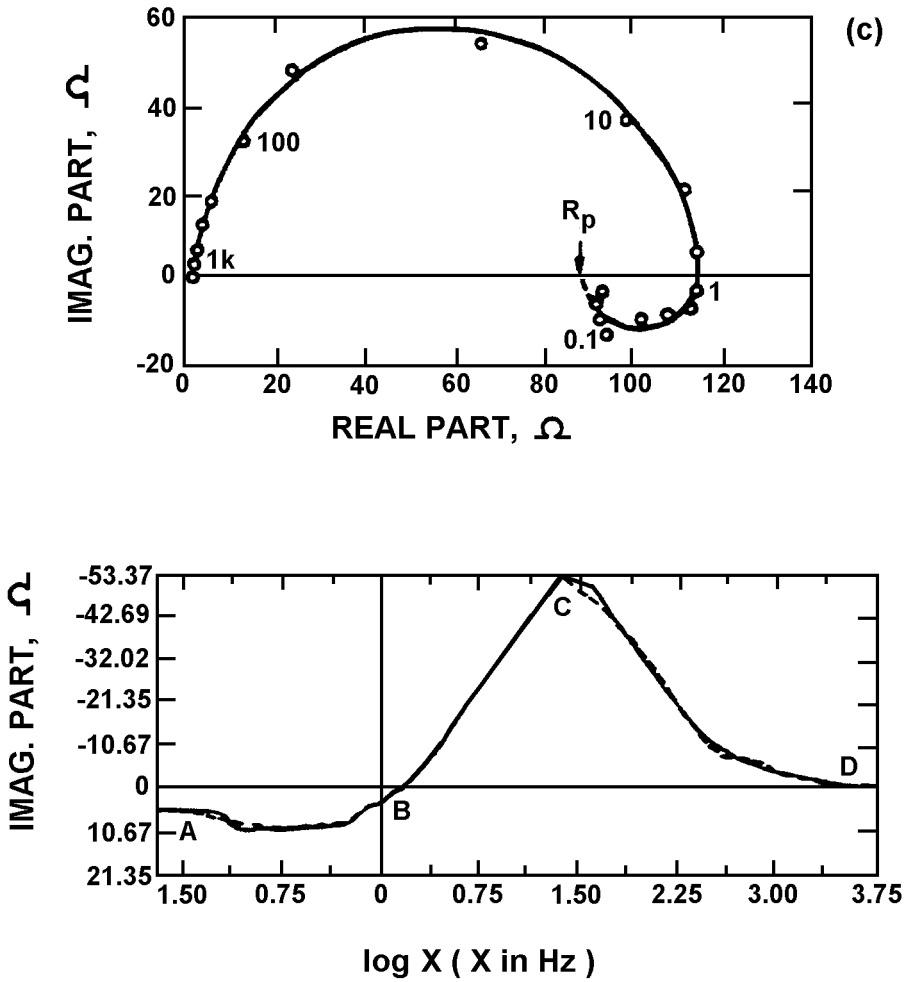

Fig. 23

(a) Complex plane impedance plot for TiO_2-coated carbon steel in HCl/KCI solution. pH = 2. T = 25°C. The numbers refer to frequency in hertz.

(b) Plot of lm[Z] vs $\log_{10}$x (x in hertz) for TiO_2-coated carbon steel in HCl/KCI solution. pH = 2. T = 25°C.

(c) Impedance diagram for Al-0.1P-0.1In-0.2Ga-0.01Tl alloy in 4M KOH at 25°C and at the open-circuit potential (-1.760V vs Hg/HgO).

(d) Plot of lm[Z] vs $\log_{10}$x (x in hertz) for Al-0.1P-0.1In-0.2Ga-0.01Tl alloy in 4M KOH at 25°C under open-circuit conditions(E=-1.76V vs Hg/HgO).

Chapter 3
Applications of Impedance Techniques

3.1 Introduction

The investigation of electrochemical processes are carried out either to understand the fundamental aspects of the processes involved or to test an overall process of practical interest. However even if an impedance technique is used for a simple test or a non-destructive material characterization, this implies a prevalidation of the procedure on simpler systems. It is undeniable that electrochemical systems of practical interest are very often complicated by their structure, composition, reaction mechanism etc. This has a restraining effect on the impedance development in the industrial world where the use of this technique is often restricted to testing or characterization.

In order to validate the technique itself even in its elementary uses, simple systems of academic interest, i.e. of theoretical interest without having an immediate practical or useful aim, have to be evaluated. In this case the electrochemist is able to devise a model of these systems from their physico-chemical properties. These are expressed in terms of mathematical evolution equations (generally differential or partial differential equations) which describe the kinetics of chemical or electrochemical reactions and mass transport by means of mass and electrical charge balances. By comparison with experiment it is possible to assess the validity of the model and to choose the parameter which gives the best estimation of a given phenomenon (e.g. the choice of the charge transfer resistance or of the polarization resistance in corrosion studies is based on such investigations). Hence even the crudest testing used on an assembly line or on a working site should have been preceded by a theoretical study in the laboratory to validate it. Between the simple search for the parameters of a known, or assumed, model and the description by a full set of differential equations there is an intermediate approach based on the equivalent circuit. However this method has been avoided here as when the elements of an equivalent circuit have been obtained it is generally difficult to ascribe an origin to each element.

In the following some new developments of the model derivation and of the practical applications are reviewed.

3.2 Interpretation of Impedance Measurements in Terms of Reaction Mechanism

Heterogeneous kinetics, i.e. electrochemical reactions and mass transport, above all diffusion, are the main types of elementary phenomena which take place at the electrochemical interface. In order to theoretically interpret the experimental impedance data it is necessary to take these various types of processes into account. Two approaches are proposed in the literature. First of all the species adsorbed on the surface are considered as located on macroscopic areas where the reactant species diffuse through a classical Nernst layer. In another approach the species are supposed to be adsorbed on active sites located on definite areas at a microscopic or macroscopic scale. In this case the diffusion is considered to occur in a classical Nernst layer far from the surface, but close to the surface a cross diffusion occurs from one site to another which gives rise to a lateral diffusion contribution.

3.2.1 Heterogeneous Kinetics involving a Macroscopic Coverage Approach

This approach, especially promoted by Epelboin et al considers that for a reaction mechanism involving m reactions, the adsorption of the n reaction intermediates X_i obey a Langmuir isotherm and are characterized by a surface coverage θ_i (the details of the hypotheses of this type of model and a simple example are given in [1]).

The general kinetic equation which links the potential perturbation ΔE to the concentration of the diffusing species Δc_i at the electrode surface and the coverage response $\Delta\theta_i$ can be written in linearized form:

$$\frac{d\Delta q_i}{dt} = A\Delta q + A'\Delta c + B\Delta E$$

and the Faradaic current response ΔI_F is:

$$\Delta I_F = C\Delta E + D\Delta E$$

where $\Delta\theta$ and Δc are vector columns of the superficial and volumic concentrations of the reactive species such as:

$$\Delta q = \begin{bmatrix} \Delta q_1 \\ \Delta q_2 \\ . \\ . \\ . \\ . \\ \Delta q_p \end{bmatrix} \; ; \quad \Delta_c = \begin{bmatrix} \Delta c_1(0) \\ \Delta c_2(0) \\ . \\ . \\ . \\ . \\ \Delta c_k(0) \end{bmatrix}$$

and A, A', B, C, D are matrix.

In the case where the diffusion is considered not to be a rate determining step (i.e. $c_i = c_i^*$, $\Delta c_i = 0$ where c_i^* is the concentration of species i in the bulk of the solution), one has:

$$\frac{d\Delta q_i}{dt} = A\Delta q + B\Delta E$$

In the frequency dornain, this is equivalent to:

$$jw\Delta q = A\Delta q + B\Delta E$$

i.e.

$$(jwI - A)\Delta q = B\Delta E$$

where I is the identity matrix.

$$\Delta q = (jwI - A)^{-1} B\Delta E$$

and:

$$\Delta I_F = C(jwI - A)^{-1} B\Delta E + D\Delta E$$

Hence, the Faradaic admittance is equal to:

$$Y(w) = \frac{\Delta I_F}{\Delta E}$$

$$= C(jwI - A)^{-1}B + D$$

When the diffusion rate of one of the reacting species (species number i) interferes with the Faradaic current, from [1] one has:

$$\frac{\Delta c_i(0)}{\Delta J_i(0)} = \frac{1}{D_i} tanh \frac{d_i\sqrt{jw / D_i}}{\sqrt{jw / D_i}}$$

$$= N_i(w)$$

where D_i is the diffusion coefficient, δ_i the thickness of the diffusion layer and $\Delta J_i(0)$ the flux of the ith diffusing species, which is more or less simply related to ΔI_F (e.g. $\Delta J_i(0) = \Delta I_F$ in the example given in [1], page16-18.

Then:

$$jw\Delta q = A\Delta q + A' N_i(w)\Delta J_i(f) + B\Delta E$$

in the case reported in [1]:

$$\Delta I_F = C(jwI - A)^{-1}[B\Delta E + A' N_i(w)\Delta I_F]$$

i.e.

$$Y(w) = \frac{C(jwI - A)^{-1}B}{1 - C(jwI - A)^{-1}A' N_i(w)}$$

Given the time constant of the mass transport (δ_i^2/D_i) the diffusion loop is usually found at the lowest part of the useful frequency range in the model simulations (e.g. see Fig. 3.11(b) of [1]). In this framework all the loops except the diffusion one are semi-circles centred on the real axis. The validity of this approach has been exploited in various metal-electrolyte systems. One of the most intricate and the most thoroughly investigated seems to be the iron dissolution in acidic medium.

3.2.2 Iron Dissolution in Acidic Medium [20]

The steady-state polarization curves and the electrode impedances were measured during the dissolution of an iron electrode in 1M $Na_2 SO_4$ solution acidified by the addition of 1M H_2S0_4. These experiments were performed within a very wide pH (0- 5), current density (up to 0.1 $A.cm^2$) and frequency (10^{-3}-10^5Hz) ranges. In addition to the high frequency capacitive loop attributed to the double layer capacity and the charge transfer resistance, three time constants were observed before the onset of the passivation process (Fig. 24).

CURRENT DENSITY, mA. cm -2
POTENTIAL, V S.S.E.
Re [Z], Ω . cm2
-Im [Z], Ω . cm2
C4
H4
F3
D2
D0
F5
E5

On the other hand, the appearance of three simultaneous inductive loops is a very selective criterion which eliminated 18 other schemes (marked B in the tables). The change of the diagram shape from E_5 to F_5 is rather selective too, and four more schemes are eliminated (marked C in the tables). Examination of these three points allows 32 schemes out of 40 to be eliminated from an analytical point of view. The behaviour of the remaining eight schemes have been investigated by numerical simulation.

Only one model (3-D) covering wide experimental conditions is kept using reasonable hypotheses:

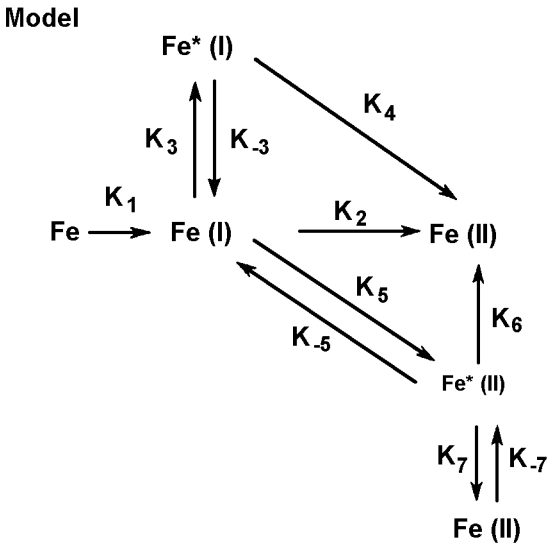

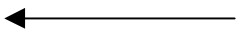

Fig 24 Steady-state polarization curves; Fe (johnson-matthey) disc electrode; diameter = 3mm; rotation speed = 1600 rev. min^{-1}; mixture in various proportions of 1m Na_2SO_4 and 1m H_2S0_4; 25° ± 0.2°c; deoxygenated by Ar. solution pH: curve 0, pH = 0 - curve 1, pH = 1.0 - curve 2, pH = 2.0 - curve 3, pH = 2.6 - curve 4, pH = 4.0 - and curve 5, pH = 5.0. the electrolyte resistance for the actual electrode (3mm in diameter) was: pH 0, 4.3Ω:-pH1, 14Ω:-pH2, 15Ω:-pH2.6, 15Ω:-pH4, 16Ω:-pH5, 17Ω. In the inserts: impedance diagrams measured about polarization points indicated on the current-voltage curves (from [20]).

3.2.3 Partially Active Electrode Approach [21,22]

The impedance of an electrode where only a reversible charge transfer and bulk diffusion towards a non-uniform interface occurs has been derived. In this approach it is assumed that the electrode surface is divided into active sites of area S_1 and an inactive part of area S_2 (Fig. 25). The reactive species of concentration c are supposed to diffuse towards the surface through a diffusion layer of thickness **l**. However close to the surface, for $0 \le x \le \mathbf{l}^*$, lateral interaction occurs due to the fact that the consumption wells are not uniformly distributed. Hence the evolution equations of the concentration of the reactive species in the bulk of the solution are:

$$\frac{d\Delta c_1}{dt} = D\frac{d^2\Delta c_1}{dx^2} + \Delta J_{12} / S_1 \quad in\ S_1 and 0 \le x \le \ell^*$$

$$\frac{d\Delta c_2}{dt} = D\frac{d^2\Delta c_2}{dx^2} + \Delta J_{12} / S_2 \quad in\ S_2 and 0 \le x \le \ell^*$$

$$\frac{d\Delta c_1}{dt} = \frac{d\Delta c_2}{dt} = \frac{d\Delta c}{dt} = D\frac{d^2\Delta c}{dx^2} \quad \ell^* \le x \le \ell^*$$

where C_1 and C_2 are average concentrations over areas S_1 and S_2; ΔJ_{12} is the perturbation of the lateral interaction flux:

$$\Delta J_{12} = (\Delta c_2 - \Delta c_1) k (S_1 + S_2)$$

These equations are similar to those which describe a chemical-electrochemical- chemical reaction mechanism. They can be solved under the following boundary conditions:

$$D \left.\frac{d\Delta c_i}{dx}\right|_{x=0} = -\Delta J_i \qquad for\ S_i = S_1 or S_2$$

If the double layer and adion charging are neglected, the total current density is obtained through an averaging procedure:

$$\Delta I_F = F(\Delta J_1 + s\Delta J_2)\frac{\Delta E}{1+s}$$

and the generalized admittance density relative to the total surface is:

$$Y_F(w) = \frac{1}{Z_N + sZ_s}$$

where:

$$Z_N(w) = H_1(w)\frac{RT}{F^2 C_{SS}{}^o}$$

and:

$$Z_s(w) = H_2(w)\frac{RT}{F^2 C_{SS}{}^o}$$

are respectively the Nernst diffusion impedance and the impedance related to the lateral transport contribution where:

$$H_1(w) = \frac{1}{\sqrt{jwD}} \tanh \ell\sqrt{\frac{jw}{D}}$$

and:

$$H_2(w) = \frac{1}{\sqrt{(jw+W)D}} \tanh \ell\sqrt{\frac{jw+W}{D}}$$

where:

$$s = S_2 / S_1 \quad \text{and} \quad W = k\frac{1+s}{s}$$

Due to the respective value of t and **l***, Z_N will usually act in the low frequency range and Z_σ in the high frequency range (Fig. 26). It is noticeable that theoretically, the slope of the high frequency portion is unity. However the authors have shown that often a capacitive contribution due to the charging of the adion or of the double layer increases the $\pi/4$ departure angle of the high frequency part of the impedance diagram up to 70° to 80°.

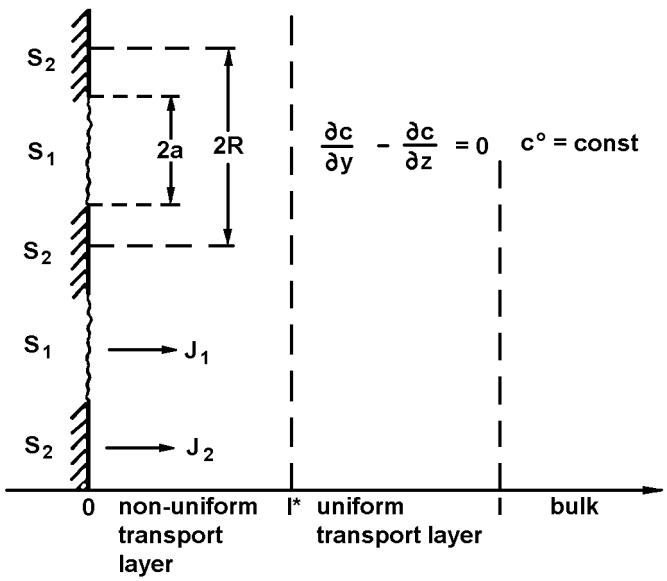

Fig.25 Schematic representation of a partially active electrode, J_1 and J_2 fluxes at S_1 (active) and S_2 (inactive) areas respectively (from [21]).

Numerical simulations given in Fig. 26 show that a high a value (high blockage) is necessary for observing Z_σ. It should be noticed that for a given value of σ the granulation of the domain structure, expressed by R in Fig. 25, is essential:

- for small sites very close

  $R \rightarrow 0 \quad (W \rightarrow \infty) \quad \Rightarrow \quad Z_F \rightarrow Z_N$

- for large sites far away

  $R \rightarrow \infty \quad (W \rightarrow 0) \quad \Rightarrow \quad Z_F \rightarrow Z_N(1+\sigma)$

Hence if in addition the double layer charging problem is considered it seems that very special conditions have to prevail for observing Z_σ.

Fig 26

Numerical simulation of ac impedance of inhomogeneous reversible Me/Me^{z+} electrodes:

(a) Impedances calculated for various values of $\sigma = S_2/S_1$.

Impedances calculated for a current dependent activation.

(b) $\sigma = 10$, $W = 280 s^{-1}$, $G_E = 0$, $\mathbf{l} = \mathbf{l}^* = 1.3\ 10^{-2}$cm, $C_{SS} = 6.10^{-4}$Mol/cm^3

(1) $G_i = 0$

(2) $G_i = 0.875 s^{-1}$, $\tau = 1s$

(3) $G_i = 2.33 s^{-1}$, $\tau = 0.375s$

(4) $G_i = 7 s^{-1}$, $\tau = 0.\ 125s$

(c) $\sigma = 150$, $W = 10^{-3} s^{-1}$, $G_E = 0$, $\mathbf{l} = \mathbf{l}^* = 1.8\ 10^{-2}$cm, $C_{SS} = 5.10^{-4}$Mol/cm^3

(1) $G_i = 0$

(2) $G_i = 5 s^{-1}$, $\tau = 0.0667s$

(3) $G_i = 15 s^{-1}$, $\tau = 0.04s$ (from [22])

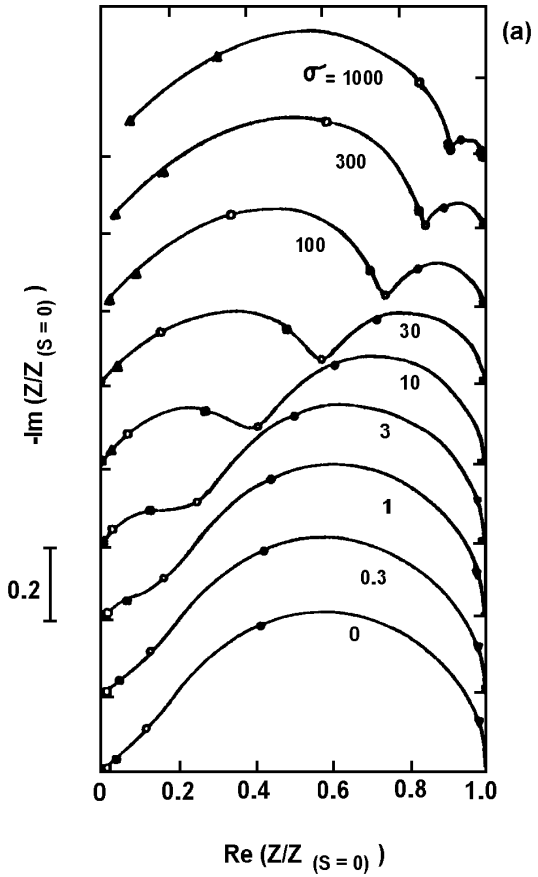
(a)
σ = 1000
300
100
30
10
3
1
0.3
0
0.2
-Im (Z/Z (S = 0))
Re (Z/Z (S = 0))
0
0.2
0.4
0.6
0.8
1.0

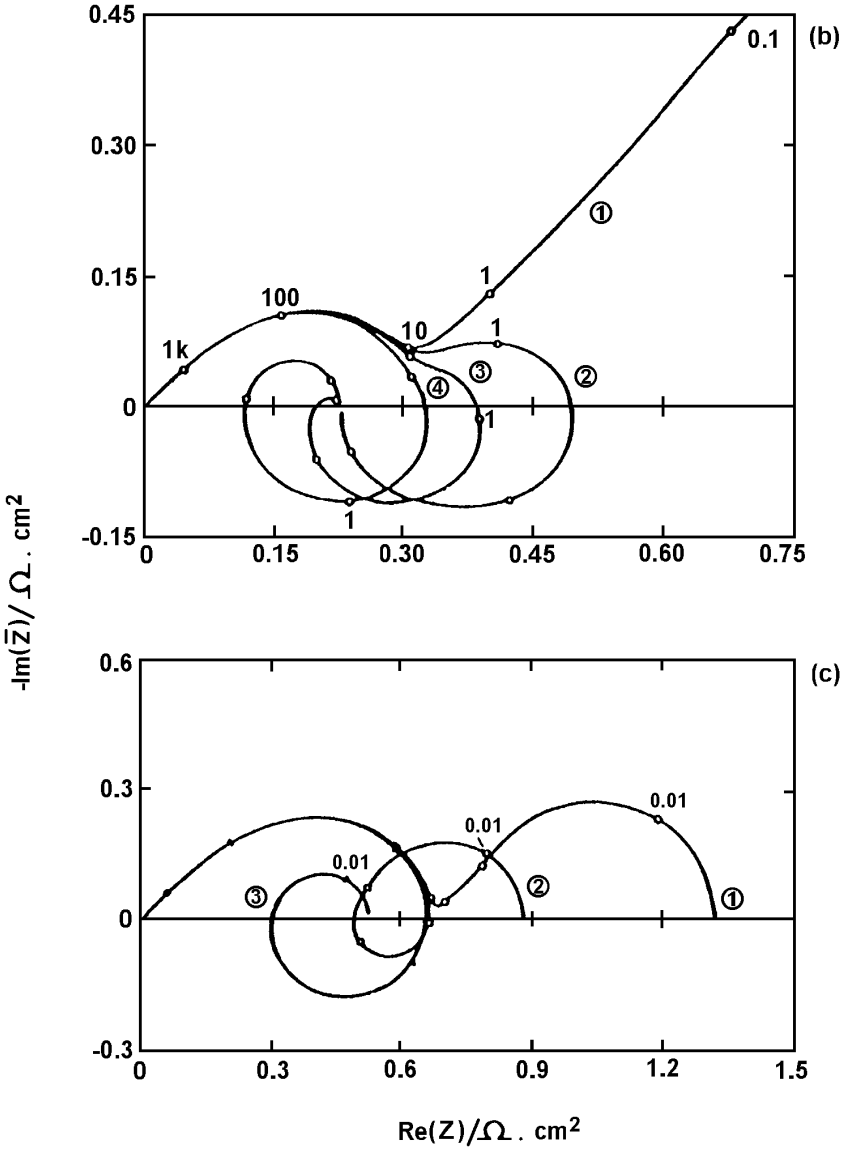
(b)
0.1
1
100
10
1
1k
①
②
③
④
1
1
0.45
0.30
0.15
0
-0.15
0
0.15
0.30
0.45
0.60
0.75
-Im(Z̄)/ Ω . cm²
(c)
0.01
0.01
0.01
①
②
③
0.6
0.3
0
-0.3
0
0.3
0.6
0.9
1.2
1.5
Re(Z)/Ω . cm²

In order to take into account a possible surface activation and de-activation, the authors proposed that the coefficient σ could be potential and current controlled. It would follow the phenomenological law:

$$\frac{ds}{dt} = A(E, I_F, s)$$

Then the whole impedance is:

$$Y(w) = Y_F(w)\frac{1 + Z_F G_E \left(t^{-1} + jw\right)^{-1}}{1 - G_i \left(t^{-1} + jw\right)^{-1}}$$

where:

$$t^{-1} = -\left(\frac{dA}{ds}\right)_{E,I_F}$$

$$G_i = \left(\frac{di_{SS}}{ds}\right)_E \left(\frac{dA}{dI_F}\right)_{I_F,s}$$

$$G_E = \left(\frac{di_{SS}}{ds}\right)_E \left(\frac{dA}{dE}\right)_{I_F,s}$$

Some simulations are given in Fig. 26 where $G_i\tau$ is kept constant for curves 2, 3 and 4 which explains the same R_p value. This model has been used in the case of silver electrocrystalization.

3.2.4 Ag/Ag$^+$ System [21, 22]

The dc and ac polarization behaviour was studied on stationary and rotated disc electrodes of polycrystalline and monocrystalline silver in 0.1M $AgNO_3$ + 1M $HCl0_4$ solution.

In Fig. 27 one of the interesting features of this approach seems to be revealed. For a good separation between Z_N and Z_σ optimum fit curves lead to values of σ ranging between 10 and 20. When the rotation speed of the rotating disc electrode is increased, only Z_N is decreased and an inductive loop is revealed in the lowest frequency range which seems to indicate a potential or current activation of the active sites. In fact as from the model Z_σ is **I**-independent, it is therefore Ω- independent and the lateral contribution cannot be eliminated by increasing Ω. For the d-e-f curves the fitting procedure has given respective σ values: 5.6; 3.0; 0.25. In agreement with the model prediction, sufficiently high σ value (5.6) shows a good separation between Z_N and Z_σ whereas for low values (0.25) only Z_N appears.

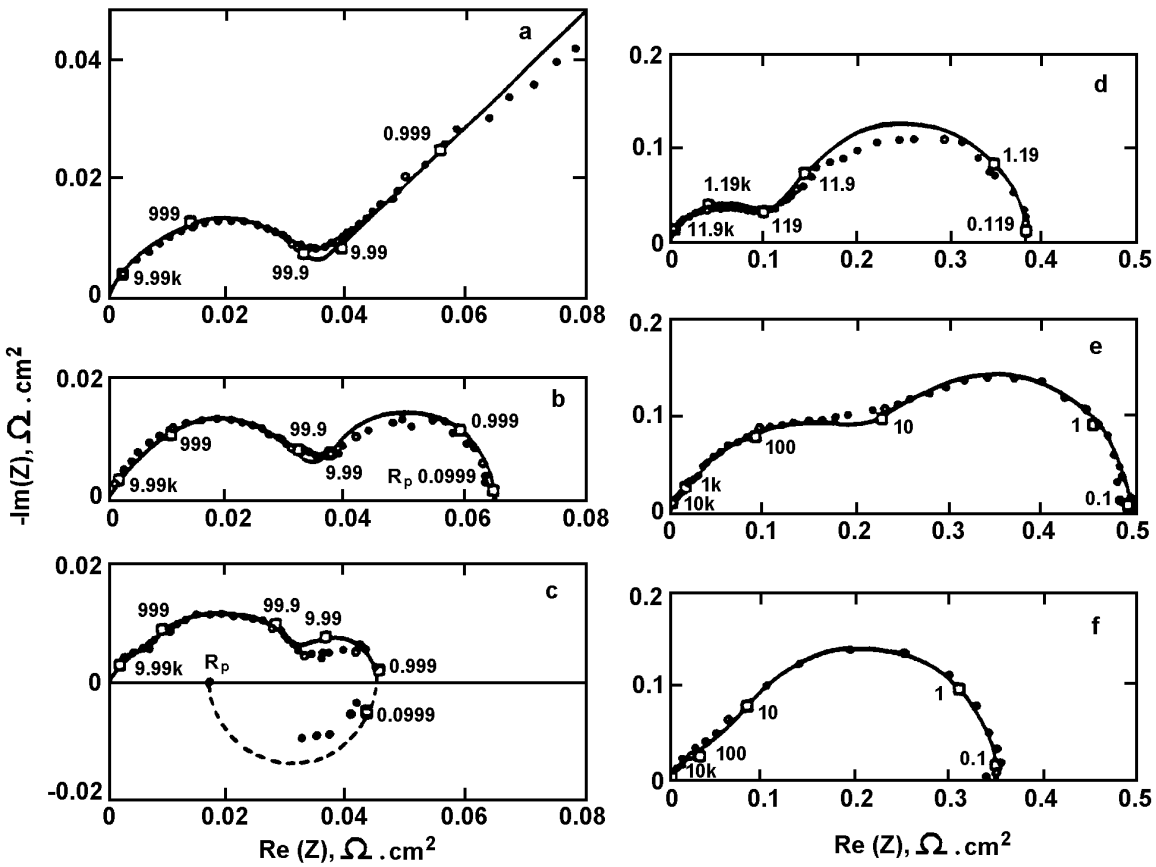

Fig. 27 AC impedance of cathodically polarized polycrystalline Ag electrodes:

(•) experimental values

( ) optimum fit curves

Ω = 0 (a); 300 (b); 120Orpm (c), (d), (e), (f)

electrolyte 1M $AgNO_3$ + 1M $HClO_4$ (a), (b), (c)

0.IM $AgClO_4$ + 1M $HClO_4$(d)

0.IM $AgNO_3$ + IM $HClO_4$ + 10^{-6}M Cl^- (e)

0.IM $AgNO_3$ + IM HNO_3 (1) (from[22]).

3.3 Applications To Practical Problems

Some examples of application of impedance analysis to systems of practical interest are surveyed below. They pertain to various fields of the real world: corrosion, batteries, bioelectrochemistry, semiconductor, etc. Each paragraph is devoted to one topic but is not at all an exhaustive review. In fact in each case only one (or a few) papers are taken into consideration without any reference to other work in the same field. The objective is to show in a particular circumstance how the authors have tackled the practical problem and how they have solved it.

3.3.1 Corrosion of Steel Bars Embedded in Concrete [23]

Reinforced concrete is one of the most widely used structural materials in construction (buildings, bridges,etc). However, loss of serviceability as a result of reinforcement corrosion is a serious problem as it can lead to dramatic accidents. Generally the corrosion state of the reinforcement bars is unknown until rust stains appear on the structure. In addition, the corrosion products themselves occupy a greater volume than the steel from which they form; the resulting increase in volume can provoke cracking and disintegration of the concrete. A technique is researched for detecting the first stages of the bars corroding in order to take precautions or repair the construction.

In the concrete the steel bars are in contact with the interstitial liquid which is inside the pores. This liquid is generally very alkaline (pH ≈ 13) just after the casting and should become more and more alkaline when the concrete is ageing. In such a medium, the steel is passive and corrosion cannot occur. Unfortunately during the life of the construction several processes can develop defects in the concrete. Porosity and microcracks are due to mechanical stresses or thermal cycles (frost - thaw) and to chemical attacks by the external surroundings (carbonation, acidic industrial pollution, etc). All these defects allow easy penetration of aggressive reagents (oxygen, chloride for structures in marine environment or subject to de-icing salts) and cause a pH decrease of the interstitial liquid. In these areas the reinforcement is less well protected and corrosion attacks may be initiated by galvanic action between the poorly protected surroundings. At the anodic areas the pH decreases as a result of hydrolysis of iron corrosion products so the adjacent concrete becomes neutralized and the anodic area extends. Highest corrosion rates are found in circumstances involving intermittent wetting of the structure. AC impedance techniques are used for a non-destructive in-situ evaluation of the corrosion of reinforcing steel in concrete. Firstly laboratory experiments on steel embedded in mortar exposed to different environments have been carried out. Secondly the in-field corrosion monitoring is approached.

→

Fig 28 Corrosion of reinforcement steel in concrete:

(a) Cross section of the sample.

(b) Impedance diagram for mortar sample at free potential (-400mV/SCE) one month after cure.

(c) Impedance diagram for mortar sample at free potential (-700mV/SCE) six months after cure.

(d) Impedance diagram for mortar sample at free potential (-724mV/SCE) eleven months after cure (from [23]).

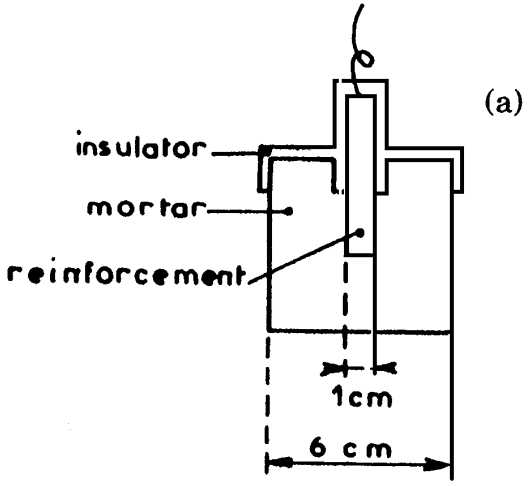
(a)
insulator
mortar
reinforcement
1cm
6 cm

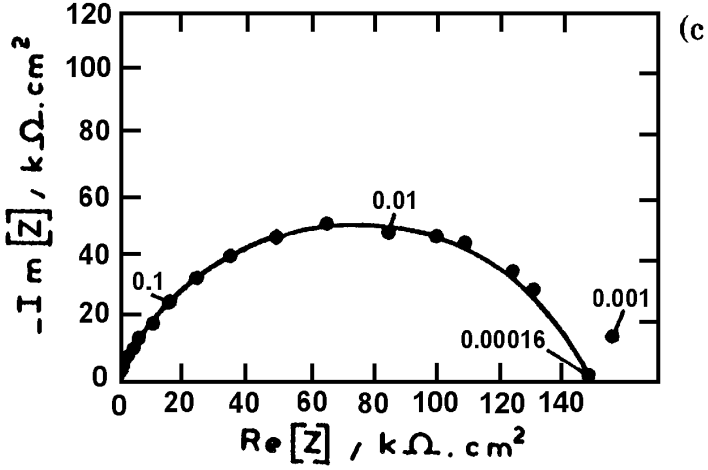
(c
-Im [Z] , kΩ.cm²
Re [Z] , kΩ.cm²
0.1
0.01
0.001
0.00016

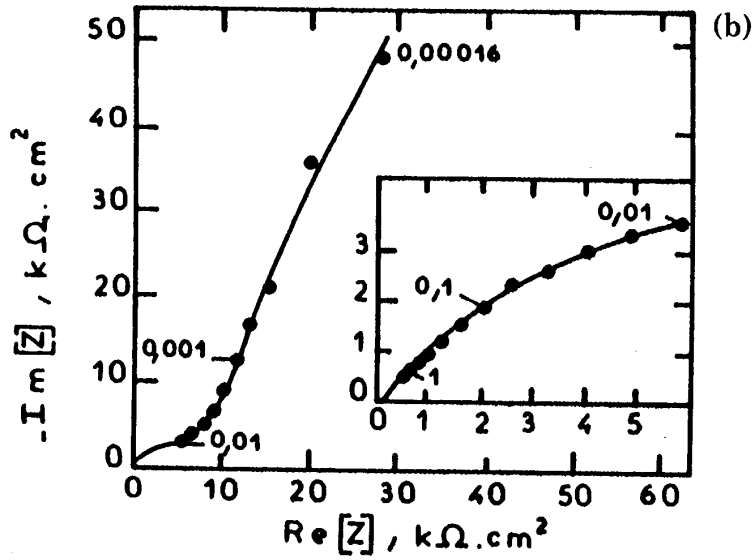
(b)
-Im [Z] , kΩ.cm²
Re [Z] , kΩ.cm²
0,00016
0,001
0,01
0,1
1

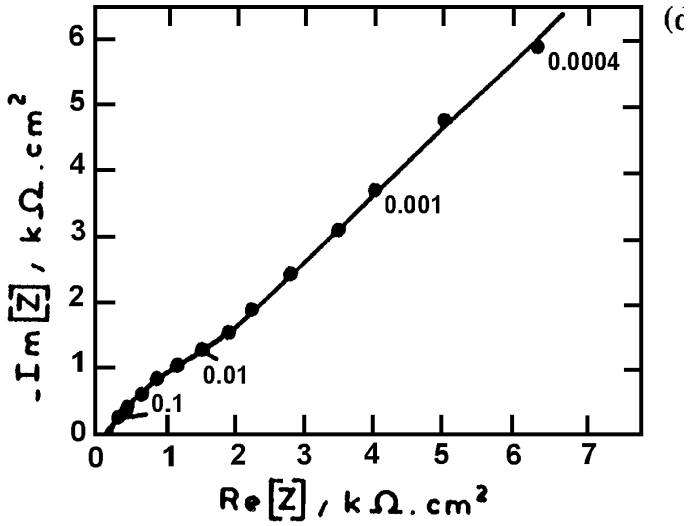
(c
-Im [Z] , kΩ.cm²
Re [Z] , kΩ.cm²
0.0004
0.001
0.01
0.1

At the laboratory scale it has been shown that the depassivation of the reinforcement in presence of chloride ions can be detected before the corrosion is evident from the outside. As an example (Fig. 28(a)) Fe-25% Ni alloy is embedded in mortar with $CaCl_2$ and immersed during two years in aerated KCl 0.5M solution in order to follow the variation of the shape of the diagram with time after a one month cure (ie. the sample is kept in a saturated atmosphere). Fig. 28(b) has been measured one month after the end of the cure. It has the shape of a passivated electrode but the diameter of the loop is much lower (for a passivated reinforcement immersed in a mortar without $CaCl_2$ the diameter is of the order of several $M\Omega.cm^2$). A month later a low frequency loop appears. In Fig. 28(c) the impedance is plotted six months after cure: the diameter of the high frequency loop has decreased considerably. This shape is similar for more than a year, but a 45° straight line is shown in the lower frequency range for another specimen 11 months after cure (see Fig. 28(d)). This linear part of the diagram seems to be due to the oxygen diffusion towards the metal. A general trend is the decrease of the diameter of the high frequency loop concomitant with an increase of the corrosion rate: this quantity could be related to a transfer resistance.

As a test the measurement of the electrochemical impedance of the reinforcement allows the depassivation of the latter to be detected before the corrosion becomes visible from the outside. However a more quantitative investigation is in progress to resolve some problems: systems where active and passive zones coexist are not well known, the long bars involved in large dimension structures lead to deformation of the high frequency part of the diagram due to a potential distribution along the bars [24], various compositions and castings can lead to various porosity [25], bright or pre-rusted steel influences the corrosion immunity [26].

As far as the in-field application is concerned the impedance technique is already used. In new or partly restored constructions, isolated test bars (two in each probe) can be built-in. These bars provide information on the actual corrosion rate. On existing old structures, the rebars (connected as working electrode) are measured against a combined auxiliary and reference electrode put on the concrete surface [27].

3.3.2 Quality Control and Corrosion Test for Anodized Al Alloys [28,29]

The corrosion resistance of anodized Al alloys is usually evaluated in a 300 hour salt spray test. The alloy has to show less than a certain number of pits at the completion. ASTM B457 describes a procedure to measure the impedance at 1000Hz to determine the quality of scaling. Some authors have considered that given the complexity of the anodized Al surface which consists of a thin non-porous barrier layer and a thick porous partially hydrated layer which needs to be adequately sealed, it seems obvious that recording the entire impedance spectrum is necessary to judge the quality of the anodized surface. As an example the Al alloys which are commonly used in aerospace applications with chromic acid anodization and sealing with hot water or dichromate is presented here. The samples are "good" in the sense that they passed the salt spray test. The large variation of the impedance modulus, from 1Ω to more than $10^6\Omega$ lead the authors to plot the data in a Bode plane. The tests were performed in aerated 0.5N NACl solution in potentiostatic mode at the corrosion potential. In this way the authors were able to compare the efficiency of two sealing procedures: hot water sealing and dichromate sealing (Fig. 29(a)). They also compared the change in corrosion protection with time for the dichromate sealing (Fig. 29(b)).

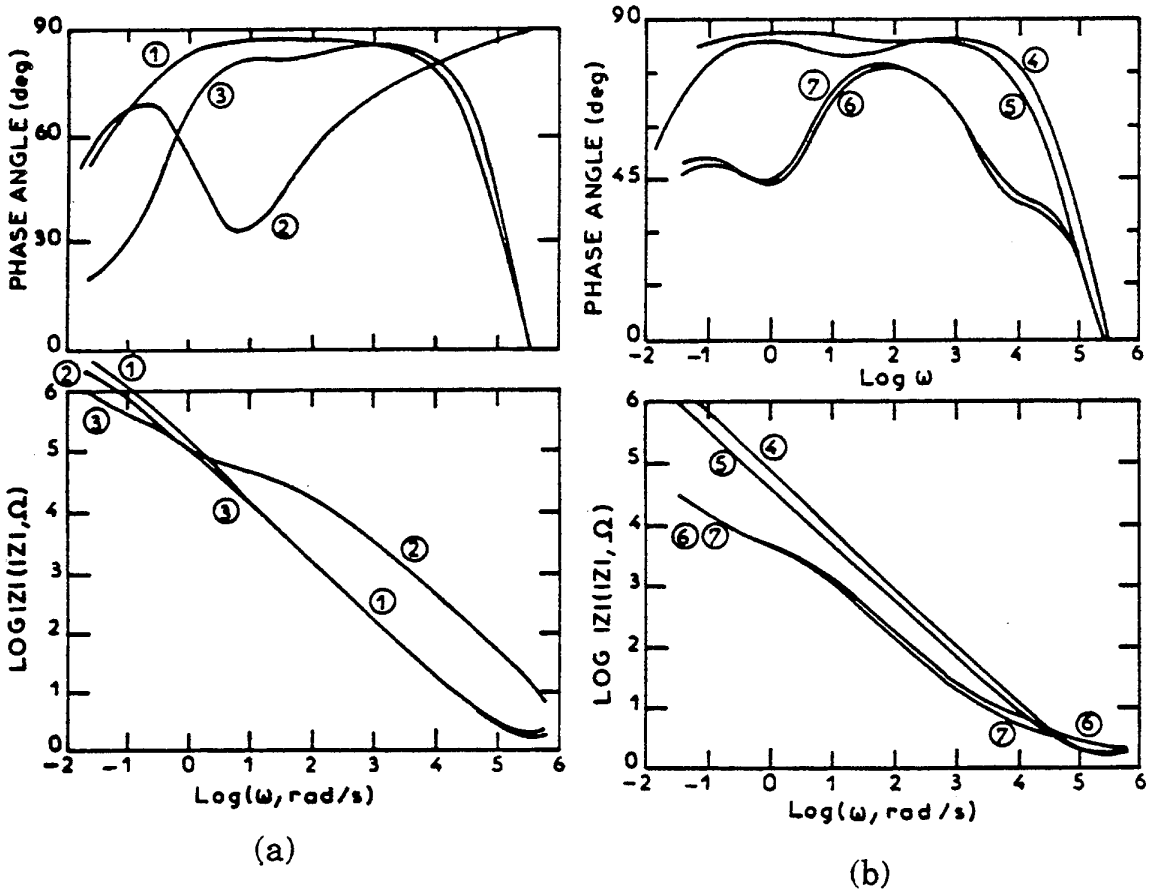

Fig. 29 Bode plots of the impedance of a 20cm^2 sample:

(a) CAA Al 7075 samples exposed during t_{corr} to 0.5N NaCl for different types of sealing:

(1) unsealed, t_{corr} = 3h

(2) hot water seated, t_{corr} = 20h

(3) dichromate sealed, t_{corr} = 4h

(b) CAA Al 2024 samples with dichromate seal as functions of exposure time to 0.5N NaCl:

(4) t_{corr} = 2h

(5) t_{corr} = 50h

(6) t_{corr} = 122h

(7) t_{corr} = 144h (from [29]).

It is established that the high frequency portion of the impedance spectra reflects the properties of the porous layer while the properties of the barrier layer determine the low frequency portion. Two time constants occur for the two sealing procedures but pronounced differences in the spectra are observed at high frequencies when the ASTM test applies, while very similar values are obtained at low frequencies. This indicates a difference in the sealing mechanism, nevertheless poor corrosion behaviour is observed for both sealing procedures even if the ASTM predictions are different. The present norm results in an erroneous conclusion concerning the quality of the dichromate sealing procedure and the resulting corrosion resistance.

Considering all of the experimental data it appears that the corrosion resistance can be better determined from the low frequency impedance data. However for the "good" anodized AI alloys the low frequency limit (f = 0) cannot be determined in the practical frequency range which is experimentally accessible. Hence the authors propose to define a damage function D based on Z_t which is the value of the impedance at a higher frequency (f = 0.1Hz) at times t:

$$D = log \frac{Z_o}{Z_t}$$

where Z_o is the initial impedance value at 0.1Hz.

The table shows a summary of damage functions for dichromate sealed and unsealed three different AI alloys for sulphuric (SAA) and chromic (CA.A) anodizations exposed to 0.5N NaCI solution.

TABLE

Damage functions for t = 7 days (Dichromate seal)

	Sealed	Unsealed
CAA Al 2024	1.51	1.37
SAA Al 2024	0.11	0.60
CAA Al 6061	0.04	0
SAA Al 6061	0.0	0
CAA Al 7075	0.18	1.91
SAA Al 7075	0.0	0.1

Some anodized AI alloys are so corrosion resistant (D = 0) that no corrosion occurs in seven days.

Hence impedance measurements can be used as a quality control test for the sealing and anodizing procedures as well as a corrosion resistance test for anodized AI alloys.

3.3.3 Characterization of Porous Layers by EHD Impedance Techniques [30,31]

Porous non-reacting layers covering a metal electrode, such as those due to insoluble corrosion products may slow down the mass transfer rate of the diffusing species. The mass transport properties of the reacting species in the layer have to be characterized in terms of the diffusion coefficient D and the layer thickness L.

By freezing the voltage polarization, i.e. the heterogeneous kinetics, and perturbing the rotation speed of a rotating disc electrode, i.e. the hydrodynamic flow, a special transfer function can be defined between the response of the current and the rotation speed in the potentiostatic regime (or the response of the potential in the galvanostatic regime). If the perturbation is a small amplitude sine wave the Electro Hydro Dynamical (EHD) irnpedance is measured. The general scheme of the measurement arrangement is given in the first monograph [1]. Usually on a bare electrode the Schmidt number (v/D where v is the viscosity of the solution) of the solution is obtained.

A well defined porous layer can be investigated as a first step by this technique. The concentration gradient is assumed to be distributed between the porous layer where the transport of the reacting species occurs only by molecular diffusion and the solution where the transport occurs by convective diffusion in a Nernst layer of thickness δ and a diffusion coefficient of the reacting species D_N. In these conditions the EHD iinpedance can be derived and numerically simulated for comparison with the experimental data.

The EHD impedance measurements are usually plotted in a Bode plane as the asymptotic tendencies (at zero and infinite frequencies) are of great interest. In addition it can be demonstrated that this quantity is equal to the product of three transfer functions respectively due to the contributions of the heterogeneous kinetics, the mass transport and the hydrodynamics. Usually the former is constant in the useful frequency range (except sometimes in the higher range) but if the mass transport has to be investigated the raw data have to be corrected for the hydrodynamics contribution which is perfectly known; such a correction is much easier in the Bode plane (where it is only a subtraction) than in the Nyquist plane. The variable parameter is a dimensionless frequency $p = \omega/\Omega$ where ω is the modulation frequency and Ω is the mean rotation frequency of the electrode.

Experimental results are given in Fig. 30 for a polymer film (Tyramine) electrochemically grafted onto a platinum electrode. The resulting coating is strongly bonded to the substrate and has a rather uniform aspect. The theoretical value was fitted to the experimental data thanks to a simple algorithm. As an example the best parameters obtained at 1600 rpm are L = 0.12μm and D = $10^{-7}cm^2.s^{-1}$ although an optical measurement shows L = 1000A. In contrast with a bare electrode the curves are not reducible in p (i.e. the experimental curves obtained for various Ω are not identical when plotted in p).

For a layer grown from the insoluble products of the corrosion of a carbon steel electrode in aerated chloride solution (3% NaCI) the results are given in Fig. 30(c). In this case the layer is characterized by an apparent Schmidt number which depends upon the mean rotation speed Ω of the electrode. Now some investigations are in progress for obtaining the thickness and the diffusivity of the layer.

Compared with the classical impedance measurements, due to the fact that the potential is frozen, the experimental results avoid the limitations due to the electrolyte resistance, double layer capacity and heterogeneous kinetics. Therefore the parameters extracted by a fitting procedure (L, v/D) are much more accurate.

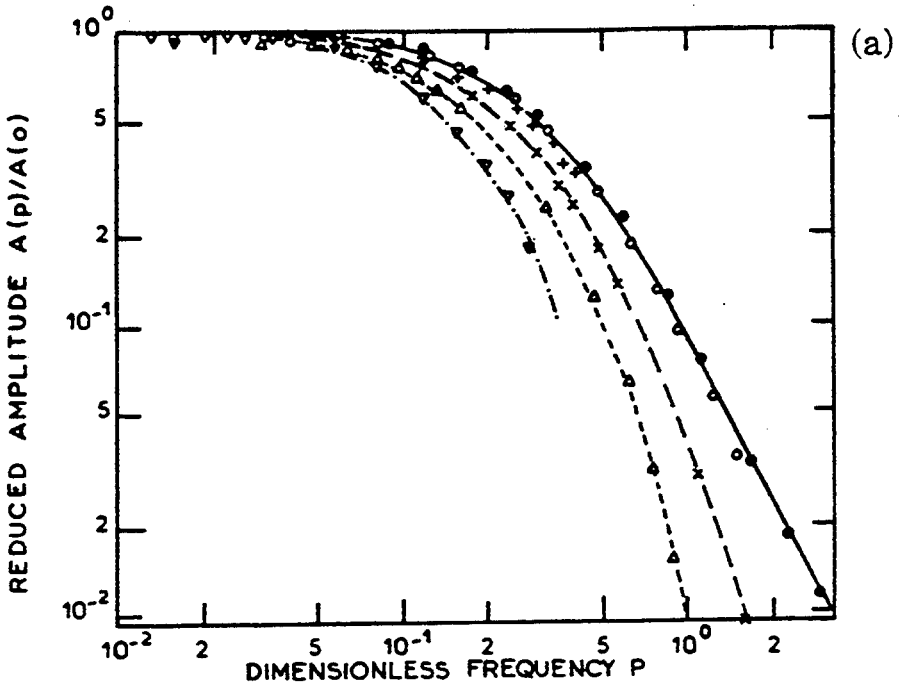
(a)
REDUCED AMPLITUDE A(p)/A(o)
10^0
5
2
10^-1
5
2
10^-2
10^-2 2 5 10^-1 2 5 10^0 2
DIMENSIONLESS FREQUENCY P

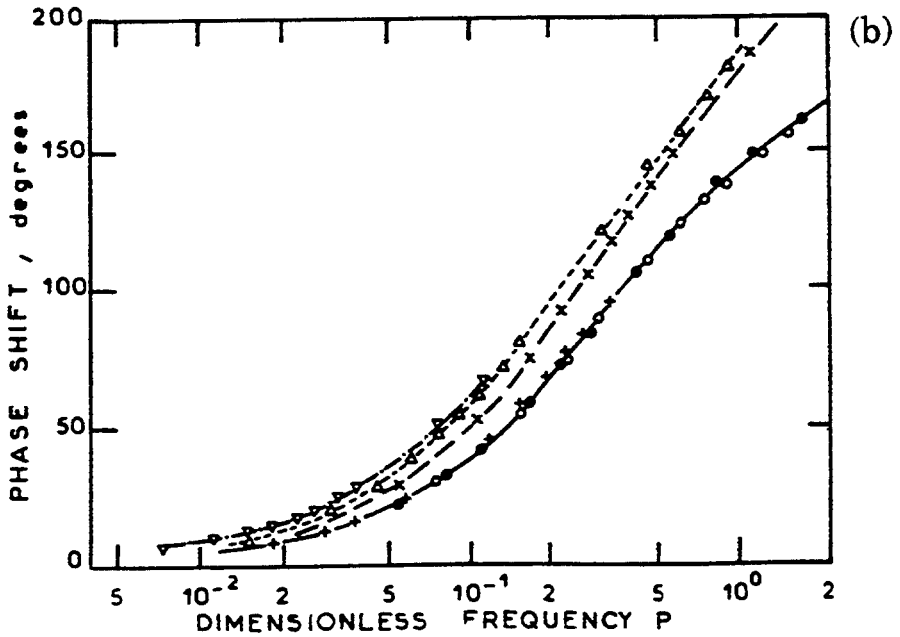
(b)
PHASE SHIFT , degrees
200
150
100
50
0
5 10^-2 2 5 10^-1 2 5 10^0 2
DIMENSIONLESS FREQUENCY P

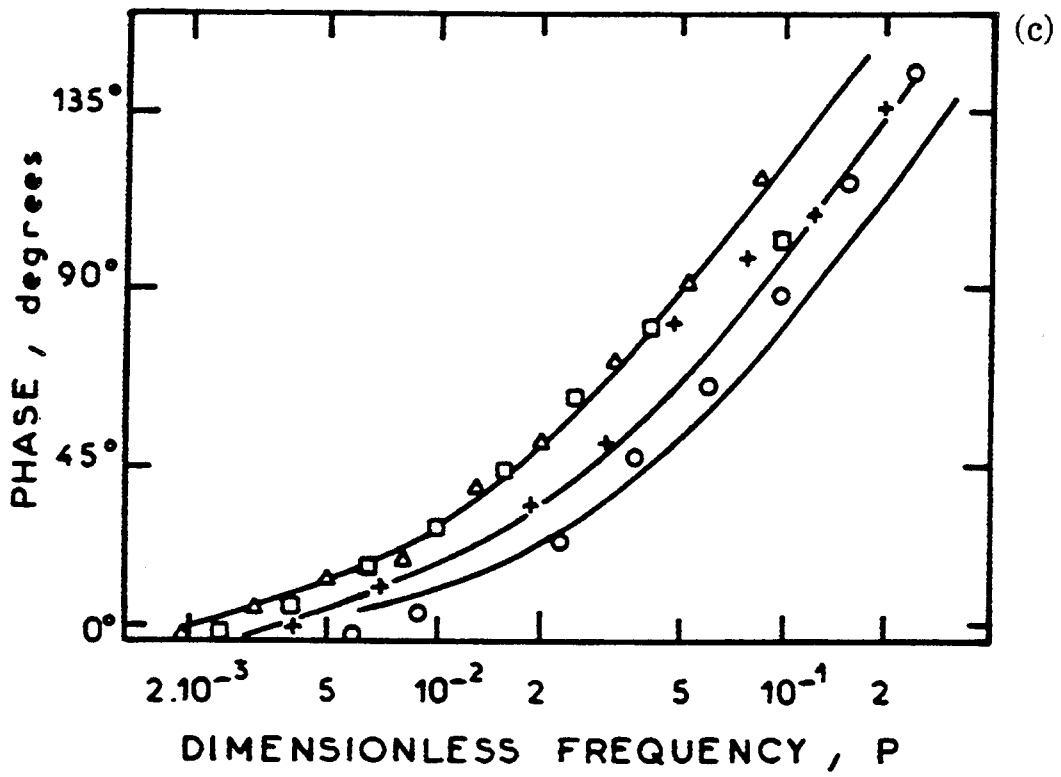

Fig. 30 Experimental impedances obtained for various layers plotted in a Bode plane:

(a) Reduced amplitude A(p)/A(0) for a polymeric porous coating.

(b) Phase shift for a polymeric porous coating (from[30]).

Bare electrode: Ω_o = 110 rpm (•-); 400rpm (o-); 1600rpm (+ -)

Coated electrode: Ω_o = 110 rpm (x---); 400rpm (Δ….); 1600rpm (∇ -.-)

On a bare electrode the three impedances are reduced by use of the dimensionless frequency $p = \omega/\Omega_o$, where ω is the modulation frequency and Ω_o the electrode rotation frequency (from [30]).

(c) Phase shift obtained for a layer of corrosion products on carbon steel in NaCl solution in galvanostatic mode for an anodic current (250μA.cm^{-2}) at Ω = 200rpm (o); 1000rpm (+); 1500rpm (Δ); 3000rpm ( ) (from [31]).

3.3.4 Characterization of Porous Electrodes [32,33]

Porous metallic electrodes are used in various fields (power sources, electrochemical reactors, etc.) due to their large specific area which is necessary when a large reactive surface is needed in a small volume. This porosity leads to potential and concentration distributions in the electrolyte paths between the bulk of the solution and the metal surface. The simplest basic model is given by a narrow cylindrical pore of finite length in which the potential and concentration profiles are characterized in terms of the penetration depth of an ac signal. At high frequencies the electrode admittance is generally large and the ac signal is damped within a short distance. As the frequency decreases, the ac signal penetrates more and more deeply in the pore and at low frequency the impedance is the same as for a flat surface having the same developed area. Therefore, the impedance is closely related to the geometry and size of the pores. If in the gas phase these parameters can be determined by various methods (e.g. BET), on the contrary in a liquid phase the characterization of the pore texture is poorly established.

For more intricate pore texture, an equivalent cylindrical pore electrode characterized by a radius, depth and pore number can be estimated.

Two examples of this procedure are given: a gold powder electrode and a nickel Raney electrode. The results are compared with experimental values obtained by BET techniques. The impedance of a bed electrode of geometric area $1cm^2$ made with a gold powder is measured in 1N KOH (Fig. 31). The low frequency rising part is equivalent to a resistance-capacity circuit whose values can be evaluated from the experimental data. By measuring the double layer capacitance C_d on a plain electrode, the ratio C/C_d gives the specific surface area. By assuming the sphere packing depicted in Fig. 31(c) the impedance can be derived and numerically simulated (Fig. 31(b)). As the experimental and theoretical impedances are very similar to that of a cylindrical pore characterized by a radius r, a length **l** and a number of pores n, these quantities can be estimated from Ω, C and V_e which is the volume of electrolyte inside the pores.

→

Fig 31

(a) Impedance diagram of a gold powder electrode with a $1cm^2$ apparent surface area in 1N KOH 20°C quantity of material: curve 1, m = 1.18g, curve 2, m = 2.3g.

(b) Simulated impedance diagram of gold powder electrode with $r = 1.15\ 10^{-3}$cm, P = 0.132, $C_d = 3\ 10^{-5} F.cm^{-2}$, $p = 4.5\Omega.cm$, $n = 2.4\ 10^4$; curve 1: 1.18g electrode, 43 packing units similar to Fig. (c) are stacked; curve 2: 2.30g electrode, 85 packing units stacked.

(c) Four packing units of spheres, r sphere radius, P geometrical factor (from [32]).

(d) Impedance diagram of Raney-nickel electrode in 5N KOH at 20°C, m = 28mg, $S_a = 1cm^2$; R electrolyte resistance outside the catalyst layer; R_o: R without catalyst layer; R_t: parallel resistance with C;$\Omega = R_p - R_t - R$ where R_p is the polarization resistance.

(e) Impedance diagrams of Raney-nickel electrode (high frequency range), m = 7, 18 and 23mg, $S_a = 0.1m^2$; R_o indicates the electrolyte resistance without catalyst layer; (o) experimental results; (-) fitted curves with appropriate R, R_e, R_t and C values (from [33]).

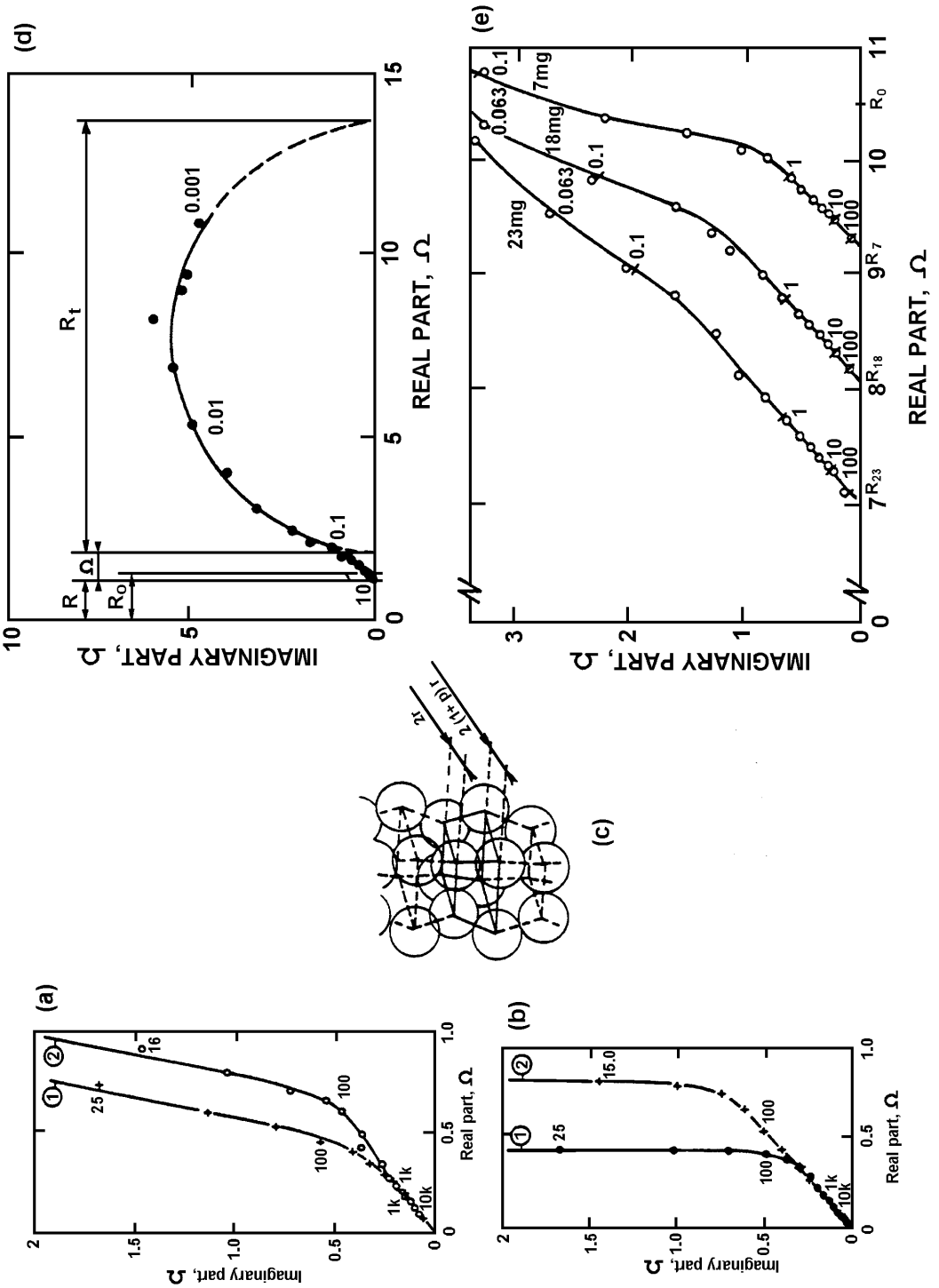
(a)
(b)
(c)
(d)
(e)
IMAGINARY PART, Ω
REAL PART, Ω
Real part, Ω
Imaginary part, Ω
R_t
R_Ω
R_0
0.001
0.01
0.1
1
10
16
25
100
1k
10k
15.0
23mg
18mg
7mg
0.063
R_{23}
R_{18}
R_7
R_0

For the electrode of Fig. 31a, the following values have been obtained: $n = 1.3\ 10^{6}$; $r = 1.1\ 10^{-3}$cm; **l** = 1.4mm and in addition the frequency f_o, at which the penetration depth is equal to the pore length, is equal to 16.2Hz for a 1.8g electrode.

Figure 31(d) shows the impedance diagram obtained with 28mg of Raney nickel in 5N KOH.

The apparent surface area is $1cm^2$. For frequencies greater than 1Hz the impedance diagram reveals a unit slope, enlarged in Fig. 31(e); on the contrary for frequencies lower than 0.6Hz a capacitive loop plotted as a slightly depressed semi-circle can be seen. Several resistive terms can be defined: R_t is the diameter of the low frequency loop; R is the resistance of the electrolyte between the capillary tip of the reference electrode and the upper surface of the catalyst layer; R_p is the polarization resistance, equal to $R + \Omega + R_t$; R_o indicates the electrolyte resistance measured in a cell without a catalyst.

In a first approximation, a Raney nickel electrode can be characterized, as previously, by an equivalent cylindrical pore. From the value of the capacity C, the specific surface area S is estimated ($S = 68m^2.g^{-1}$). The charge transfer resistance R_t is due to the oxidation of the adsorbed hydrogen at the Raney nickel electrode at open-circuit potential. This value allows the exchange current per unit catalyst mass J_o, to be evaluated ($J_o = 0.146\ A.g^{-1}$) which shows a high reactivity of the electrode. The R_o - R value gives the global porosity, as the gas phase measurement leads to the porosity inside a catalyst grain, by difference the intergranular porosity is obtained.

However if a single porosity is assumed, the estimated pores are too large compared to the value obtained from the gas phase measurement. If micropores are supposed to exist into the catalyst grain and to have a length equal to the grain radius, the number of cylindrical pores per catalyst grain can be calculated ($n_p = 2.10^7$). The slight deviation from the vertical of the high frequency part can be explained by a random distribution of the pore length. The depression of the low frequency semi-circle is very common in solid electrode impedances. Hence these results show that the complicated double porosity texture of the Raney nickel electrode has been decrypted and described as a double family of pores.

3.3.5 Surface-state Characterization at Semiconductor/ Electrolyte Junction [34,35]

The investigation of the semiconductor/electrolyte interface is attractive both for solar energy conversion and for the preparation and characterization of semiconductor materials for electronics. Photoelectrochemical conversion research has been very active these last years and a large variety of systems have been tested for improving the performance and long term stability of liquid junctions.

In order to thoroughly characterize the semiconductor/electrolyte interface impedance measurements have been used for a long time in the high frequency domain in order to obtain the space charge capacity. Its value is used to draw the classical Mott-Schottky plot in order to obtain information about the position of the energy levels of the semiconductor versus those of electrolyte and to know the potential distribution across the junction. However the investigation of the medium frequency range can give information about the surface states. The n-GaAs/aqueous electrolyte junction with a redox couple in solution under various illumination shows a good example of the type of information accessible through impedance measurements in the medium frequency range.

The equivalent circuit of this junction is shown in Fig. 32(a) where the various parameters are defined in the legend. Examples of impedance diagrams are given in Fig. 32(b) and 32(c). The photocurrent - voltage curve is given in Fig. 32(d). Every impedance diagram is analyzed by means of a non-linear least squares method, in accordance with the classical electrical equivalent circuit (schematic a).

In order to obtain non-frequency dependent components of the circuit it is necessary to take into account two R_{ss}, C_{ss} series circuits which mimic fast and slow surface state relaxations. However another, more physical, description of the time constants of the surface states is required in order to properly fit the experimental data (the fitting procedure leads to the various parameters). The value of space charge capacity allows the Mott-Schottky plot to be drawn. It gives the flat band potential and shows that under illumination the semiconductor band-edges are shifted with respect to their positions in the dark. It is shown that the C_{ss} (V) variation presents a sharp peak; its height increases with illumination. The surface state capture cross-sections are obtained from the relaxation time R_{ss} C_{ss}. A model for the electron occupation rate of a surface state distribution can be derived for explaining the C_{ss} variation. However the explanation of the flat band potential shift at the illuminated electrode necessitates that some chemical surface modifications are taken into account which are not very clear yet. These effects might be detected by means of very low frequency experiments which are not exploited so far, except in a few cases (eg. mass transport in [35]).

3.3.6 Prediction of the State-of-Charge of Batteries [36]

Electrochemical power cells deliver energy as a consequence of the cell reaction which starts to deteriorate from the moment that manufacture is complete. This self-discharge may be quite significant and can be dangerous for starting equipment that has long periods of inactivity. Hence in order to assess the reliability of a power cell a cell status indicator is required if a high wastage rate of partially discharged but still usable batteries is to be avoided.

The properties of the impedance of various batteries have been investigated especially with the aim of characterizing their state-of-charge. The change of some impedance components has been recorded when a prescribed amount of charge is withdrawn from the storage cell. A priori it seems that the problem is less convoluted in the case of primary cells than for secondary cells. The reason for this is that primary cells are not subjected to cycling as are secondary cells.

Usually a 2-electrode arrangement is used for the impedance measurements. The inclusion of a third electrode inside the commercial cell is always a possibility - which is attractive for a fundamental kinetic investigation - but the incorporation is not very convenient for practical applications. A test of the state-of-charge of a cell based upon parameters obtained from data on its impedance would only be satisfactory, reliable and credible if sufficient kinetic interpretation could also be provided to justify the selection of those parameters for the test. In this preliminary investigation the problem is to find the parameter which changes more markedly than others due to the discharge.

In a general way it can be shown (Fig. 33) that the locus of the impedance follows a semi-circular shape at the higher frequencies and becomes mainly resistive when the highest frequency is approached (10kHz). The resistive character observed as the frequency becomes infinite clearly corresponds to the ohmic resistance of the cell, electrolyte, electrodes and current conductors. The high frequency semi-circular loop represents the Faradaic process which controls the current and is generally to be identified with the electrode that forms the negative terminal of the cell, namely the anode as the cathode is usually of larger area.

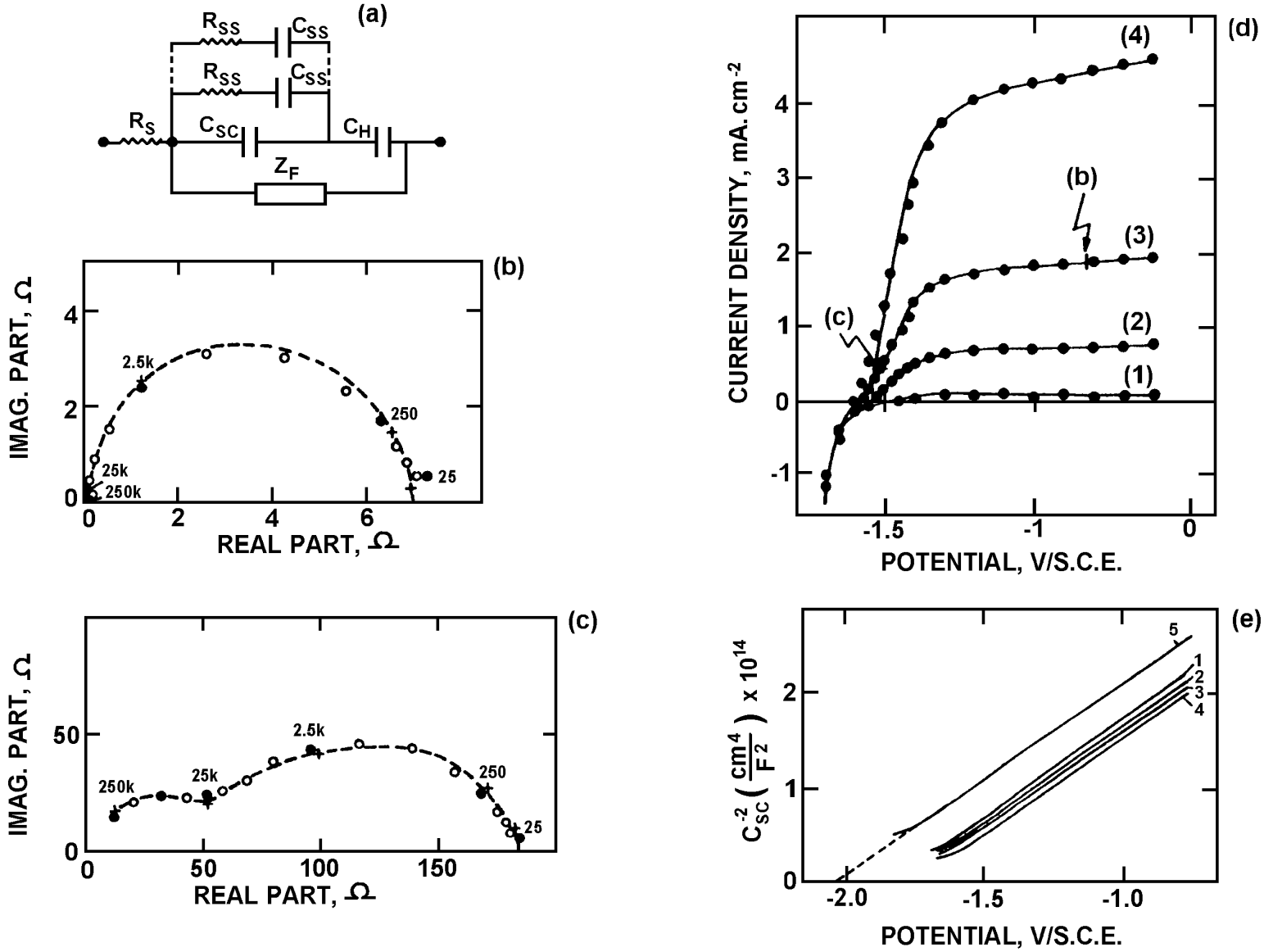
(a)
R_{SS}
C_{SS}
R_{SS}
C_{SS}
R_S
C_{SC}
C_H
Z_F
(b)
IMAG. PART, Ω
REAL PART, Ω
2.5k
250
25k
250k
25
(c)
IMAG. PART, Ω
REAL PART, Ω
250k
25k
2.5k
250
25
(d)
CURRENT DENSITY, mA. cm^{-2}
POTENTIAL, V/S.C.E.
(1)
(2)
(3)
(4)
(b)
(c)
(e)
$C_{sc}^{-2}\left(\frac{cm^4}{F^2}\right)$ x 10^{14}
POTENTIAL, V/S.C.E.
1
2
3
4
5

The depolarizing reaction at the cathode is quite often the slowest of the two electrode reactions in the kinetic sense, however the limitation imposed by the anode electrode area is generally sufficient to provide the major current control at the higher frequencies. The change in the diameter of the semi-circle which occurs when a charge is delivered by the cell is clearly an attractive parameter for examination.

At least for the highest state-of-charge (between 100% and 90%) there is a linear relationship between the state-of-charge and the diameter of the high frequency loop for the alkaline Zn/HgO and Li/$S0_2$ cells. With the Leclanche cell the low frequency part of the semi-circle is so merged with the Warburg line that the graphical determination of the diameter is quite difficult. Only a numerical fitting procedure is possible and has shown to the authors that the real part of the impedance measured at 31.2Hz is a linear function of the state-of-charge in the 100-90% range.

For alkaline Zn/MnO_2 and Li/CuO cells it seems rather difficult to devise a simple one or two frequency test. The cell impedance has to be analyzed over a wider frequency range in order to assess the charge status. For the Li/$SOCl_2$, in spite of a thorough kinetic investigation, a state-of-charge test has not been devised yet.

From these studies it is concluded that the impedance techniques can be taken as a basis for a charge status identification.

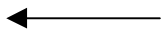

Fig.32

(a) Electrical equivalent circuit of a semiconductor-electrolyte junction. C_{sc} is the space-charge capacitance in the semiconductor, C_H the Helmholtz capacitance, R_s the series resistance and Z_p the Faradaic impedance. The series $R_{ss}C_{ss}$ circuit accounts for a charge relaxation in surface states. At some potential, a second $R_{ss}C_{ss}$ circuit is necessary to fit impedance spectra. (b) and (c) impedance spectra of the n-GaAs/selenide junction under 22mW/cm^2 illumination at different potentials (electrode area = 0.34cm^2). (o) experimental data (---) calculated spectrum according to the scheme in (a). The calculated (+) and experimental (•) points correspond to the same frequency indexation.

(b) V = -0.60V/SCE; C_{sc} = I5.InF, R_f = 7020Ω; R_{ss} = 664Ω; C_{ss} = 4.2nF; R_s = 5.7Ω; C_H = lμF.

(c) V = -1.575V/SCE; C_{sc} = 36.2nF; R_F = 176Ω; R_{ss} = 106Ω; C_{ss} = 181 nF,. R'_{ss} = 211Ω; C'_{ss} = 1800nF; R_s = 7.9Ω; C_H = 1μF. The polarization points where (b) and (c) are measured are indicated in Fig. (d).

(d) I-V curves of the n-Ga.As/selanide junction under:

(1) 1.5mW/cm^2 (2) 9mW/cm^2

(3) 22mW/cm^2 (4) 50mW/cm^2 illumination

(•) experimental data and (-) theoretical curve according to the model. Parameters are a = 26,000cm^{-1}; L = 0.2μm; c = 1.45 x 10^{-10}s; N_D = 2.3 x $10^{16}cm^{-3}$; V_{FB} = -2.06V/SCE; V_{redox} = -096V/SCE; λ = 1eV.

(e) Mott-Schottky plots (1), (2), (3) and (4) correspond to the I-V curves (1), (2), (3) and (4), respectively. In the dark, V_{FB} = -2.06V/SCE (curve (e)) (from [34]).

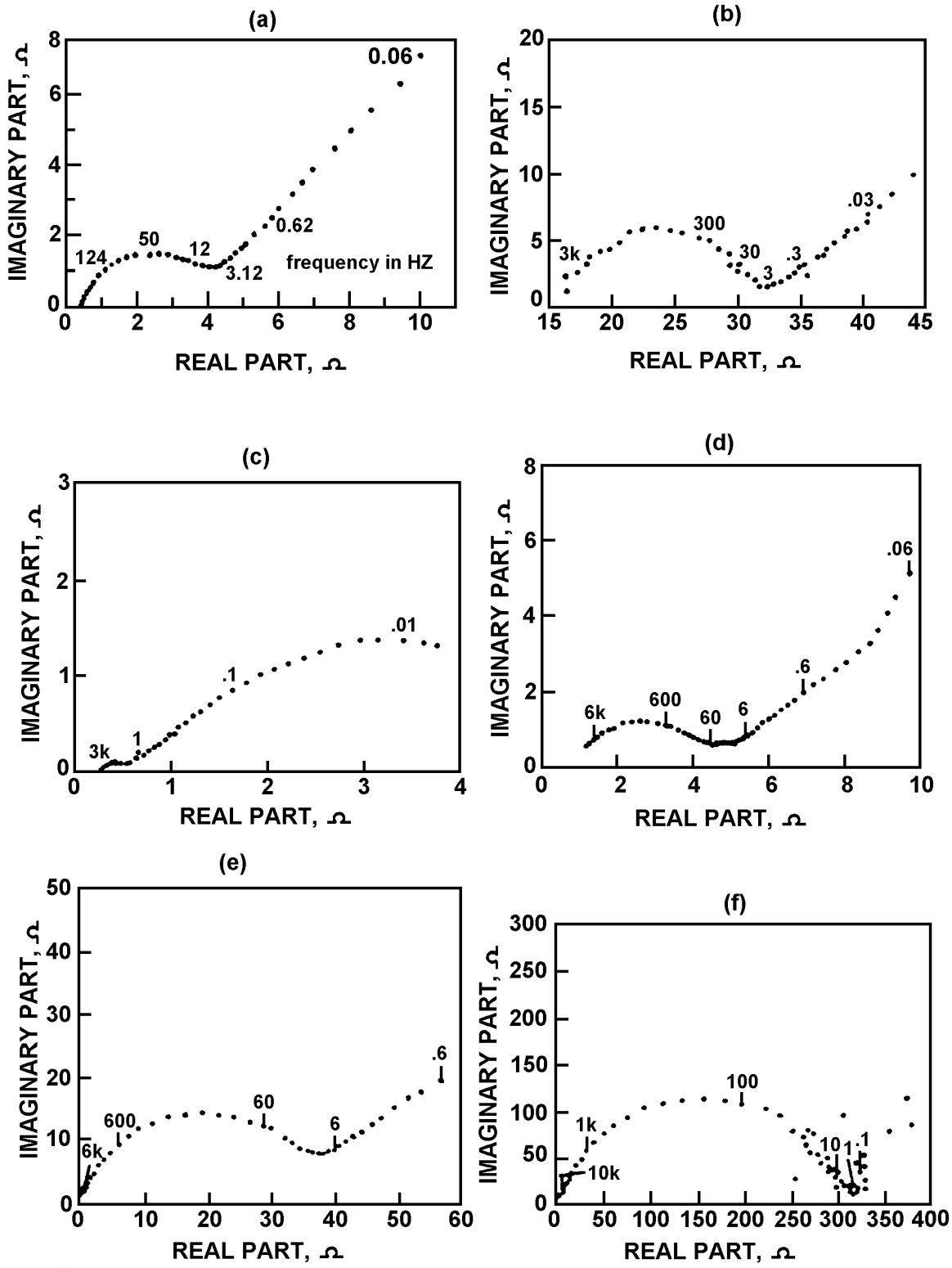
(a)
IMAGINARY PART, Ω
REAL PART, Ω
0.06
0.62
50
124
12
3.12
frequency in HZ
(b)
IMAGINARY PART, Ω
REAL PART, Ω
3k
300
30
3
.3
.03
(c)
IMAGINARY PART, Ω
REAL PART, Ω
3k
1
.1
.01
(d)
IMAGINARY PART, Ω
REAL PART, Ω
6k
600
60
6
.6
.06
(e)
IMAGINARY PART, Ω
REAL PART, Ω
6k
600
60
6
.6
(f)
IMAGINARY PART, Ω
REAL PART, Ω
1k
10k
100
10
1
.1

3.3.7 Electrodes Modified with a Redox Polymer Film [37]

The classic technique for these studies is linear sweep voltammetry coupled with chronoamperometry. The latter is used to determine the characteristic transport time of the charge within the film. Several models have been suggested to describe the kinetics of the modified electrodes under steady-state conditions with a substrate (i.e. a redox couple whose reaction is mediated by the redox polymer film) in solution. To interpret the simple case with no substrate in solution, the charge transfer at the electrode/polymer interface and the charge transport within the polymeric film have to be considered.

The charge transport in the film of thickness ϕ is understood to be a diffusion-like process. Since the redox centres are fixed to the polymer, they are not able to diffuse in a proper way, even though these centres may have a certain mobility. By mutual electron transfer between two adjacent redox centres however, a charge transport through the entire film is possible without significant displacement of the redox centres themselves. This charge transport obeys Fick's law where the diffusion coefficient depends not only on the electron exchange rate (self exchange rate) between the redox centres but also on the diffusion of these centres themselves.

In general this charge transport process is accompanied by counterion diffusion which assures electroneutrality throughout the film. The charge transport within the film depends therefore on the counterion diffusion in the film, the self exchange rate of the redox centres and the mobility of the polymer "fixed" redox centres.

A simple model has been tested by impedance technique; the oxydo-reduction of the redox active centres at the electrode / film interface and the diffusion of the redox couple within the polymer film. By assuming that the redox centres cannot leave the film to go in the solution a Faradaic impedance can be derived which agrees well with the experimental results.

Glassy carbon disc electrodes (diameter: 3mm) were coated with

$$Ru\ (bpy)_2\ [poly\ (4'\text{-vinylpyridine})Cl]\ Cl$$

by a spincoating technique using a methanolic solution of the redox polymer 10mg/10ml. With a micro-syringe about 1µl of this solution was placed at the surface of the glassy carbon electrode. The electrode was then spun immediately after deposition maintaining the disc in an upward position. The procedure was repeated until a coverage $\Gamma_o = 2.10^{-8} mole.cm^{-2}$ was attained. Γ_o was measured by integrating the anodic or cathodic wave of a linear sweep voltammogram.

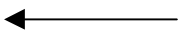

Fig. 33 Complex plane plots at high states-of-charge for some primary cells.

(a) Leclanche (SP11, Ever Ready).

(b) Alkaline Zn-MnO_2 (MN 150, Duracell).

(c) Alkaline Zn-HgO (RM 502R, Mallory Batteries Ltd.).

(d) Li-CuO (LC01, SAFT Sogea).

(e) Li-$S0_2$ (L032S, Mallory Batteries Ltd.).

(f) Li-$SOCl_2$ (LA30944 LAA-1, GTE Products Ltd.)

The impedance measurements were performed at various potentials using redox polymer coated glassy carbon electrodes in 1M HCI. The results are displayed in Fig. 34. The low frequency capacity C_{lf} has been determined by considering the low frequency equivalent resistance-capacity circuit. The variation of C_{lf} is plotted versus potential. The integration of this graph leads to a value of $\Gamma_o = 1.9 \times 10^{-8}$ mole.cm^{-2} which is very close to the value obtained by cyclic voltamrnetry. By plotting the transfer resistance versus the potential the Tafel coefficients b_i'S and the Ko'S/ϕ of the reaction rates where $K = K_o \exp.bV$, $K = K_o \exp.bV$, can be attained.

The impedance analysis of a polymer coated electrode allows all the accessible parameters to be evaluated by using only one technique. Hence this approach is very attractive for investigating modified electrodes.

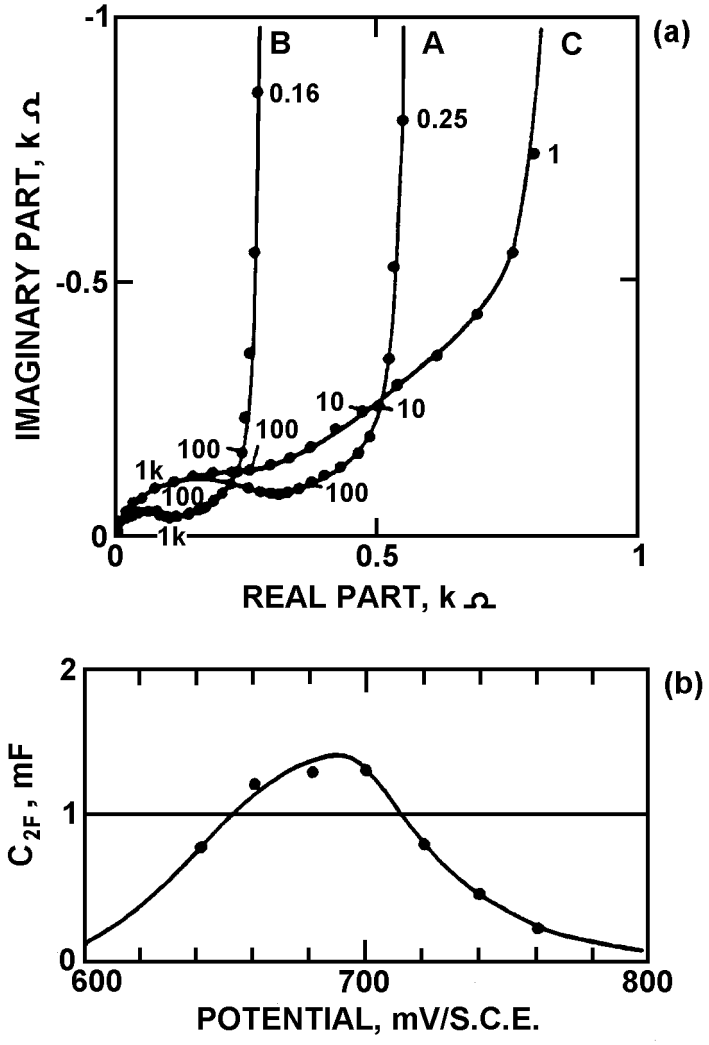

Fig. 34 Vitreous carbon disc electrode (diameter 3mm) modified with a redox polymer film: [Ru (bpy)$_2$[poly(4'vinylpyridine)CI] CI] in HCI, 1M.

(a) Impedance measured at A 0.64V/ECS; B 0.7V/ECS; C 0.76V/ECS.

(b) Change of the low frequency capacity C_{lf} vs potential (from [37])

3.3.8 Mass Transfer Phenomena in Blood [38]

Exchange of mass (particularly oxygen) between a vascular wall and the blood medium is of high physiological importance. It depends on the rheological characteristics of the blood, on the diffusion coefficient of the considered species and on the rate of the heterogeneous reactions to the wall. In addition, as the blood involves red blood cells and plasma the flux of matter will also depend on the exchange rate between the electroactive species dissolved in these two phases. The role of the blood diphasic character has been studied in the framework of homogeneous non-Newtonian fluid of the Ostwald type. In fact the special blood rheology gives a remarkable fluidity to the blood when compared to the other particle suspensions. As an example, at a haematocrit (i.e. volume fraction of cells) of 45% the relative viscosity (viscosity of suspensions/viscosity of suspending phase) is considerably lower in the case of blood ($\eta_r = 3$) than in suspension of rigid spheres or discs ($\eta_r = 200$).

In order to study these problems an electroactive haemacompatible species, the ferrocyanide anion, has been used as a mass transport tracer. The rotating disc electrode has been employed because it generates a well-def'ined flow and the uniform accessibility of the diffusion is worthwhile even for fluids notably departing from Newtonian rheological behaviour. The impedance of a platinum electrode immersed in various solutions (Fig. 35(a)) has been measured in whole human blood, in a suspension of red blood cells in a Ringer-Hartmann solution and in a homogeneous Ringer-Hartmann solution for a 3-electrode potentiostatic arrangement. The working electrode is a 3mm diameter rotating disc immersed in a solution at 37°C.

The rheological parameters:

a) fluidity index of the Ostwald fluid and

b) the apparent viscosity

are determined from viscosity measurements. The experimental impedances are fitted to a Randles-like equivalent circuit where the diffusion impedance is relative to a homogeneous non-Newtonian Ostwald fluid and a uniformly reactive electrode. The transfer resistance R_{ct}, the diffusion coefficient D and the diffusion resistance R_D have been determined. Hence the variation of the product $R_t.I$ and of the quantities D and R_D with the potential (Fig. 35(b)) and the rotation speed (Fig. 35(c)) have been investigated for the two types of red blood cell suspensions and for RH solution. This has shown the importance of the microenvironment at the electrode and the influence of the free exchange area as the electrode surface is partially blocked. The exchanges between the artificial wall and the blood medium are partly conditioned by electrostatic interactions between the wall and the red blood cells which can lead to the formation of a structure on or in the immediate vicinity of the exchange area. These structures which modify the exchanges are sensitive to the electrode charge, to the hydrodynamic conditions and to the temperature.

On another point of view this study of the interaction of red blood cells with platinum (and also vitreous carbon in [38]) could emerge on a more general investigation of the interaction of living cells with biomaterials. This can yield a diagnosis on the compatibility or possible rejection of an artificial prosthesis.

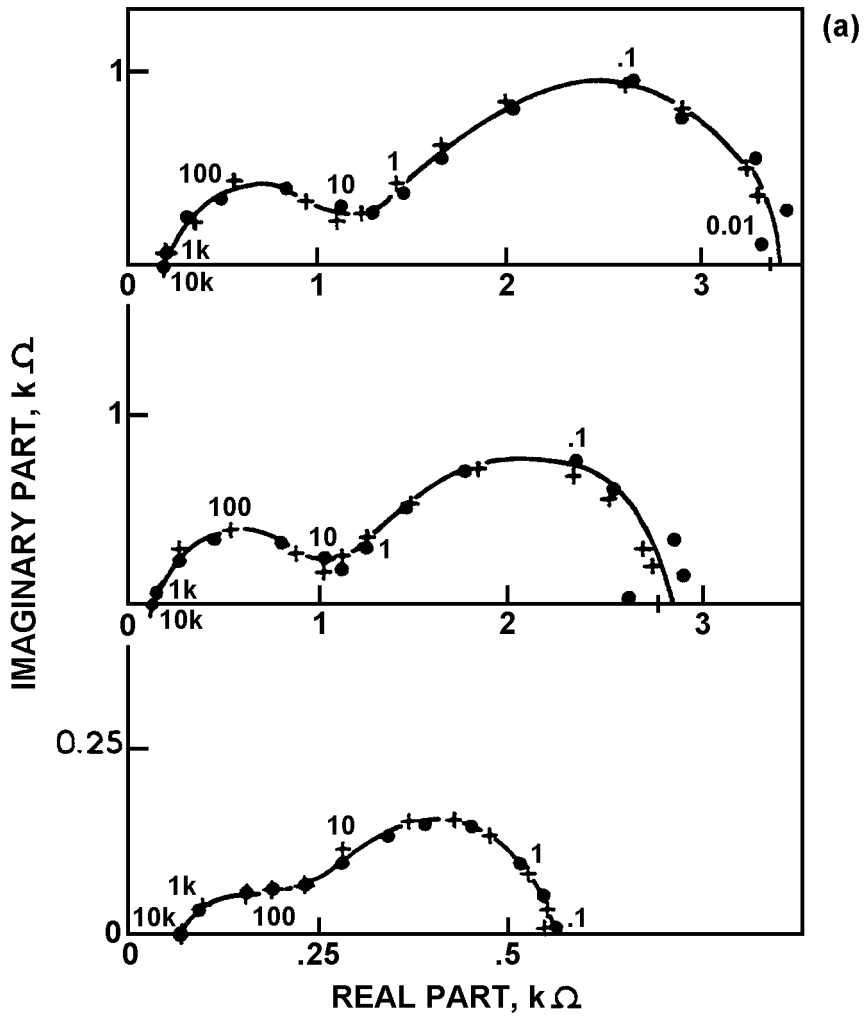

Fig. 35 Impedance of a 3mm diameter platinum electrode immersed in human blood.

(a) Experimental (•) and theoretical (+) impedance diagrams for a 170mV/SCE potential at 37°C.

(A) whole blood, Ω = 225rpm.

(B) red blood cells in RH solution, Ω = 225rpm.

(C) homogeneous RH solution, Ω = 2400rpm.

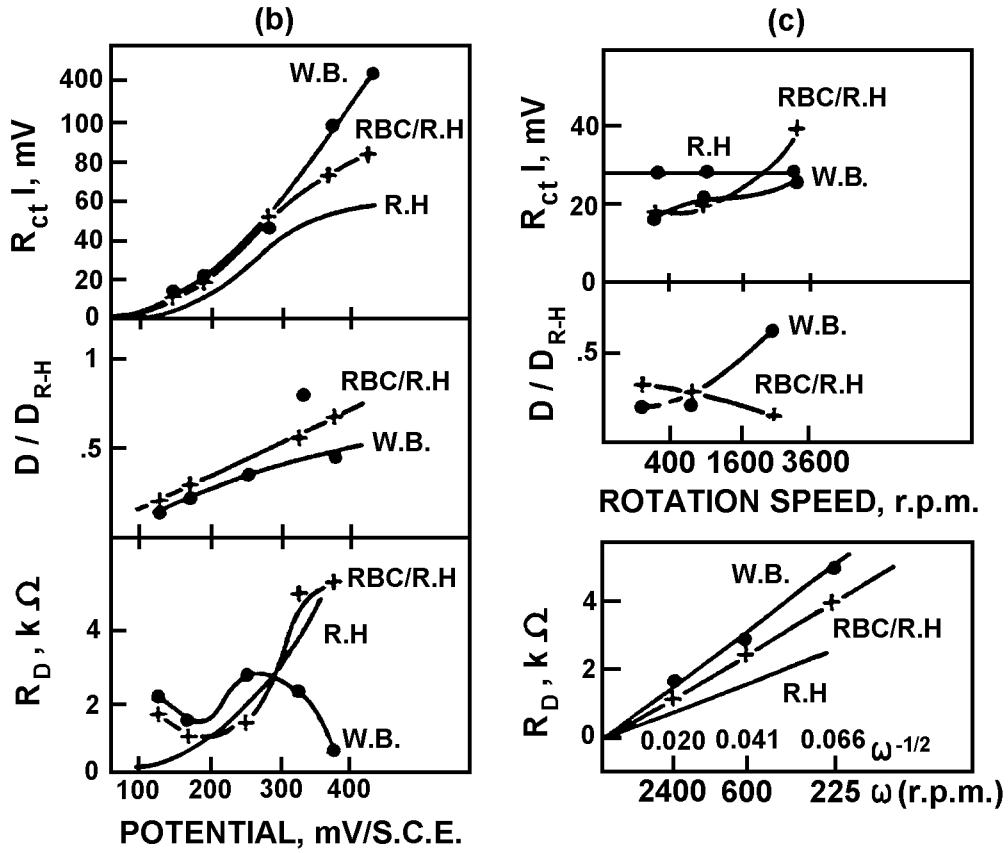

Variation of R_{ct}.I,D/D_{RH}, and R_D for RH solution where I.2 $10^{-5} \leq D \leq 1.610^{-5} cm^2 s^{-1}$(-); whole blood (•); and red blood cell suspension (+) (from [38]).

(b) with potential at Ω = 600rpm

(c) and rotation speed at 170mV/SCE

References

[1] C. GABRIELLI Identification of electrochemical processes by frequency response analysis Solartron Instruments, Farnborough, UK (1980)

[2} A.J. BARD and L.R. FAULKNER Electrochemical methods, fundamentals and applications John Wiley and Sons, Inc. (1980)

[3] D. D. MACDONALD Transient techniques in electrochemistry Plenum Press, New York (1977)

[4] Comprehensive Treatise of Electrochemistry Vols. 1 to 10. Ed. by E. YEAGER, J.O'M. BOCKRIS, B.E. CONWAY and S. SARANGAPANI Plenum Press, New York (1984)

[5] J.A. GONZALEZ, A. MOLINA, M.L. ESCUDERO and C. ANDRADE Errors in the electrochemical evaluation of very small corrosion rates I. Polarization resistance method applied to corrosion of steel in concrete Corr. Sci., 25 (1985) p. 917-930

[6] T. HEPEL Linear potential scan voltammetry for irreversible co-adsorption of electroactive species J. Electroanal. Chem., 193 (1985) p. 89-101

[7] C. GABRIELLI, F. HUET and M. KEDDAM (to be published)

[8] J.S. GILL, L.M. CALLOW and J. D. SCANTLEBURY Corrosion measurements derived from small perturbation non-linearity Part 1 harmonic analysis Corrosion NACE, 39 (1983) p. 61-66

[9] C. GABRIELLI, M. KEDDAM, H. TAKENOUTI, VU QUANG KINH and F. BOURELIER The relationship between the impedance of corroding electrode and its polarization resistance determined by a linear voltage sweep technique Electrochim. Acta, 24 (1979) p. 61-65

[10] C. GABRIELLI, M. KEDDAM and J.F. LIZEE On an impedance measurement error arising for fast swept sinusoidal excitation J. Electroanal. Chem., 163 (1984) p. 419-427

[11] A.A. PILLA Laplace plane analysis of electrode kinetics in "Electrochemistry Simulation and Instrumentation" Ed. by J.S. MATTSON, H.B. MARK and H.C. McDONALD Marcel Dekker, New York, 1972 Calculation, Intro Elect Imp Tech I CSB 1A01 R. 1

[12] H.B. SIERRA ALCAZAR, A.N. FLEMING and J.A. HARRISON J. Electroanal. Chem., 87 (1978) p. 339

[13] C. GABRIELLI, M. KEDDAM and J.F. LIZEE Frequency analysis of electrochemical step responses. Complex and operational impedances J. Electroanal. Chem., 205 (1986) p. 59

[14] C. GABRIELLI, F. HUET, M. KEDDAM and J.F. LIZEE Measurement time versus accuracy trade-off analyzed for electrochemical impedance measurements by means of sine, white noise and step signals J. Electroanal. Chem., 138 (1982) p. 201-208

[15] H. GOHR, M. MIRNIK and C.A. SHILLER Distortions of high frequency electrode impedance. Their causes and how to avoid them J. Electroanal. Chem., 180 (1984) p. 273-285

[16] S.A.G.R. KARUNATHILAKA, R. BARTON, M. HUGHES and N.A. HAMPSON Faradaic impedance measurements of small magnitudes encountered in high capacity electrical storage cell J. Applied Electrochem., 15 (1985) p. 251-257

[17] D. D. MACDONALD and M. URQUIDI-MACDONALD Application to Kramers-Kronig transforms in the analysis of electrochemical systems. 1. Polarization resistance J. Electrochem. Soc., 132 (1985) p. 2316-2319

[18] M. KENDIG and F. MANSFELD Corrosion rates from impedance measurements: an improved approach for rapid automatic analysis Corrosion NACE, 39 (1983) p. 466-467

[19] M. URQUIDI-MACDONALD, S. REAL and D. D. MACDONALD Application of Kramers-Kronig transforms in the analysis of electrochemical impedance data. 11. Transformations in the complex plane J. Electrochem. Soc., 133 (1986) p. 2018

[20] M. KEDDAM, O.R. MATTOS and H. TAKENOUTI Reaction model for iron dissolution studied by electrode impedance 1 - Experimental results and reaction model J. Electrochem. Soc., 128 (1981) p. 257-266 11 - Determination of the reaction model J. Electrochem. Soc., 128 (1981) p. 266-274

[21] J. HITZIG, J. TITZ, K. JUTTNER, W.J. LORENZ and E. SCHMIDT Frequency response analysis of the Ag/Ag+ system: a partially active electrode approach Electrochim. Acta, 29 (1984) p. 287-296

[22] E. SCHMIDT, J. HITZIG, J. TITZ, K. JUTTNER and W.J. LORE@;Z Inhomogencous electrodes. A polarization model of the partially blocked reversible metal ion electrode Electrochim. Acta, 31 (1986) p. 1041

[23] F. WENGER, L. LEMOINE and J. GALLAND Etude de la corrosion de l'acier doux dans le beton par les methodes electrochimiques 9th Intern. Congress of Metallic Corr., June 1984 Toronto (Canada) Proceedings Vol. 2 p. 349-356

[24] J. ZHANG, F. WENGER, M. JEROME and J. GALLAND Controle de la corrosion par la mesure de l'impedance electrochimique: probleme des structures de grandes dimensions C.R. Acad. Sci. Paris, 301 II(1985) p. 995-998

[25] P. LAY, P.F. LAWRENCE, N.J.M. WILKINS and D.E. WILLIAMS An ac impedance study of steel in concrete J. Applied Electrochem. 15 (1985) p. 755-766

[26] D.G. JOHN, A.T. COOTE, K.W.J. TREADAWAY and J.L. DAWSON The repair of concrete - a laboratory and exposure site investigation

[27] B. ELSENER and H. BONHI Monitoring corrosion of steel in concrete - an impedance approach 8eme Congres Europeen de Corrosion Nov. 1985, Nice (France), Proc. 1, p. 1-6

[28] F. MANSFELD and M.W. KENDIG Impedance spectroscopy as quality control and corrosion test for anodized AI alloys Corrosion NACE, 41 (1985) p. 490-492

[29] F. MANSFELD and M.W. KENDIG Electrochemical impedance spectroscopy of protective coatings in "Electrochemical Methods in Corrosion Research" Ed. by M.DUPRAT. Materials Science Forum Trans.Tech. Pub. Switzerland. 8 (1986) p. 337

[30] C. DESLOUIS and B. TRIBOLLET Electrohydrodynamical impedance in corrosion in "Electrochemical Methods in Corrosion Research" Ed. by M.DUPRAT. Materials Science Forum Trans.Tech. Pub. Switzerland. 8 (1986) p. 1

[31] A. BONNEL, F. DABOSI, C. DESLOUIS, M. DUPRAT, M. KEDDAM and B. TRIBOLLET Corrosion study of a carbon steel in neutral chloride solutions by impedance techniques J. Electrochem. Soc., 130 (1983) p. 753-761

[32] J.P. CANDY, P. FOUILLOUX, M. KEDDAM and H. TAKENOUTI The characterization of porous electrodes by impedance measurements Electrochim. Acta, 26 (1981) p. 1029-1034

[33] J.P. CANDY, P. FOUILLOUX, M. KEDDAM and H. TAKENOUTI The pore texture of Raney-nickel determined by impedance measurements Electrochim. Acta, 27 (1982) p. 1585-1593

[34] P. ALLONGUE and H. CACHET Band-edge shift and surface charges at illuminated n-GaAs/aqueous electrolyte functions J. Electrochem. Soc., 132 (1985) p. 45-52

[35] P. ALLONGUE, H. CACHET and G. HOROWITZ Detailed analysis of a redox stabilized liquid junction solar cell J. Electrochem. Soc., 130 (1983) p. 2352-2357

[36] S.A.G.R. KARUNATHILAKA, N.A. HAMPSON, M. HUGHES, W.G. MARSHALL, R. LEEK and T.J. SINCLAIR The prediction of the state-of-charge of some commercial primary cells J. Applied Electrochem. 13 (1983) p. 577-586

[37] C. GABRIELLI, 0. HAAS and H. TAKENOUTI Impedance analysis of electrodes modified with a reversible redox polymer film J. Applied Electrochem. 17 (1987) p. 82

[38] A. CAPRANI and M. NAKACHE Model of mass transfer phenomena in whole blood. Electrochemical impedance measured with ferrocyanide anion oxidation on a rotating disc electrode Bioelectrochem. and Bioenerg., 10 (1983) p. 213-228

Table I Reaction Schemes with three monovalent intermediates

	Schemes	Eliminated		Schemes	Eliminated
1-A	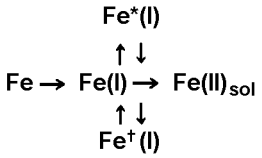	A	1-B	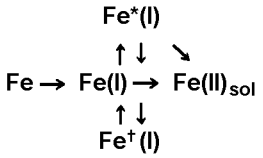	B
1-C	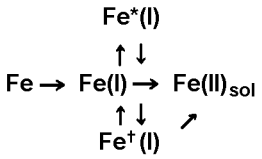	B	1-D	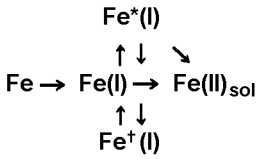	C
1-E	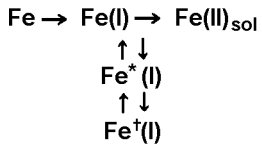	A	1-F	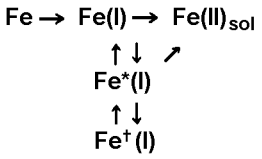	B
1-G	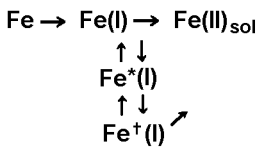	B	1-H	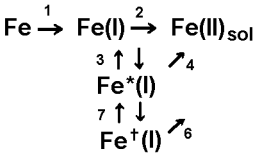	C

Table II Reaction Schemes with one mono- and two-divalent intermediates

	Schemes	Eliminated		Schemes	Eliminated
2-A	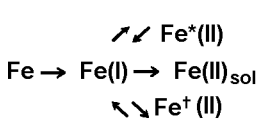	A	2- B	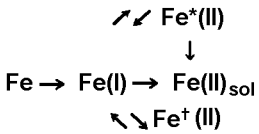	B
2-C	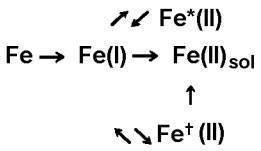	B	2-D	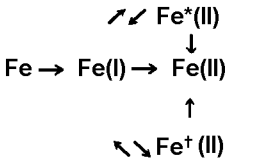	C
2-E	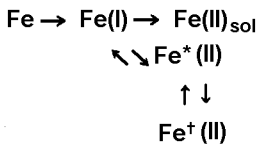	A	2-F	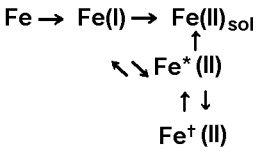	B
2-G	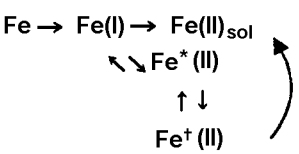	B	2-H	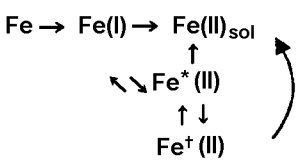	C
2-I	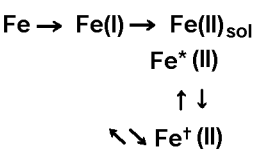	A	2-J	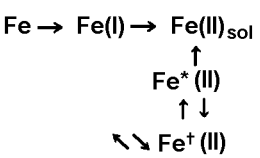	B
2-K	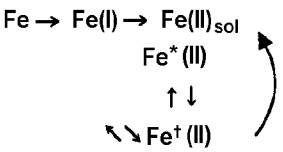	B	2-L	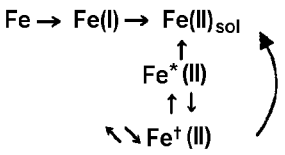	C
2-M	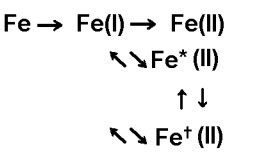	A	2-N	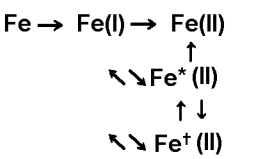	B
2-O	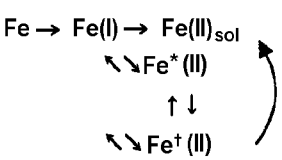	B	2-P	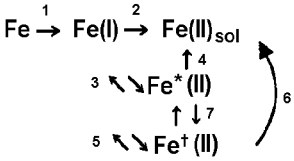	C

Table III Reaction Schemes with two mono- and one-divalent intermediates

	Schemes	Eliminated		Schemes	Eliminated
3-A	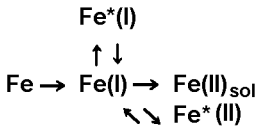	A	3-B	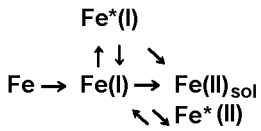	B
3-C	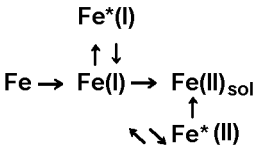	B	3-D	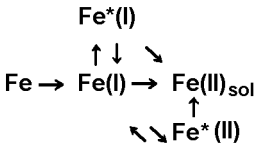	
3-E	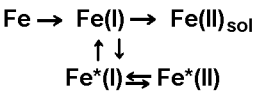	A	3-F	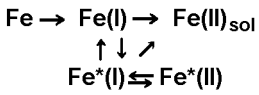	B
3-G	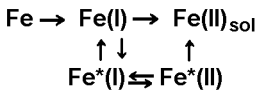		3-H	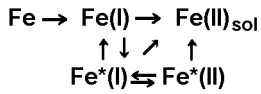	
3-I	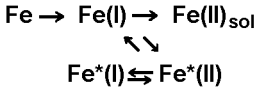	A	3-J	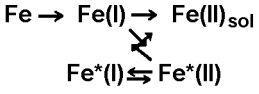	B
3-K	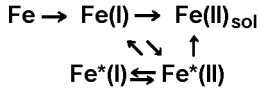	B	3-L	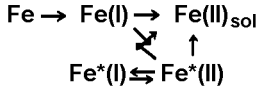	
3-M	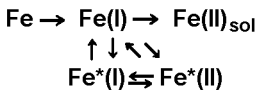	A	3-N	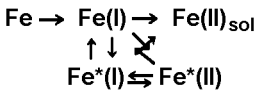	B
3-O	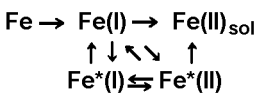		3-P